Supporting Information

Meso-Zn(II)porphyrins of Tailored Functional Groups for Intensifying the Photoacoustic Signal

Amina Yasin, Vijayakumar S. Nair, Assa S. Aravindh, Shaheen M. Sarkar, Maryam Hatamimoslehabadi, Somak Mitra, Mohd Hasbi Ab Rahim, Jeffrey La, Iman S. Roqan, Mashitah M. Yusoff, Chandra S. Yelleswarapu,* Rajan Jose*

Abstract:

Development of efficient molecular photoacoustic contrast agent plays significant role in the next generation biomedical imaging techniques. This article demonstrates a design criterion for small molecules to exhibit large photoacoustic effect by density functional theory (DFT) and its experimental validation. The method relies on controlling the effect of resonating structures on the vibrational energies of small molecules such that rapid thermalization pathways exist near higher-order unoccupied molecular orbitals. A series of Zn(II)porphyrin derivatives (Por-C_n-RA_m, where n=12 or 8 and m=1–4) is designed as a model system by DFT and demonstrated a systematic variation in the absorption coefficients of C-H vibrational modes occurring at high-frequency spectral region. A systematic decrease in absorption coefficients was observed; and therefore, a similar variation in the photoacoustic signals is predicted. To validate the theoretical results, four Zn(II)porphyrin based molecules showing systematic variation in absorption coefficients, viz. Por-C_{12}-RA_1, Por-C_{12}-RA_2, Por-C_{12}-RA_3, and Por-C_8-RA_4 are synthesized in good yields (40–70%) and their optoelectronic properties are systematically studied as well as the effect of resonating structures in these molecules in determining the vibrational energies are discussed. Theoretical predictions are validated by photoacoustic coefficients measurements and photoacoustic tomography. The photoacoustic coefficients and tomographic intensities decreased in the order Por-C_{12}-RA_1>Por-C_{12}-RA_2>Por-C_{12}-RA_3>Por-C_8-RA_4, as predicted by DFT. Large photoacoustic coefficients are observed for the Por-C_{12}-RA_1, which is superior to that of the existing small molecules. Besides offering a superior molecule for photoacoustic tomography, the present criterion adopted here would enable to design simpler molecules with superior photoacoustic and other nonlinear optical properties.

Table of Contents

Experimental Methods

I. Computational Calculations

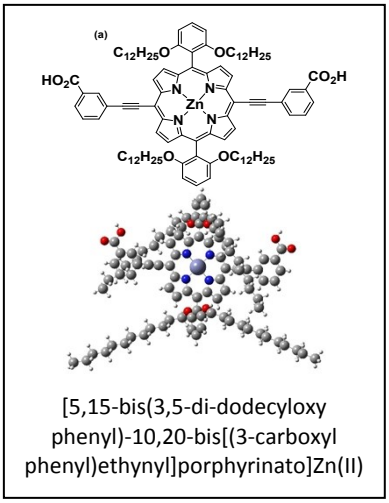

[5,15-bis(3,5-di-dodecyloxy phenyl)-10,20-bis[(3-carboxyl phenyl)ethynyl]porphyrinato]Zn(II)

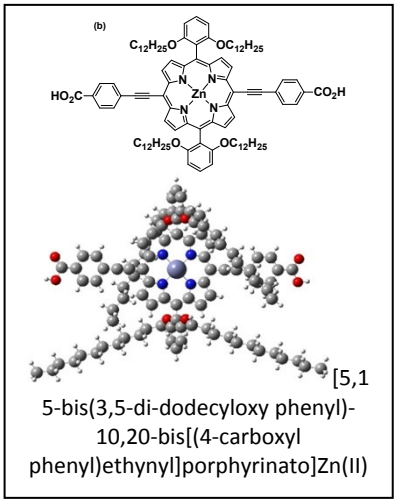

[5,15-bis(3,5-di-dodecyloxy phenyl)-10,20-bis[(4-carboxyl phenyl)ethynyl]porphyrinato]Zn(II)

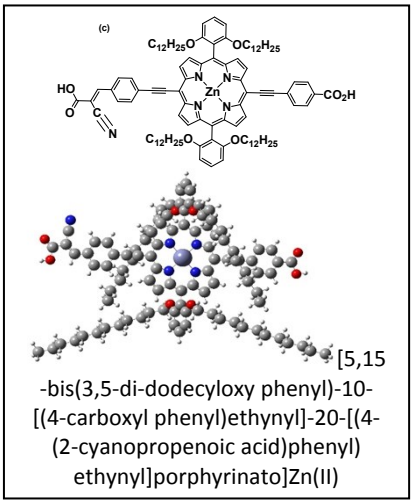

[5,15-bis(3,5-di-dodecyloxy phenyl)-10-[(4-carboxyl phenyl)ethynyl]-20-[(4-(2-cyanopropenoic acid)phenyl) ethynyl]porphyrinato]Zn(II)

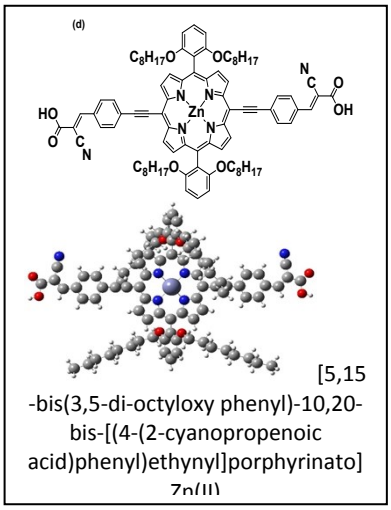

[5,15-bis(3,5-di-octyloxy phenyl)-10,20-bis-[(4-(2-cyanopropenoic acid)phenyl)ethynyl]porphyrinato] Zn(II)

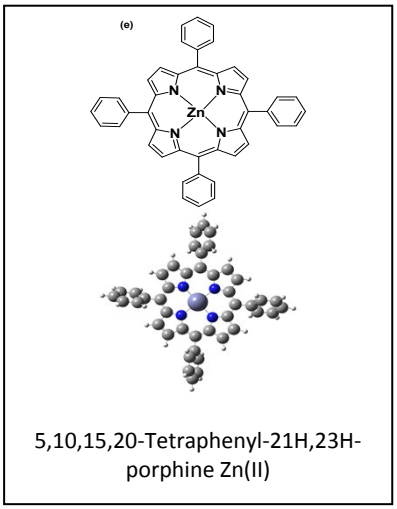

5,10,15,20-Tetraphenyl-21H,23H-porphine Zn(II)

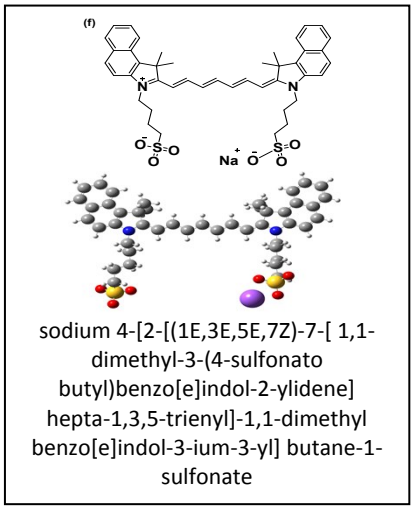

sodium 4-[2-[(1E,3E,5E,7Z)-7-[1,1-dimethyl-3-(4-sulfonato butyl)benzo[e]indol-2-ylidene] hepta-1,3,5-trienyl]-1,1-dimethyl benzo[e]indol-3-ium-3-yl] butane-1-sulfonate

Figure S1a. Structures and IUPAC naming of porphyrin molecules. The left panel shows planer ChemDraw sketch and right panel are the computed geometry developed using Gauss View. (a) Por-C_{12}-RA_1; (b) Por-C_{12}-RA_2; (c) Por-C_{12}-RA_3; (d) Por-C_8-RA_4; (e) ZnTPP and (f) ICG

Full geometry optimizations of the Por-C_n-RA_m series complexes in their singlet ground state were calculated using the Gaussian 09W program package[1] at the Universiti Malaysia Pahang, Malaysia with the computer facilities supported by King Abdullah University of Science and Technology (KUAST), Kingdom of Saudi Arabia. Geometry optimizations were performed with the use of the following levels of DFT: B3LYP[2]/ lanl2dz,[3, 4] B3LYP/6-31G*,[5, 6] M06[7]/lanl2dz, M06/6-31G*, CAM-B3LYP[8]/lanl2dz and CAM-B3LYP/6-31G*. However, calculations using the Becke's three-parameter hybrid method with the Lee, Yang, and Parr gradient corrected correlation functional (B3LYP)[2] with the effective core potential employing basis set 6-31G*[5] gave the best match with experimental results; therefore, results from these calculations are discussed here. Upon completion of geometry optimization, it is vital to examine whether or not the optimized geometry is with a global minimum energy structure. This is because the iterative minimization technique can lead to a "false" minimum energy point (synonymously "local" minimum) where the optimization program accidently falls into the convergence criteria – that the forces on the atoms are at a certain minimum value such that its first derivative is zero. Computational chemistry routinely employs harmonic frequency calculations to determine whether or not the optimized geometry is at a global minimum energy structure – the frequencies are real (positive) for a global minimum energy; and observe imaginary frequencies (negative) in the case of fall minimum. Therefore, the acceptability of the geometry of all studied porphyrin molecules were verified by determining vibrational frequencies by calculating their IR spectra at the same levels of the theory. All the studied compounds were optimized in the presence of implicit solvent effects. These condensed-phase effects were considered using a self-consistent reaction-field (SCRF)[9, 10] model. Within the different approaches that can be followed to calculate the electrostatic potential created by the polarized continuum in the cavity, we have employed the integral equation formalism of the polarizable continuum model (IEF-PCM),[11] in which the solvent used as a polarizable continuum rather than an individual molecule. All the calculations were performed in methanol to be consistent with experimental measurements. The molecular orbitals were mapped from the corresponding checkpoint files. Molecular representation of Por-C_n-RA_m porphyrins and their energy orbitals were obtained with the Gaussview.[12] Molecular structures alone with their IUPAC naming as well as optimized geometries of Por-C_n-RA_m porphyrins are shown in Figure S1a.

a. Calculated Vibrational Spectra

The primary purpose for vibrational energy calculations was to study the effect of various vibrational modes on photoacoustic properties of porphyrin molecules by substituting the meso-position of porphyrins with various π–conjugated functional groups. All the vibrational frequencies (IR spectra) were calculated from the optimized geometries at the same levels of the theory used for geometry optimization. As per consideration, the high frequency vibrational modes could be the source of non-radiative decays through thermalization by absorption of high energy quanta (photons) causing the excitation of electrons from υ=0 to υ=n vibrational energy levels (where n= 2,3,4……). Representative IR spectra and source of the vibrations are shown in Figure S1b.

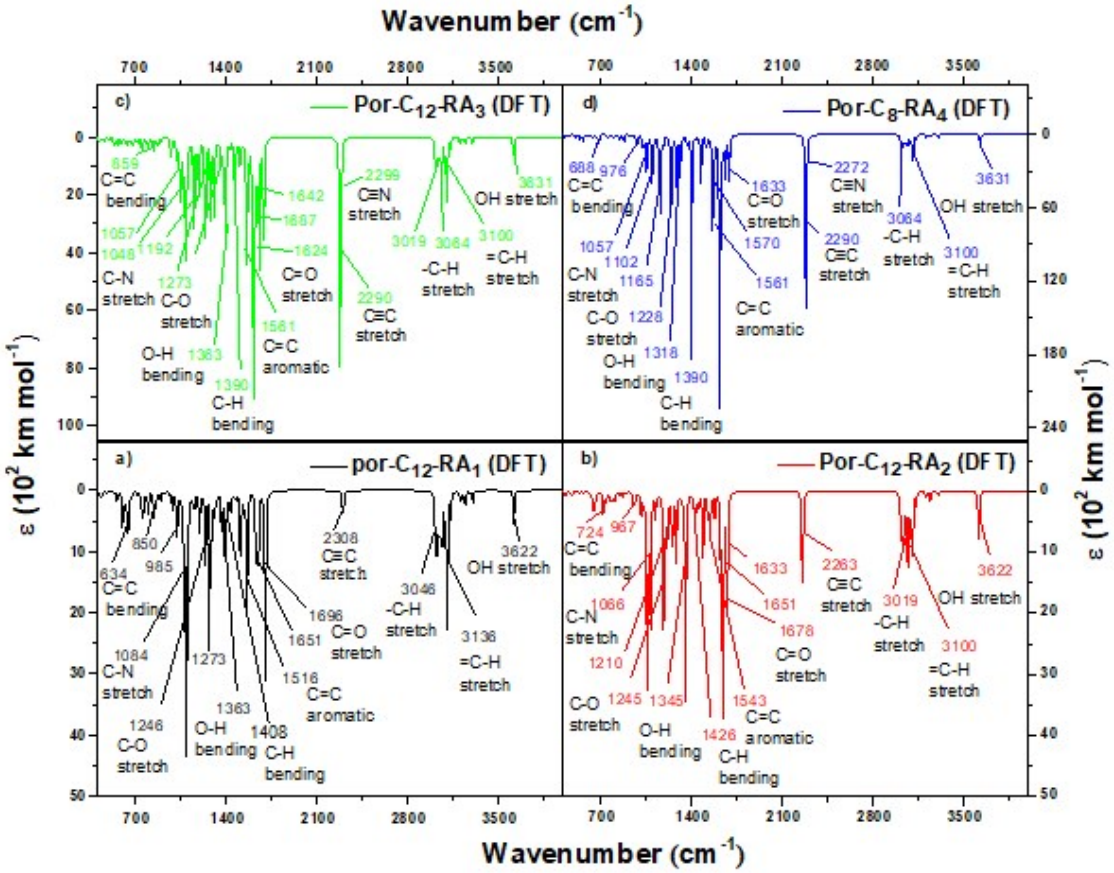

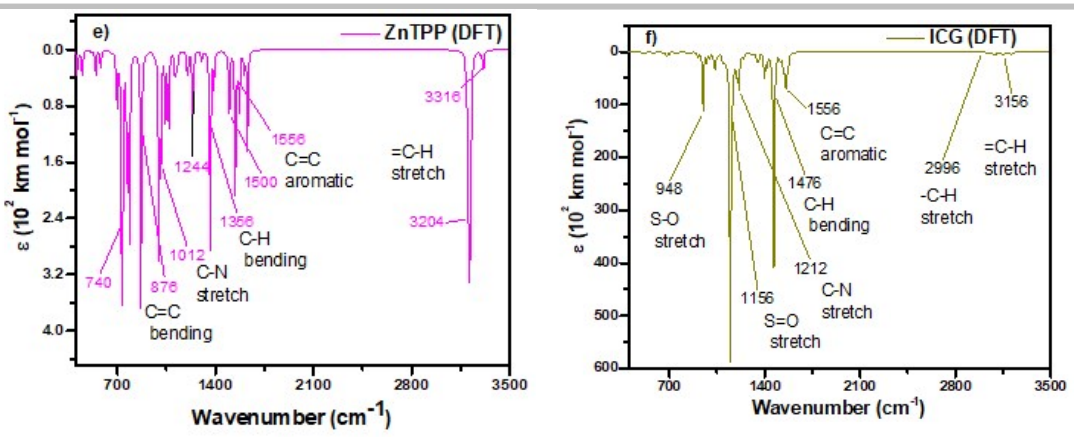

Figure S1b. Calculated FTIR spectra of (a) Por-C_{12}-RA_1; (b) Por-C_{12}-RA_2; (c) Por-C_{12}-RA_3; (d) Por-C_8-RA_4; (e) ZnTPP and (f) ICG

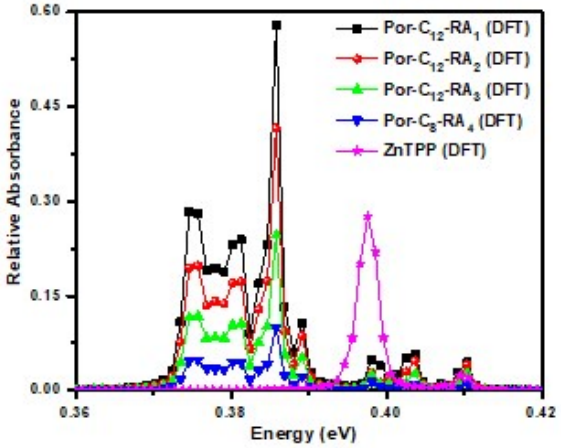

Figure S1c. Vibrational modes for Por-C_{12}-RA_1, Por-C_{12}-RA_2, Por-C_{12}-AY_3, Por-C_8-RA_4 and ZnTPP.

As noted from calculated vibrational energy spectra, there are 699, 699, 714 and 585 modes of vibrations in compounds **Por-C_{12}-RA_1**, **Por-C_{12}-RA_2**, **Por-C_{12}-RA_3** and **Por-C_8-RA_4** respectively, and the vibrational spectra of all molecules are similar (Figure S1b). However, some obvious differences could be very informative in the high-frequency region of C-H bands providing evidence for non-radiative decay. In the calculated IR spectrum of **Por-C_{12}-RA_1**, out of 699 transitions, there are 122 stretching vibration modes which belong to C–H groups in the region 0.411–0.373 eV. The highest frequencies at ~0.411–0.407 eV correspond to C_β–H stretching vibrations of the pyrrole rings. The calculated C–H stretching vibrations in benzene rings substituted with porphyrin core either directly or through ethynyl groups are observed in the region of ~0.403–0.398 eV. The absorption coefficients of the C_β–H vibrations are higher than that of C–H stretching in benzene rings. The C–H stretching vibration modes of the long alkoxy groups are observed in the interval ~0.389–0.373 eV. As it is clearly observable, the absorption coefficients of the C–H stretching vibration modes for long alkoxy chain are of much higher intensity than that of C–H stretching in benzene rings and C_β–H vibrations of pyrrole rings. Similar trends are observed in the calculated vibrational energy spectra of **Por-C_{12}-RA_2**, **Por-C_{12}-RA_3** and **Por-C_8-RA_4**. However, the intensity of C–H stretching vibrations of **Por-C_n-RA_m** series complexes increase in the order of **Por-C_{12}-RA_1** > **Por-C_{12}-RA_2**> **Por-C_{12}-RA_3**> **Por-C_8-RA_4** (Figure S1c).

b. Calculated Optical Properties

The absorption spectra of the **Por-C_n-RA_m** porphyrins were developed from the energy calculation carried out at linear response time-dependent DFT (LR-TD-DFT)[13, 14] theory. This method calculates the discrete singlet excitation energies (oscillation strengths) from the optimized geometries from where continuous absorption spectra of the molecules could be developed. All the energy calculations were done from ground state to singlet state excitation using IEF-PCM[11] model to study the effect of methanol as a solvent on absorption spectra because the experimental absorption spectra of all the **Por-C_n-RA_m** porphyrins were measured in methanol. At each singlet geometry, LR-TD-DFT/IEF-PCM calculations were performed for the first 50 excited singlet states by using the B3LYP functional with 6-31G*[4] and LANL2DZ[3, 4] basis sets. However, the excitation energies obtained from B3LYP/6-31G* agreed well with experimental data compared to that of B3LYP/lanl2dz for example; the first transition of **Por-C_{12}-RA_2** measured experimentally is at 661 nm and is calculated at 647 nm (1.916 eV) by 6-31G*. Based on same computational protocol, the lanl2dz basic set gives this first transition at 631 nm (1.964 ev). Singlet transitions and their oscillation strength of the four molecules, ZnTPP and ICG are in the Figure S1d.

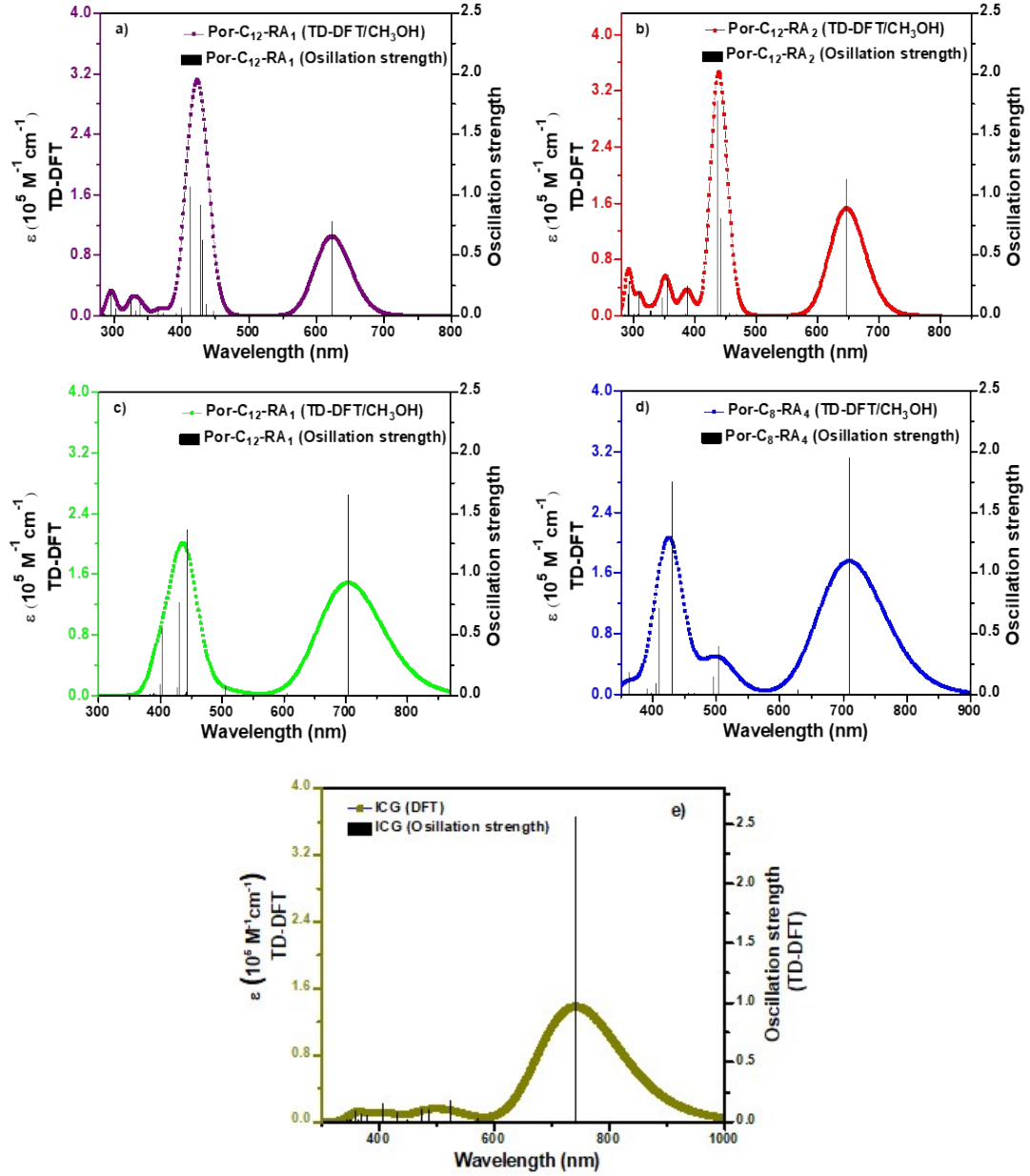

Figure S1d. Calculated absorption spectra of (a) Por-C_{12}-RA_1; (b) Por-C_{12}-RA_2; (c) Por-C_{12}-RA_3; (d) Por-C_8-AR_4 and (e) ICG

II. Synthetic Materials

a. General Methods

All the reactions were carried out under N_2 atmosphere by using Schlenk-tube apparatus. All glasswares were oven-dried at about 100 °C prior to use. All solvents and chemicals were used in reagent grade and purchased from commercial sources and used without further purification, unless otherwise stated. All solvents were dried and double distilled from appropriate drying agents. Pyrrole was freshly distilled before use. Tetra-butylammonium fluoride (TBAF) was recrystallized twice from absolute ethanol and further dried for two days under vacuum. Thin-Layer Chromatograph (TLC) was performed with Merck pre-coated TLC silica gel 60 F_{254} aluminium sheets, visualizing with UV light where required. Flash column chromatography and preparative TLC were performed using Silica gel 60 from Merck (0.02-0.06 mm).

b. Instrumentation

^{1}H and ^{13}C-NMR spectra were recorded on a Bruker ultra-shield plus 500 (500MHz) using tetramethylsilane (TMS) as an internal standard. The coupling constant are calculated in Hz and chemical shifts (δ) in ppm. Multiplicities of peaks are denoted as: s= singlet, d= doublet, dd= double doublet, t= triplet and m= multiplet. The absorption spectra in solution were obtained by UV-vis-NIR spectrophotometer UV-2600 SHIMADZU, Japan. All the spectra were measured by preparing fresh samples. The steady state fluorescence and the corresponding excitation spectra were recorded on an Edinburgh Instruments FLS920 phosphorimeter equipped with single monochromators.

Fluorescence lifetime measurements were made a mode-locked Ti:sapphire laser (Coherent Mira 900) having a laser power output of 1.90 W at 800 nm. Thermogravimetric analysis (TGA) measurements were performed on Mettler Toledo thermogravimetric analyzer, model Perkin-Elmer TGA/DSC 1, at 10 °C min^{-1} heating rate. FTIR data were measured on a PerkinElmer Spectrum using thin films KBr method. The photoacoustic measurements were conducted using the Nd:YAG laser (3 ns pulse width) at 532 nm and using OPO laser (3 ns pulse width) at 680 nm. For all the experiments performed at 532 nm, the **Por-C_n-RA_m** porphyrins were compared to ZnTPP as a reference. The PAZ-Scan experiments were conducted at 100 µJ laser energy and at 130 µJ laser energy on all the samples prepared in DMF absorbing 0.1 OD at 532 nm and at 680 nm in 2 mm quartz cuvettes. PAT experiments were carried out by using a doubled Nd:YAG laser, a transducer (Olympus V311-SU) and a pulse amplifier that is fed to a Lecroy WavePro oscilloscope for display and data collection.

c. Procedure for the synthesis of Starting Materials

*Synthesis of Cyano-3-(4-iodophenyl)acrylic Acid (**3**)*

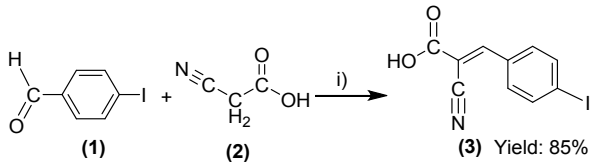

Scheme S1. i) CH_3COOH, NH_4Ac reflux, overnight

To a solution of ammonium acetate (22 mg, 0.28 mmol) in acetic acid (3 ml), 4-Iodobenzaldehyde (200 mg, 0.86 mmol) and cyanoacetic acid (88 mg, 1.04 mmol) were added and the solution was refluxed overnight. The reaction mixture was allowed to cool at room temperature; the product was crystallized as off-white precipitate from the solution. The precipitate was washed with distilled water and then recrystallized from hexane and dichloromethane (DCM) (1:1) to yield the compound **3** as off-white solid (219.1 mg, 85% yield).

^{1}H NMR (CD_3OH, 500 MHz): δ 8.25 (s, 1H), 7.93 (d, *J* = 8.55 Hz, 2H), 7.76 (d, *J* = 8.55 Hz, 2H). ^{13}C NMR (CD_3OH, 125 MHz): δ 164.66, 154.69, 139.76, 138.97, 133.08, 132.57, 132.26, 116.56, 105.66, 101.19.

*Synthesis of 1,3-Dialkoxybenzene (**5a-5b**)*

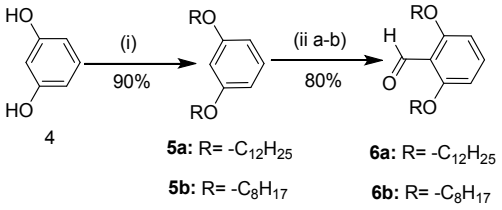

Scheme S2. (i) $C_{12}H_{25}Br$, K_2CO_3, $(CH_3)_2CO$, reflux, 2 days; (ii) a) TMEDA, $(C_2H_5)_2O$, N_2, 0 °C, 3hr; b) n-BuLi, $(C_2H_5)_2O$, DMF, N_2, 2 hr.

Compound **5a** and **5b** were synthesized by modified method of literature procedure.[15] In a mixture of resorcinol (5 g, 0.045 mol) and K_2CO_3 (31.10 g, 0.22 mol), 1-bromoalkane (0.18 mol) was added and the reaction mixture was refluxed for 3 days in dry acetone (500 mL). The reaction progress was monitored by TLC analysis. When all reactants were consumed, the solvent was removed under reduced pressure. The residue was extracted with EtOAc (3 × 100 mL), washed with water and dried over anhydrous $MgSO_4$. The solvent was removed under reduced pressure and the product was purified by column chromatography eluting with *n*-hexane to afford 1,3-di(alkoxy)benzene **5a** and **5b** with 90% and 90% yield respectively.

5a: ^{1}H NMR ($CDCl_3$, 500 MHz): δ 7.15 (t, *J* = 8.15 Hz, 1H), 6.48 (d, *J* = 2.35 Hz, 1H), 6.46 (m, 2H), 3.92 (t, *J* = 6.65 Hz, 4H), 1.78-1.72 (m, 4H), 1.43-1.42 (m, 4H), 1.33-1.26 (m, 32H), 0.89 (t, *J* = 7.1 Hz, 6H). ^{13}C NMR ($CDCl_3$, 125 MHz): δ 160.39, 129.72, 106.62, 101.44, 67.96, 31.97, 29.71, 29.68, 29.65, 29.63, 29.44, 29.40, 29.32, 26.10, 22.73, 14.15.

5b: ^{1}H NMR ($CDCl_3$, 500 MHz): δ 7.15 (t, *J* = 8.3 Hz, 1H), 6.48 (d, *J* = 2.35 Hz, 1H), 6.46 (m, 2H), 3.93 (t, *J* = 6.5 Hz, 4H), 1.78-1.73 (m, 4H), 1.46-1.40 (m, 4H), 1.35-1.26 (m, 16H), 0.89 (t, *J* = 6.95 Hz, 6H). ^{13}C NMR ($CDCl_3$, 125 MHz): δ 160.40, 129.73, 106.63, 101.44, 67.97, 31.86, 29.41, 29.32, 29.29, 26.10, 22.70, 14.12.

*Synthesis of 2,6-Dialkoxybenzenaldehyde (**6a-6b**)*

Compound **6a** and **6b** were synthesized by modified method according to the literature procedure.[16] A solution of compound **5a**/**5b** (11.21 mmol) and tetramethylethylenediamine (TMEDA) (2.24 mmol) in 100 mL of anhydrous ether was degassed with N_2 for 25 min using Schlenk-tube apparatus and cooled to 0 °C. A solution of *n*-butyllithium (2 M solution in hexanes, 16.80 mmol) was then added drop-wise over 2 hr and allowed the mixture to stir for additional 2 hr at 0 °C. The reaction mixture was warmed to room temperature and stirred for 30 min and then anhydrous dimethylformamide (DMF) (22.40 mmol) was added dropwise. The reaction mixture was again stirred for

an additional 2 hr and it was quenched with water, extracted with ether (3 × 80 mL), and dried over anhydrous $MgSO_4$. The solvent was removed under reduced pressure. The product was recrystallized from *n*-hexane to yield a white solid **6a** and **6b** with both 80% yield.

6a: ^{1}H NMR ($CDCl_3$, 500 MHz): δ 10.53 (s, 1H), 7.38 (t, *J* = 8.45 Hz, 1H), 6.53 (d, *J* = 8.55 Hz 2H), 4.03 (t, *J* = 6.5 Hz, 4H), 1.84-1.79 (m, 4H), 1.49-1.43 (m, 4H), 1.34-1.26 (m, 32H), 0.89 (t, *J* = 7.1 Hz, 6H). ^{13}C NMR ($CDCl_3$, 125 MHz): δ 189.51, 161.85, 135.69, 114.93, 104.67, 69.11, 32.10, 29.84, 29.81, 29.78, 29.74, 29.53, 29.23, 26.16, 22.87, 14.30.

6b: ^{1}H NMR ($CDCl_3$, 500 MHz): δ 10.26 (s, 1H), 7.10 (t, *J* = 8.4 Hz, 1H), 6.25 (d, *J* = 8.4 Hz 2H), 3.74 (t, *J* = 6.5 Hz, 4H), 1.56-1.50 (m, 4H), 1.21-1.15 (m, 4H), 1.07-1.03 (m, 16H), 0.63 (t, *J* = 6.95 Hz, 6H). ^{13}C NMR ($CDCl_3$, 125 MHz): δ 189.10, 161.61, 135.52, 114.68, 104.45, 68.85, 31.79, 29.29, 29.24, 29.20, 29.16, 29.04, 25.97, 22.63, 14.05.

*Synthesis of 2,6-Dioctoxybenzenaldehyde (**9**)*

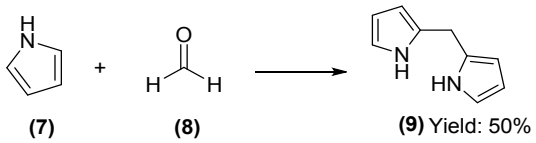

(7) **(8)** **(9)** Yield: 50%

Scheme S3. (a) TFA, N_2, 70 °C, 2 hr; (b) 0.4 M NaOH, stirring, 30 min

Method 1: Compound **9** was synthesized by previously reported procedure with modification.[17] To the freshly distilled pyrrole (104.50 mL, 1.5 mol) in 500 mL flask shielded from light, was added paraformaldehyde (1.80 g, 0.06 mol by formaldehyde) and the solution was degassed for 15 min under N_2 atmosphere. The reaction mixture was heated at 70 °C and at this temperature, trifluoroacetic acid (TFA) (1.30 mL, 17.14 mmol) was added in one portion. The reaction mixture was stirred for 2 hr until it became clear and dark. After cooling at room temperature, the mixture was quenched by addition of 10% NaOH (40 mL) solution and was stirred for additional 30 min. The reaction mixture was then extracted with DCM (3 × 30 mL). The combined organic layer was washed with water twice and dried over anhydrous $MgSO_4$. The solvent was removed under reduced pressure. Excess of pyrrole was distilled off by vacuum distillation. The remaining crude product was purified by silica gel column chromatography with DCM: hexane (2:1) as eluent to afford the off-white product **9** with 50% (4.38 g) yield.

^{1}H NMR ($CDCl_3$, 500 MHz): δ 7.69 (s, 2H), 6.59 (q, 2.7 Hz, 2H), 6.14 (q, 2.75 Hz, 2H), 6.02 (br s, 2H), 3.91 (s, 2H). ^{13}C NMR ($CDCl_3$, 125 MHz): δ 129.14, 117.37, 108.33, 106.47, 26.36.

Method 2: Trifluoroacetic acid (1.30 mL, 0.017 mol) was added in a mixture of freshly distilled pyrrole (20.80 mL, 0.3 mol) and paraformaldehyde (1.74 g, 0.06 mol) in dry methanol (100 mL). The reaction mixture was stirred for 5 hr at 70 °C under N_2 environment. After cooling at room temperature, the mixture was quenched by addition of 10% NaOH (40 mL) solution and was stirred for additional 30 min. The reaction mixture was then extracted with DCM (3 × 30 mL). The combined organic layers were washed with water twice times and dried over anhydrous $MgSO_4$. The solvent was removed under reduced pressure. The crude product was purified by silica gel column chromatography with DCM: hexane (2:1) as eluent to afford **9** as an off-white color solid with 28.5% (2.5 g) yield.

^{1}H NMR ($CDCl_3$, 500 MHz): δ 7.69 (s, 2H), 6.59 (q, 2.7 Hz, 2H), 6.14 (q, 2.75 Hz, 2H), 6.02 (br s, 2H), 3.91 (s, 2H). ^{13}C NMR ($CDCl_3$, 125 MHz): δ 129.14, 117.37, 108.33, 106.47, 26.36.

d. Procedure for the synthesis of Por-C_n-RA_m Porphyrins

*Synthesis of 5,15-bis(2,6-di(alkoxy)phenyl)porphyrin (**10a-10b**)*

A solution of compound **9** (34.24 mmol) and compound **6a/6b** (34.24 mmol) in anhydrous DCM (1 L) was degassed with N_2 for 15 min and trifluoroacetic acid (31.13 mmol) was added into the solution. The reaction mixture was stirred under N_2 for 4 hr and DDQ (51.36 mmol) was added to the reaction mixture and stirring was continued for additional 1 hr. The reaction mixture was then basified with NEt_3 (7 mL) and filtered on a glass filter by adding short silica gel bed and washed with DCM. The solvent was removed under reduced pressure. The remaining crude product was purified by column chromatography (silica gel) using DCM: hexanes (1:2) as an eluent. The product was recrystallized from MeOH/DCM to give the purple color product **10a** and **10b** with 35% and 30% yield respectively.

10a: ^{1}HNMR ($CDCl_3$, 500 MHz): δ 10.13 (s, 2H), 9.25 (d, *J* = 4.5 Hz, 4H), 8.97 (d, *J* = 4.55 Hz, 4H), 7.71 (t, *J* = 8.45 Hz, 2H), 7.02 (d, *J* = 8.5 Hz, 4H), 3.83 (t, *J* = 6.6 Hz, 8H), 1.27-1.21 (m, 8H), 1.17-1.09 (m, 16H), 1.01-0.98 (m, 8H), 0.92-0.83 (m, 28H), 0.72-0.69 (m, 8H), 0.56-0.53 (m, 16H), 0.45-0.42 (m, 8H), -3.02(s, 2H). ^{13}CNMR ($CDCl_3$, 125 MHz): δ 160.12, 157.69, 130.77, 130.40, 129.96, 119.95, 111.50, 105.28, 103.89, 68.66, 31.90, 29.49, 29.42, 29.30, 29.19, 29.05, 28.68, 28.58, 25.27, 22.69, 14.13.

10b: ^{1}HNMR ($CDCl_3$, 500 MHz): δ 10.13 (s, 2H), 9.25 (d, *J* = 4.4 Hz, 4H), 8.97 (d, *J* = 4.6 Hz, 4H), 7.71 (t, *J* = 8.5 Hz, 2H), 7.01 (d, *J* = 8.55 Hz, 4H), 3.83 (t, *J* = 6.4 Hz, 8H), 0.93-0.88 (m, 8H), 0.85-0.79 (m, 8H), 0.66-0.60 (m, 8H), 0.57-0.51 (m, 28H), 0.45-0.40 (m, 8H), -3.01 (s, 2H). ^{13}CNMR ($CDCl_3$, 125 MHz): δ 160.15, 130.79, 130.40, 129.99, 119.99, 111.51, 105.31, 103.91, 68.70, 31.31, 28.66, 28.62, 28.60, 25.30, 22.31, 13.85.

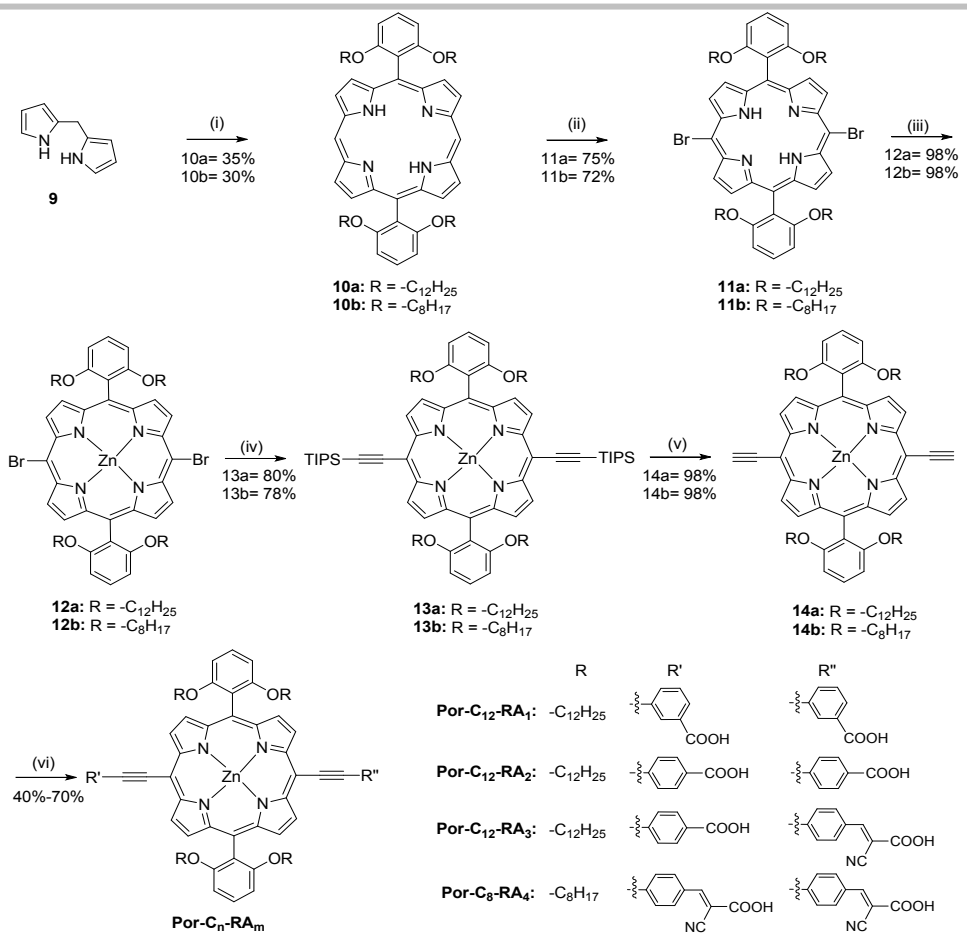

Scheme S4. Reagents: (i) a) 6, TFA, DCM, N_2, 23 °C, 4 hr; b) DDQ, 1 hr; (ii) NBS, DCM, N_2, 6 hr; (iii) $Zn(OAc)_2.2H_2O$, DCM, CH_3OH, 23 °C, 24 hr; (iv) TIPS-acetylene, THF, CuI, $Pd(PPh_3)_2Cl_2$, NEt_3, N_2, 85 °C, 8hr; (v) TBAF, THF, N_2, 6hr; (vi) various substituted phenyl iodide, THF, NEt_3, $Pd_2(dba)_3$, $AsPh_3$, N_2, 85 °C, 5hr.

*Synthesis of 5,15-bisbromo-10,20-bis(2,6-di(alkoxy)phenyl)porphyrin (**11a-11b**)*

A solution of *N*-bromo succinimide (NBS) (8.35 mmol) in anhydrous DCM (200 mL) was slowly added to a stirred solution of compound **10a**/**10b** (4.17 mmol) in anhydrous DCM (1000 mL) for 4 hr at 0°C under N_2 atmosphere. The reaction mixture was further stirred for 2 hr more at room temperature. The reaction mixture was quenched with acetone (30 mL) and the solvent was removed under reduced pressure. The crude product was purified by column chromatography (silica gel) using DCM: hexane = 0.5:2 as an eluent. Recrystallization in MeOH/DCM gave the final product **11a** and **11b** as a purple solid with 75% and 72% yield respectively.

11a: ^{1}HNMR ($CDCl_3$, 500 MHz): δ 9.50 (d, *J* = 4.75 Hz, 4H), 8.78 (d, *J* = 4.9 Hz, 4H), 7.69 (t, *J* = 8.55 Hz, 2H), 6.98 (d, *J* = 8.5 Hz, 4H), 3.84 (t, *J* = 6.5 Hz, 8H), 1.23-1.19 (m, 8H), 1.14-1.05 (m, 16H), 0.97-0.91 (m, 12H), 0.86-0.80 (m, 24H), 0.67-0.64 (m, 8H), 0.54-0.48 (m, 16H), 0.42-0.39 (m, 8H), -2.59(s, 2H). ^{13}CNMR ($CDCl_3$, 125 MHz): δ 159.94, 153.07, 139.33, 137.79, 130.24, 123.60, 119.90, 105.03, 102.24, 68.60, 31.87, 29.72, 29.46, 29.37, 29.29, 29.20, 29.04, 28.70, 28.57, 25.31, 22.69, 14.14.

11b: ^{1}HNMR ($CDCl_3$, 500 MHz): δ 9.50 (d, *J* = 4.9 Hz, 4H), 8.78 (br s, 4H), 7.70 (t, *J* = 8.55 Hz, 2H), 6.98 (d, *J* = 8.5 Hz, 4H), 3.84 (t, *J* = 6.4 Hz, 8H), 0.97-0.91 (m, 8H), 0.85-0.78 (m, 8H), 0.64-0.58 (m, 8H), 0.55-0.47 (m, 28H), 0.43-0.37 (m, 8H), -2.59 (s, 2H). ^{13}CNMR ($CDCl_3$, 125 MHz): δ 159.95, 130.26, 119.93, 114.16, 109.88, 105.05, 102.26, 68.63, 31.33, 28.66, 28.64, 28.58, 25.33, 22.27, 13.84.

*Synthesis of [5,15-bisbromo-10,20-bis(2,6-di(alkoxy)phenyl)porphyrinato]zinc(II) (**12a-12b**)*

A solution of compound **11a/11b** (2.95 mmol) and $Zn(OAc)_2 \bullet 2H_2O$ (17.70 mmol) in anhydrous DCM (400 mL) and MeOH (200 mL) was stirred at room temperature for 24 hr. The reaction mixture was quenched with water (100 mL) and was extracted with DCM (2 × 100 mL). The combined organic layers were washed with water and dried over anhydrous $MgSO_4$. The solvent was removed under reduce pressure. The crude product was purified by column chromatography (silica gel) using DCM: hexane = 1:2 as an eluent. Recrystallization by MeOH/DCM gave the final product **12a** and **12b** as a purple solid, both with 98% yield.

12a: ^{1}HNMR ($CDCl_3$, 500 MHz): δ 9.62 (d, *J* = 4.65 Hz, 4H), 8.88 (d, *J* = 4.65 Hz, 4H), 7.69 (t, *J* = 8.55 Hz, 2H), 6.99 (d, *J* = 8.7 Hz, 4H), 3.84 (t, *J* = 6.5 Hz, 8H), 1.22-1.19 (m, 8H), 1.13-1.04 (m, 10H), 0.95-0.90 (m, 20H), 0.84-0.78 (m, 22H), 0.62-0.59 (m, 8H), 0.51-0.42 (m, 16H), 0.35-

0.32 (m, 8H). ^{13}CNMR ($CDCl_3$, 125 MHz): δ 159.90, 151.36, 149.67, 132.79, 132.76, 129.99, 120.67, 114.89, 105.15, 103.91, 68.58, 31.87, 29.45, 29.34, 29.28, 29.20, 29.04, 28.67, 28.57, 25.23, 22.69, 14.14.

12b: ^{1}HNMR ($CDCl_3$, 500 MHz): δ 9.62 (d, *J* = 4.6 Hz, 4H), 8.88 (d, *J* = 4.6 Hz, 4H), 7.71 (t, *J* = 8.55 Hz, 2H), 7.00 (d, *J* = 8.55 Hz, 4H), 3.84 (t, *J* = 6.4 Hz, 8H), 0.97-0.91 (m, 8H), 0.83-0.76 (m, 8H), 0.61-0.55 (m, 8H), 0.52-0.43 (m, 28H), 0.37-0.31 (m, 8H). ^{13}CNMR ($CDCl_3$, 125 MHz): δ 159.89, 151.34, 149.67, 132.77, 132.72, 129.99, 120.70, 114.80, 105.17, 103.90, 68.60, 31.33, 28.66, 28.61, 28.56, 25.23, 22.26, 13.82.

*Synthesis of [5,15-bis(2,6-di(alkoxy)phenyl)-10,20-bis(triisopropylsilyl)ethynyl)porphyrinato]zinc(II) (**13a-13b**)*

To a degassed solution of compound **12a/12b** (1.06 mmol), (triisopropylsilyl)acetylene (2.65 mmol) and CuI (0.30 mmol) in anhydrous THF (20 mL) was added NEt_3 (9 mL) under N_2 atmosphere. $Pd(PPh_3)_2Cl_2$ (0.21 mmol) was added to the solution and the reaction mixture was stirred at 85 °C for 8 hr. The reaction mixture was cooled at room temperature and the solvent was removed under reduced pressure. The crude product was purified by column chromatography (silica gel) using DCM: hexane (1:2) as an eluent to give the product **13a** and **13b** as a purple solid with 80% and 78% yield respectively.

13a: ^{1}HNMR ($CDCl_3$, 500 MHz): δ 9.66 (d, *J* = 4.55 Hz, 4H), 8.86 (d, *J* = 4.45 Hz, 4H), 7.67 (t, *J* = 8.55 Hz, 2H), 6.98 (d, *J* = 8.5 Hz, 4H), 3.82 (t, *J* = 6.4 Hz, 8H), 1.46-1.39 (m, 42H), 1.18-1.13 (m, 8H), 1.08-0.97 (m, 16H), 0.95-0.90 (m, 10H), 0.88-0.82 (m, 8H), 0.81-0.70 (m, 26H), 0.57-0.46 (m, 16H), 0.41-0.34 (m, 8H). ^{13}CNMR ($CDCl_3$, 125 MHz): δ 159.93, 152.06, 150.68, 131.94, 130.90, 129.82, 120.94, 115.25, 109.85, 105.34, 100.49, 96.82, 68.76, 31.86, 29.46, 29.26, 29.25, 29.16, 28.96, 28.63, 28.59, 25.21, 22.68, 19.14, 14.13, 11.95.

13b: ^{1}HNMR ($CDCl_3$, 500 MHz): δ 9.58 (d, *J* = 4.5 Hz, 4H), 8.78 (d, *J* = 4.5 Hz, 4H), 7.60 (t, *J* = 8.4 Hz, 2H), 6.91 (d, *J* = 8.55 Hz, 4H), 3.73 (t, *J* = 6.5 Hz, 8H), 1.39-1.33 (m, 42H), 1.02-0.84 (m, 26H), 0.83-0.65 (m, 22H), 0.53-0.41 (m, 12H). ^{13}CNMR ($CDCl_3$, 125 MHz): δ 159.91, 152.05, 150.64, 131.86, 130.85, 129.80, 121.03, 115.11, 109.93, 105.40, 100.42, 96.75, 68.78, 31.24, 29.73, 28.56, 28.54, 28.53, 25.19, 22.16, 19.10, 13.78, 11.94.

*Synthesis of [5,15-bis(2,6-di(alkoxy)phenyl)-10,20bis(ethynyl)porphyrinato]zinc(II) (**14a-14b**)*

To a degassed solution of compound **13a/13b** (0.12 mmol) in anhydrous THF (30 mL) was added TBAF (1M in THF, 1.23 mmol). The solution was stirred at room temperature for 2 hr and was quenched with H_2O. The mixture was then extracted with DCM (3 × 30 mL) and combined organic layers were dried over anhydrous $MgSO_4$. The solvent was removed under reduced pressure to give compound **14a** and **14b** with 98% yield for both. The compound **14a** and **14b** were directly used for the synthesis of **Por-C_{12}-RA_2** and **Por-C_{12}-RA_3** without further purification.

*Synthesis of [5,15-bis(2,6-di(dodecyloxy)phenyl)-10,20-bis(3-carboxylphenyl)ethynyl)porphyrinato]zinc(II) (**Por-C_{12}-RA_1**)*

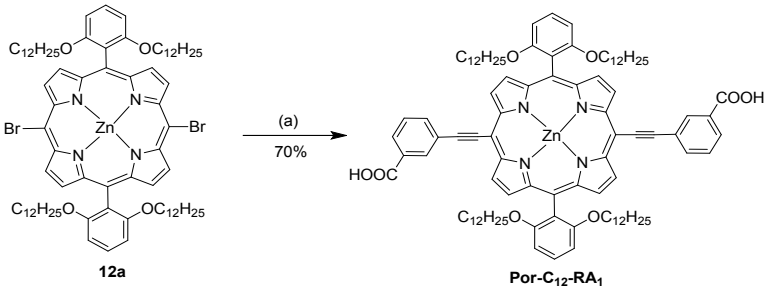

12a **Por-C_{12}-RA_1**

Scheme S5. a) 3-ethynyl benzoic acid, THF, CuI, $Pd(PPh_3)_2Cl_2$, NEt_3, N_2, 85 °C, 8hr.

To a degassed solution of compound **12a** (0.91 g, 0.81 mmol), 3-ethynyl benzoic acid (0.37 mL, 2.04 mmol) and CuI (0.047 g, 0.24 mmol) in anhydrous THF (30 mL) was added NEt_3 (5 mL) under N_2 atmosphere. $Pd(PPh_3)_2Cl_2$ (0.11 g, 0.16 mmol) was added to the solution and it was stirred at 85 °C for 8 hr. The reaction mixture was cooled at room temperature and the solvent was removed under vacuum. The crude product was purified by column chromatography (silica gel) using DCM: MeOH (1:7) as an eluent. Recrystallization from CH_3OH to give pure product **Por-C_{12}-RA_1** (88 mg, 70% yield) as a green solid.

^{1}HNMR (CD_3OH, 500 MHz): δ 9.42 (d, *J* = 4.3 Hz, 4H), 8.52 (d, *J* = 4.45 Hz, 4H), 8.44 (s, 2H), 7.85 (q, *J* = 7.6 Hz, 4H), 7.52 (t, *J* = 8.15 Hz, 2H), 7.35 (t, *J* = 7.5 Hz, 2H), 6.86 (d, *J* = 8.4 Hz, 4H), 3.79 (t, *J* = 6.0 Hz, 8H), 1.09-1.05 (m, 16H), 0.95-0.90 (m, 8H), 0.81-0.77 (m, 8H), 0.72-0.65 (m, 24H), 0.59-0.54 (m, 20H), 0.52-.048 (m, 8H), 0.37-0.34 (m, 8H). ^{13}CNMR (CD_3OH, 125 MHz): δ 173.49, 162.75, 159.95, 151.55, 150.56, 132.50, 131.24, 129.93, 124.22, 114.87, 112.64, 105.23, 103.17, 99.59, 95.16, 93.27, 68.42, 31.61, 29.35, 29.13, 29.04, 29.02, 28.83, 28.69, 28.56, 28.47, 25.18, 22.35, 13.12, 9.91

*Synthesis of [5,15-bis(2,6-di(dodecyloxy)phenyl)-10,20-bis(4-carboxylphenyl)ethynyl)porphyrinato]zinc(II) (**Por-C_{12}-RA_2**)*

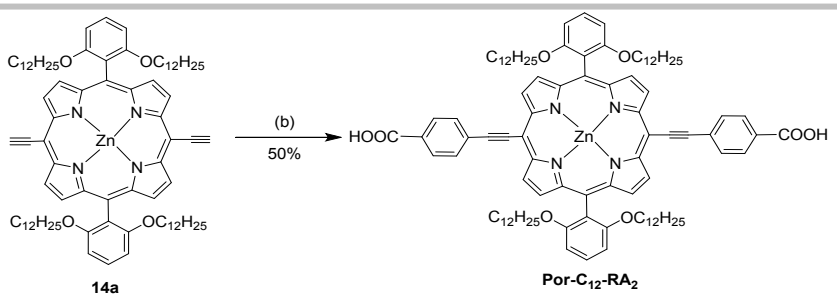

Scheme S6. b) 4-iodobenzoic acid, THF, NEt_3, $Pd_2(dba)_3$, $AsPh_3$, N_2, 85 °C, 6hr.

To a degassed solution of compound **14a** (100 mg, 0.076 mmol) and 4-iodobenzoic acid (56.54 mg, 0.23 mmol) in anhydrous THF (10 mL) was added NEt_3 (1 mL) under N_2 atmosphere. $Pd_2(dba)_3$ (17.39 mg, 0.019 mmol) and $AsPh_3$ (46.54 mg, 0.15 mmol) were added to the mixture and it was stirred at 85 °C for 6 hr. The reaction mixture was cooled at room temperature and the solvent was removed under vacuum. The crude product was purified by column chromatography (silica gel) using DCM: MeOH (1:5) as an eluent. The further purifications of the compound were carried out by pre-TLC and recrystallization from CH_3OH to give green color pure product **Por-C_{12}-RA_2** with 50% (59.16 mg) yield.

^{1}HNMR (CD_3OH, 500 MHz): δ 9.51 (d, *J* = 4.5 Hz, 4H), 8.63 (d, *J* = 4.5 Hz, 4H), 8.08 (d, *J* = 8.45 Hz, 4H), 7.90 (d, *J* = 8.45 Hz, 4H), 7.60 (t, *J* = 8.55 Hz, 2H), 6.94 (d, *J* = 8.6 Hz, 4H), 3.73 (t, *J* = 6.1 Hz, 8H), 1.10-1.04 (m, 8H), 1.02-0.94 (m, 8H), 0.92-0.79 (m, 12H), 0.74-0.63 (m, 48H), 0.52-.049 (m, 8H), 0.22-0.17 (m, 8H). ^{13}CNMR (CD_3OH, 125 MHz): δ 174.61, 159.90, 151.51, 150.60, 132.70, 131.03, 129.55, 129.31, 123.36, 115.02, 114.56, 105.16, 100.66, 97.66, 83.35, 68.35, 31.62, 29.38, 29.35, 29.15, 29.04, 28.85, 28.53, 28.45, 25.17, 22.37, 13.15.

*Synthesis of [5,15-bis(2,6-di(dodecyloxy)phenyl)-10-[(4-carboxylphenyl)ethynyl]-20-[(4-(2-cyanopropenoi cacid)phenyl)ethynyl]porphyrinato]zinc(II) (**Por-C_{12}-RA_3**)*

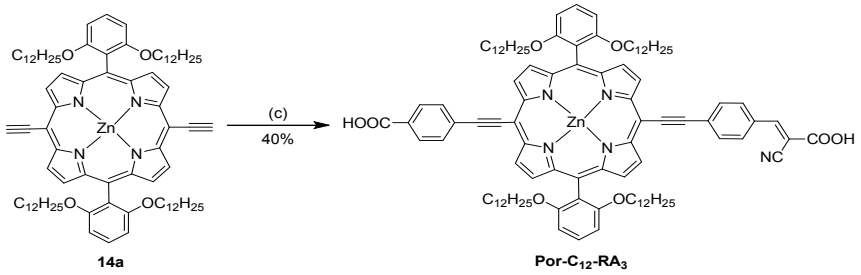

Scheme S7. c) 4-iodobenzoic acid, cyano-3-(4-iodophenyl)acrylic acid, THF, NEt_3, $Pd_2(dba)_3$, $AsPh_3$, N_2, 85 °C, 6hr.

To a degassed solution of compound **14a (**100 mg, 0.076 mmol), compound **3** (34.08 mg, 0.114 mmol) and 4-iodobenzoic acid (28.27 mg, 0.114 mmol) in anhydrous THF (10 mL) was added NEt_3 (1 mL) under N_2 atmosphere. $Pd_2(dba)_3$ (17.39 mg, 0.019 mmol) and $AsPh_3$ (46.54 mg, 0.15 mmol) were added to the mixture and stirring was continued for 6 hr at 85 °C. The reaction mixture was cooled at room temperature and the solvent was removed under vacuum. The crude product was purified by column chromatography (silica gel) using DCM: MeOH (1:7) as an eluent. The obtained compound was further purified through pre-TLC and recrystallization from CH_3OH to afford **Por-C_{12}-RA_3** (48.88 mg, 40% yield) as a green color solid.

^{1}HNMR (CD_3OH, 500 MHz): δ 9.46 (d, *J* = 4.5 Hz, 4H), 8.60 (d, *J* = 4.5 Hz, 2H), 8.58 (d, *J* = 4.5 Hz, 2H), 8.02 (s, 1H), 8.01 (d, *J* = 8.2 Hz, 4H), 7.95 (d, *J* = 8.1 Hz, 2H), 7.84 (d, *J* = 8.15 Hz, 2H), 7.59 (t, *J* = 8.5 Hz, 2H), 6.93 (d, *J* = 8.55 Hz, 4H), 3.74 (t, *J* = 6.0 Hz, 8H), 1.03-0.97 (m, 8H), 0.93-0.85 (m, 8H), 0.81-0.72 (m, 8H), 0.67-0.58 (m, 52H), 0.48-0.42 (m, 8H), 0.19-0.13 (m, 8H). ^{13}CNMR (CD_3OH, 125 MHz): δ 174.63, 159835, 151.61, 151.45, 148.80, 131.33, 130.36, 130.14, 129.75 129.31, 115.26, 105.05, 99.86, 88.89, 68.25, 31.65, 29.21, 29.15, 29.08, 28.92, 28.77, 28.46, 25.16, 22.39, 13.16.

*Synthesis of [5,15-bis(2,6-di(octyloxy)phenyl)-10,20-[(4-(2-cyanopropenoicacid)phenyl)ethynyl]porphyrin ato]zinc(II) (**Por-C_8-RA_4**)*

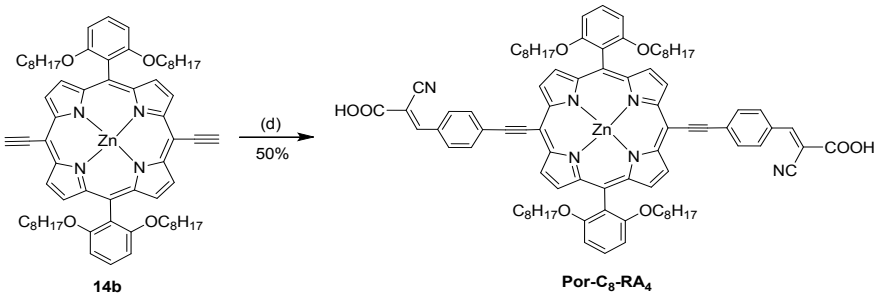

Scheme S8. d) cyano-3-(4-iodophenyl)acrylic acid, THF, NEt_3, $Pd_2(dba)_3$, $AsPh_3$, N_2, 85 °C, 6hr.

To a degassed solution of compound **14b** (100 mg, 0.092 mmol) and Compound **3** (82.64 mg, 0.27 mmol) in anhydrous THF (10 mL) was added NEt_3 (1 mL) under N_2 atmosphere. $Pd_2(dba)_3$ (21.06 mg, 0.023 mmol) and $AsPh_3$ (56.35 mg, 0.18 mmol) were added to the mixture and it was stirred at 85 °C for 6 hr. The reaction mixture was cooled at room temperature and the solvent was removed under vacuum. The crude product was purified by column chromatography (silica gel) using DCM: MeOH (1:8) as an eluent. Further purification was done by pre-TLC to get the pure compound which was recrystallized from CH_3OH to afford final product **Por-C_8-RA_4** (78.90 mg, 50% yield) as a green color solid.

^{1}HNMR (CD_3OH, 500 MHz): δ 9.49 (d, *J* = 4.4 Hz, 4H), 8.61 (d, *J* = 4.45 Hz, 4H), 8.07 (s, 2H), 8.06 (d, *J* = 8.35 Hz, 4H), 7.98 (d, *J* = 8.1 Hz, 4H), 7.55 (t, *J* = 8.45 Hz, 2H), 6.88 (d, *J* = 8.6 Hz, 4H), 3.67 (t, *J* = 5.25 Hz, 8H), 1.22-1.13 (m, 8H), 1.07-1.02 (m, 8H), 0.95-0.89 (m, 8H), 0.86-0.80 (m, 8H), 0.73-0.64 (m, 12H), 0.55-0.52 (m, 8H), 0.26-0.21 (m, 8H). ^{13}CNMR (CD_3OH, 125 MHz): δ 179.47, 178.04, 162.08, 155.85, 154.75, 147.54, 143.80, 133.00, 131.99, 128.41, 124.16, 123.08, 123.02, 117.09, 112.45, 109.36, 103.07, 101.67, 87.97, 85.70, 83.32, 62.15, 52.21, 30.93, 30.61, 29.35, 29.03, 22.32, 22.06, 20.70, 18.92, 17.44, 15.45, 13.07.

Characterizations

III. FTIR measurements

The Fourier transform infrared absorption spectra of **Por-C_n-RA_m** porphyrins were acquired by using a Perkin-Elmer 580B spectrophotometer, equipped with a Perkin-Elmer 3600 IR data station, in KBr pellets. All the samples were flushed with N_2 gas before measurements and the IR spectra were recorded at spectral range between 700 and 4000 cm^{-1}. Baseline spectra were obtained using KBr pellet only under the same conditions. The Experimental IR for all the synthesized porphyrin are shown in Figure S2a.

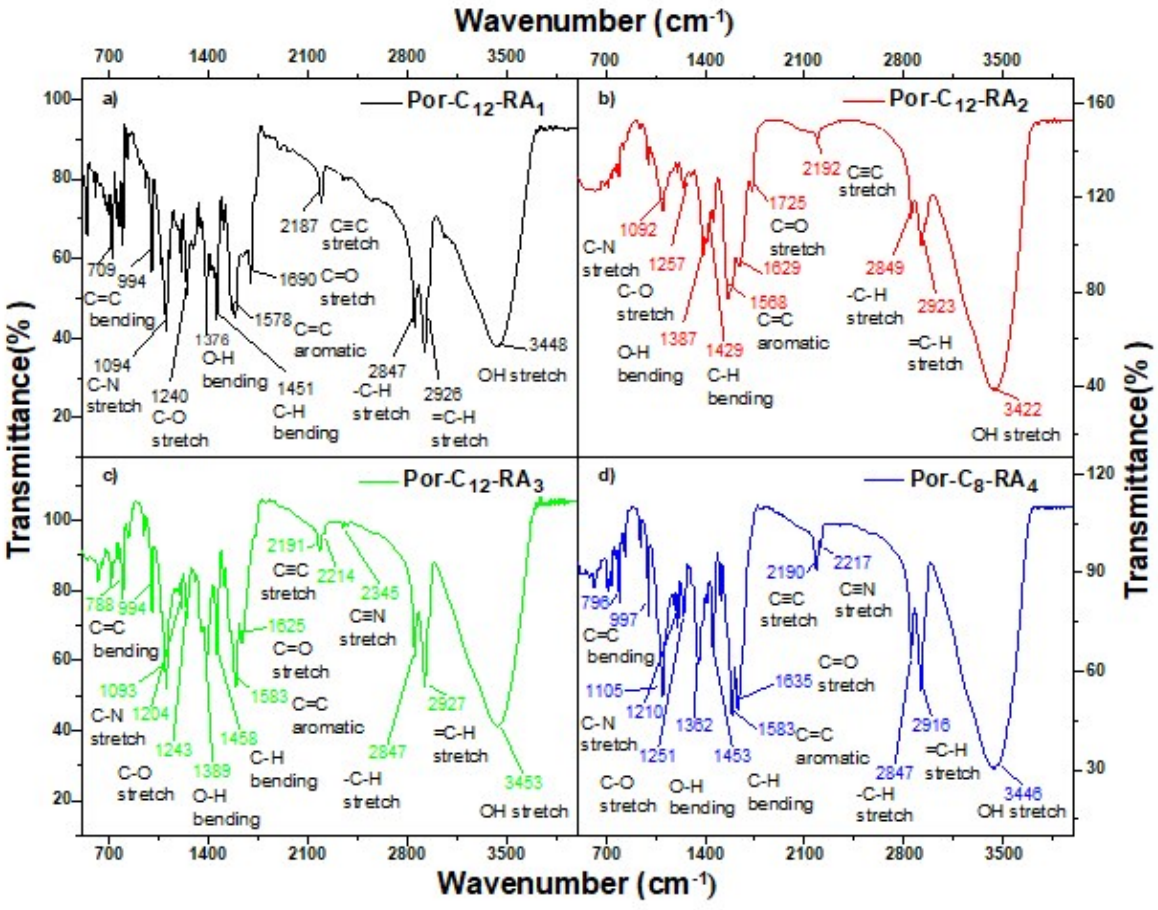

Figure S2a. Experimental FTIR spectra of (a) Por-C_{12}-RA_1; (b) Por-C_{12}-RA_2; (c) Por-C_{12}-RA_3 and (d) Por-C_8-RA_4

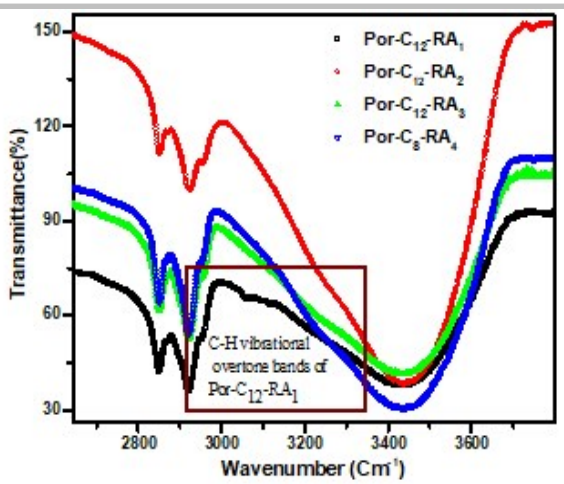

Figure S2b. Experimental C-H vibrations for Por-C_{12}-RA_1, Por-C_{12}-RA_2, Por-C_{12}-RA_3 and Por-C_8-RA_4

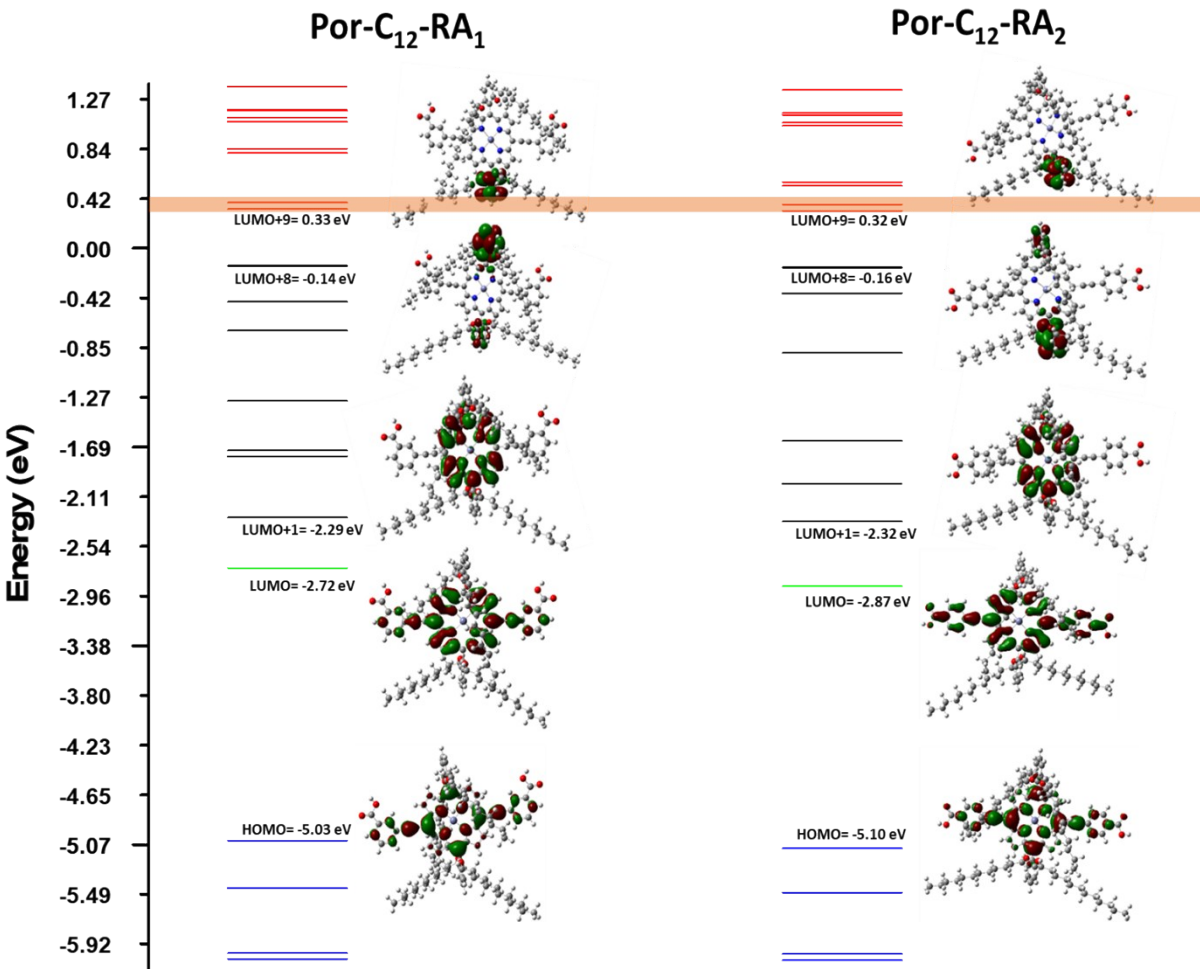

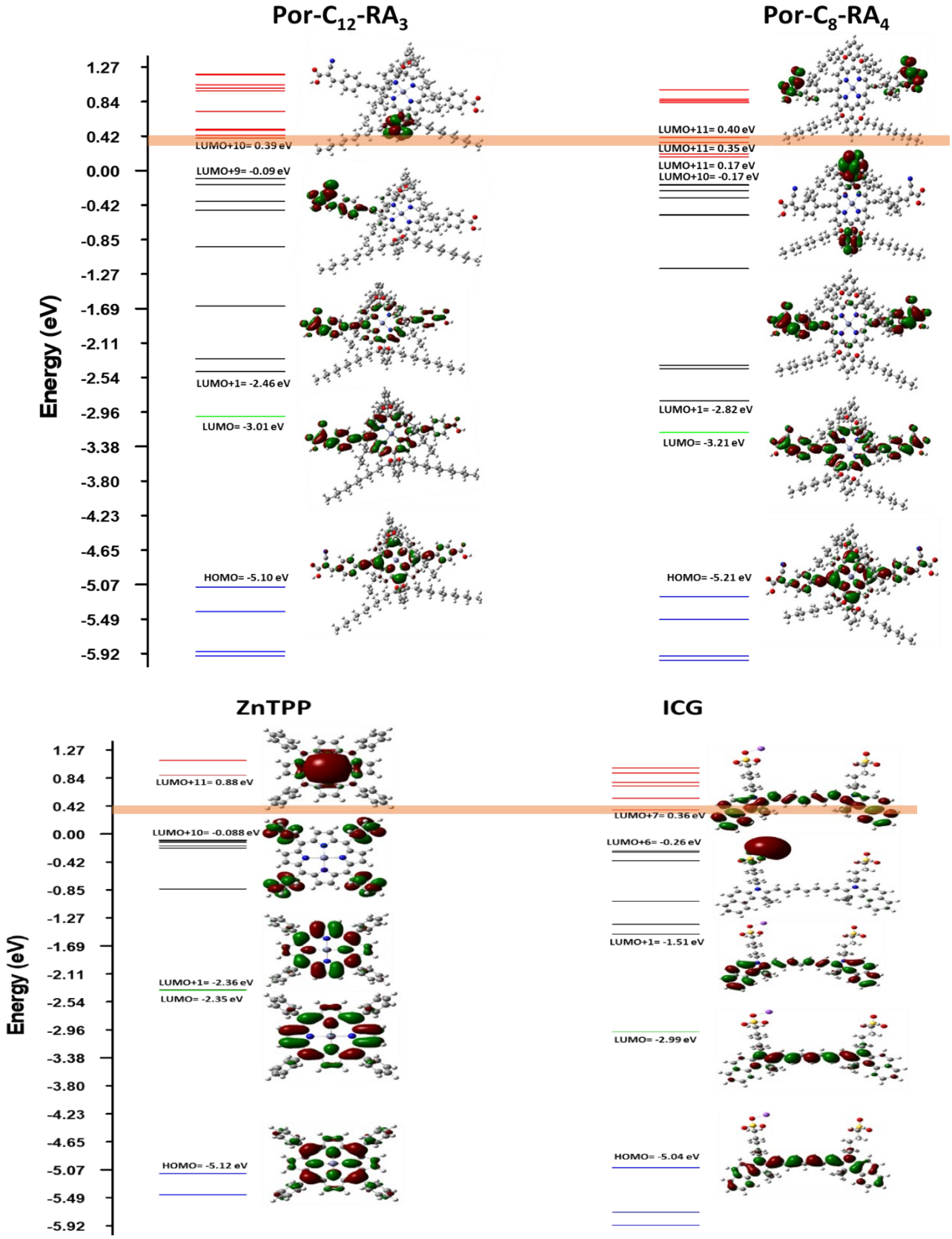

Figure S2c. Molecular orbitals energy diagram of Por-C_{12}-RA_1, Por-C_{12}-RA_2, Por-C_{12}-RA_3, Por-C_8-RA_4, ZnTPP and ICG

IV. UV-Vis Electronic Absorption measurements

The electronic absorption spectra of **Por-C_n-RA_m** porphyrins were obtained in methanol solution using an UV-Vis-NIR spectrophotometer UV-2600 SHIMADZU, Japan. The UV-Vis absorption spectra were collected at the spectral range between 200 and 900 nm with 2-nm resolution and 200 nm/min scan rate. All the spectra were measured on fresh samples at room temperature using 1 cm quartz cell and are

depicted in Figure S3a. The molar absorption coefficients (ε) were calculated from the slope of linear plots of absorbance versus concentration.

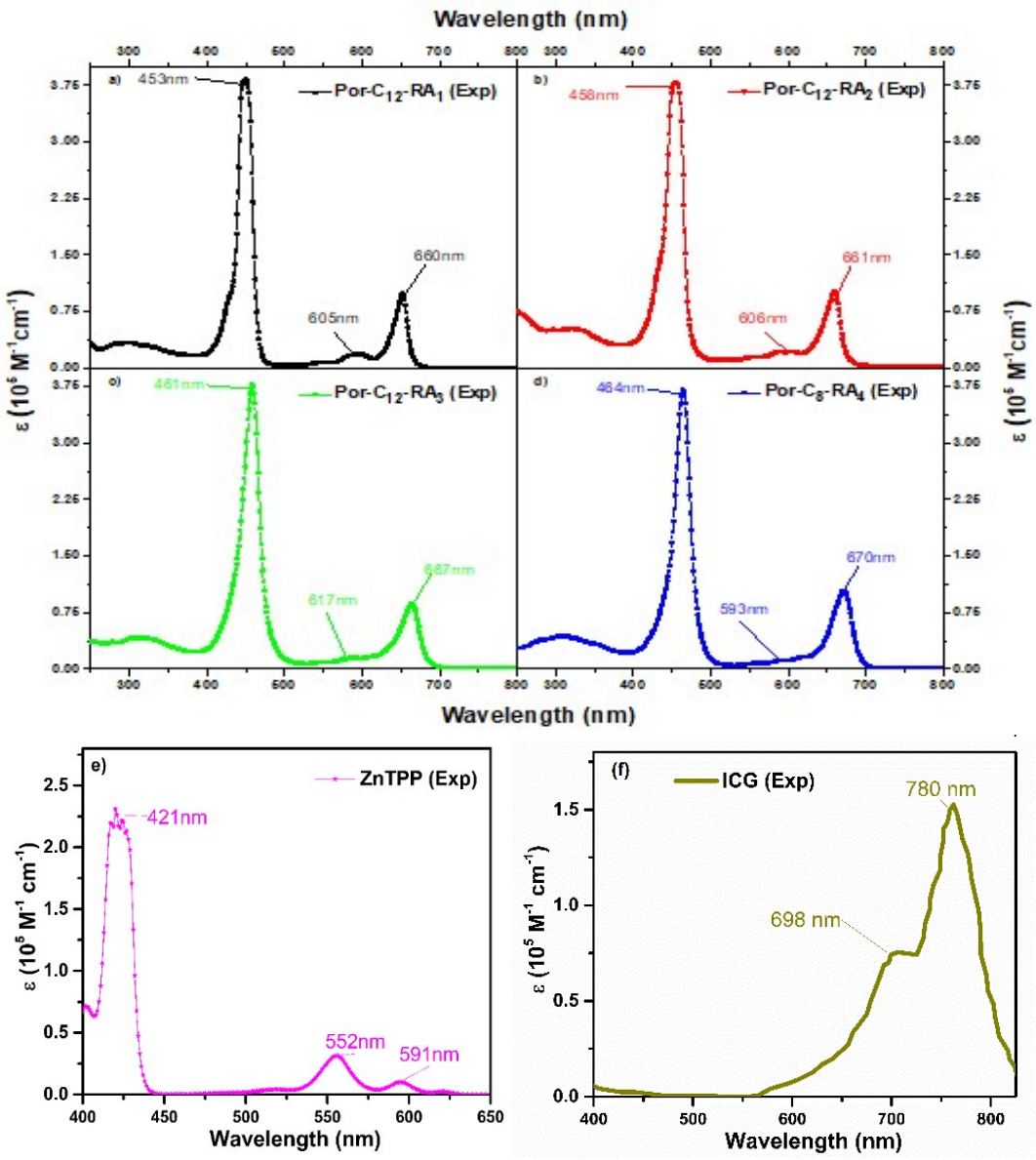

Figure S3a. Experimental electronic absorption spectra of (a) Por-C_{12}-RA_1; (b) Por-C_{12}-RA_2; (c) Por-C_{12}-RA_3; (d) Por-C_8-RA_4; (e) ZnTPP and (f) ICG

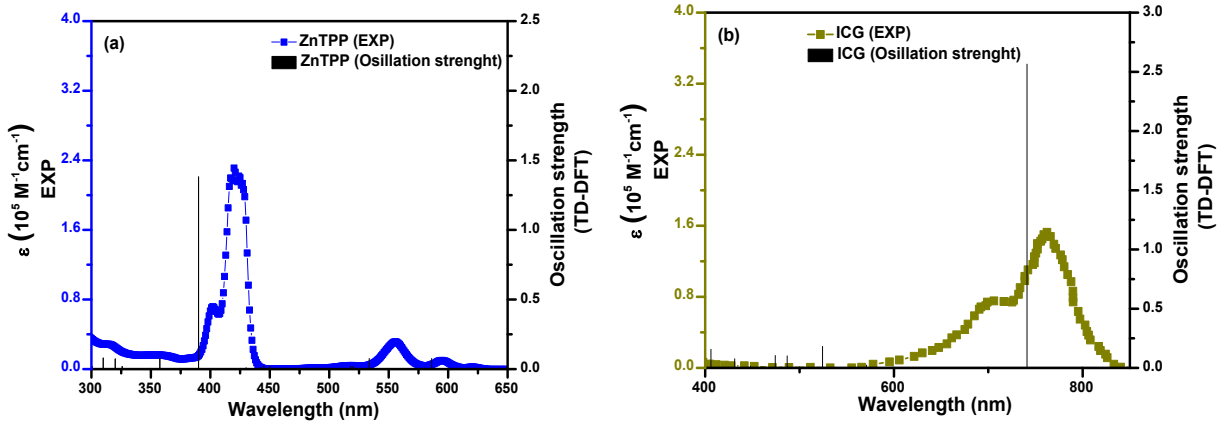

Figure S3b. UV-Vis spectra and oscillation strengths of (a) ZnTPP (reference); (b) ICG

The experimental and calculated wavelength of absorption bands alone with their molar extinction coefficients and oscillation strengths for all four Por-C_n-RA_m porphyrins are displayed in Table S1.

Table S1. Experimental and calculated absorption bands (λ) alone with their molar extinction coefficients (ε) for Por-C_n-RA_m porphyrins

		Por-C_{12}-RA_1	**Por-C_{12}-RA_2**	**Por-C_{12}-RA_3**	**Por-C_8-RA_4**
	λ{B (0,0)}/nm	453	458	461	464
Experimental	ε{B (0,0)}/ M^{-1} cm^{-1}	382635.7	378299.99	377540.10	370355.00
	λ{Q (0,0)}/nm	660	661	667	670
	ε{Q (0,0)}/ M^{-1} cm^{-1}	98139.53	101999.98	87108.97	11775.39
	λ{Q (1,0)}/nm	605	606	617	593
	ε{Q (1,0)}/M^{-1} cm^{-1}	17829.46	4409.93	15060.89	104649.05
Calculated	λ_{gau}{B (0,0)}/nm	423.4	438.8	442.98	432.49
	ε_{gau}{B (0,0)}/ M^{-1} cm^{-1}	312599.37	346763.82	195339.31	199258.21
	f {B (0,0)}	1.0656	1.7789	1.3645	1.7521
	λ_{gau}{Q (0,0)}/nm	622.62	647.4	704.14	708.58
	ε_{gau}{Q (0,0)}/ M^{-1} cm^{-1}	104814.55	152678.85	148666.24	175875.20
	f {Q (0,0)}	0.7772	1.132	1.6518	1.9488
	λ_{gau}{Q (1,0)}/nm	578.95	585.8	604.3	628.6
	ε_{gau}{Q (1,0)}/M^{-1} cm^{-1}	21700.69	10050.65	14448.64	44053.10
	f {Q (1,0)}	0.0003	0.0037	0.0215	0.0355
	$E_{g(gau)}$	2.32	2.22	2.00	1.98

V. Steady State Emission measurements

The steady state fluorescence and the corresponding excitation spectra were recorded on an Edinburgh Instruments FLS920 phosphorimeter, equipped with single monochromators at room temperature using 1 cm path-length quartz cuvette and are depicted in Figure S4. The emission spectra were recorded between 600 and 900 nm for excitation wavelengths at 550 nm, 600 nm and 650 nm. Spectroscopy grade methanol was used for the measurements of fluorescence spectra. The solutions of **Por-C_n-RA_m** in methanol with concentrations between 6 and 32 µM were measured. Table S2 shows the absorption and emission spectral data of Por-C_n-RA_m porphyrins.

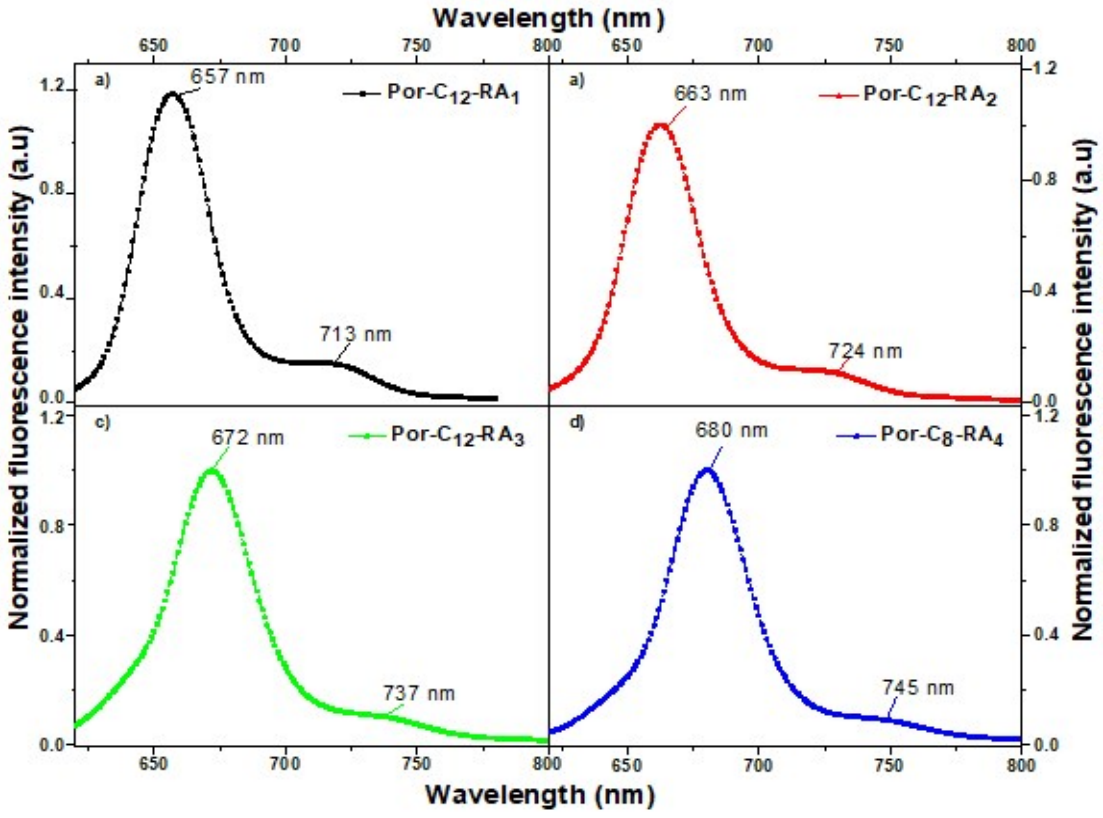

Figure S4. Steady state emission spectra of (a) Por-C_{12}-RA_1; (b) PorP-C_{12}-RA_2; (c) Por-C_{12}-RA_3 and (d) Por-C_8-RA_4

Table S2. The absorption & fluorescence spectral data for Por-C_n-RA_m porphyrin complexes

		Por-C_{12}-RA_1	**Por-C_{12}-RA_2**	**Por-C_{12}-RA_3**	**Por-C_8-RA_4**
Absorbance	Q(0,0) (λ/nm)	656	660	668	670
	Q(1,0)(λ/nm)	600	606	617	619
	Splitting ($\Delta\nu_1/cm^{-1}$)[a]	1422.77	1350.13	1237.4	1229.72
Emission	Q(0,0) (λ/nm)	675	690	693	689
	Q(1,0) (λ/nm)	731	754	763	760
	Splitting ($\Delta\nu_2/cm^{-1}$)[b]	1134.92	1230.15	1323.85	1355.90
Stokes shift ($\Delta\nu/cm^{-1}$)		429.09	658.77	540.05	411.58
Φ_f		0.52	0.53	0.52	0.22
$^1\tau$ (ps)		41.79	21.94	23.87	31.27

VI. Time-Resolved Photoluminescence measurements

Photoluminescence (PL) and ultrafast dynamics of photocarriers were studied by using wavelength-integrated time-resolved photoluminescence (TRPL) down to the sub-nanosecond regime. PL and TRPL measurements were performed with a mode-locked Ti:sapphire laser (Coherent Mira 900) having a laser power output of 1.90 W at 800 nm, and the measurements were used to study the carrier lifetimes of **Por-C_{12}-RA_1**, **Por-C_{12}-RA_2** , **Por-C_{12}-RA_3** and **Por-C_8-RA_4**. A second harmonic generator (APE-SHG) was used to excite the sample by an output wavelength of 400 nm (pulse width 150 fs, pulse repetition rate of 76 MHz), using the synchro scan mode. Emission of the sample was detected by the monochromator attached to a Hamamatsu C6860 streak camera with a temporal resolution of 2 ps. The integration time was kept 100 ms for 500 integrations. All the PL and TRPL measurements of the samples were carried out at room temperature, keeping all the measurement parameters constant.

Figure S5a shows a comparison between the PL spectra of the **Por-C_n-AY_m** porphyrins; the PL spectra showed consistent Stokes shift. Peak PL of the Por-C_{12}-AY_1 shows ~20 nm blue shifted as compared to the other porphyrins. Interestingly, the PL intensity and hence the PL quantum yield (Φ_f) varied in order of **Por-C_8-RA_4< Por-C_{12}-RA_3~Por-C_{12}-RA_1<Por-C_{12}-RA_2** indicating that the relative decrease in Φ_f in Por-C_8- AY_4 is attributed to the effect of strong electron withdrawing substituents as compared to that of other complexes of same series.

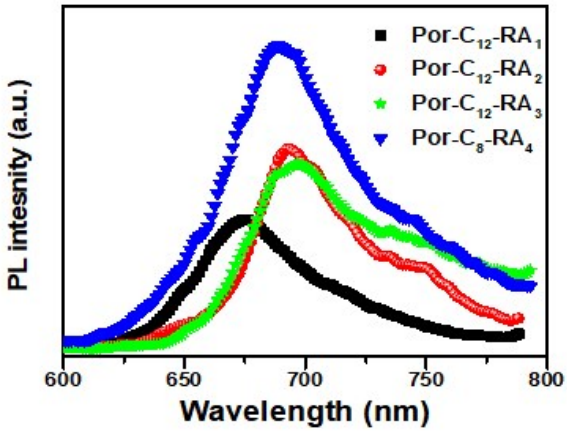

Figure S5a. PL spectra of all four Por-C_n-RA_m excited by femtosecond laser at 400 nm wavelength and having 1.4 mW power

TRPL decay curves using a two-term exponential decay model were measured by a mode-locked Ti:sapphire laser having a laser power output of 1.90 W at 800 nm and all the measurements were carried out at room temparature keeping the all the measurement parameters constant. The two-term exponential model, shown in Figure S5b, best fits the fast decay process involves the thermalization carrier dynamics and the slow decay involves slow cooling process.

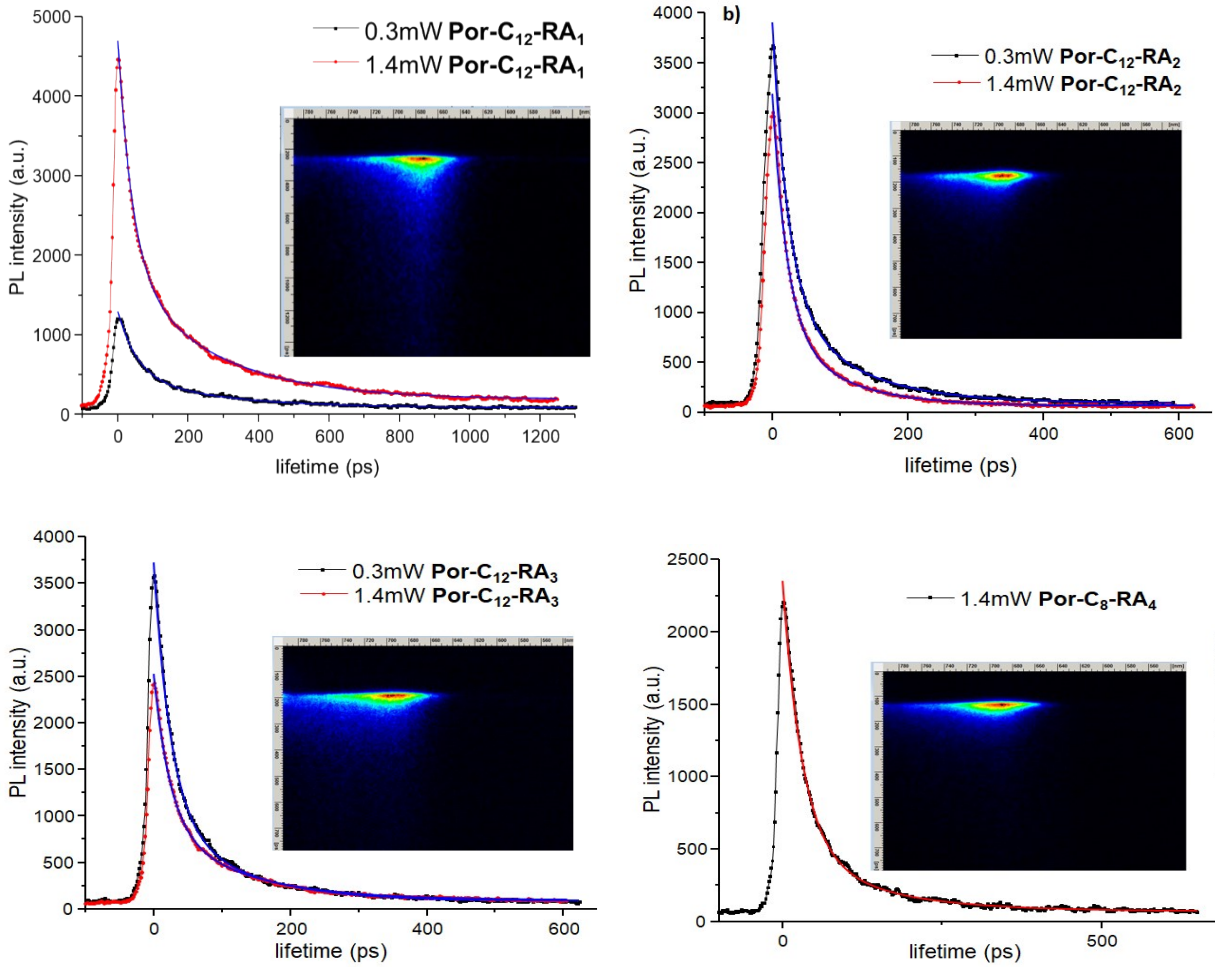

Figure S5b. Time resolved photoluminescence spectra for the fast and the slow time windows for the Por-C_n-RA_m samples annealed at room temperature. (a) Por-C_{12}-RA_1; (b) Por-C_{12}-RA_2; (c) Por-C_{12}-RA_3 and (d) Por-C_8-RA_4

VII. Quantum Yield measurements

Fluorescence quantum yield (Φ_f) of **Por-C_n-RA_m** was determined in methanol using a previously described comparable method (λ_{ex} = 600 nm in ethanol).[18] Two different methods are used to measure the relative quantum yield; (i) a single-point method and (ii) a comparative method.[19] In single-point method, the Φ_f is measured by integrating the emission intensities from a single sample and a reference at identical concentration. However, in the comparative method, the Φ_f is measured by calculating the slope of the line obtained from plotting the absorbance against the integrated emission intensities for multiple concentration of a dye. In this case, the Φ_f is calculated by using the following equation:

$$QY = QY_R\left(\frac{m}{m_R}\right)\left(\frac{n^2}{n_R^2}\right) \quad (1)$$

where "s" is the slope of the line generated from plotting the integrated fluorescence intensity vs. absorbance. "n" is the refractive index of solvent, while the subscript "R" refers to the reference of known quantum yield.[20] If the ethanol is the solvent system for both reference and sample, the n^2/n^2_R ratio will be 1. Three different measurements (i.e., different solutions) were performed for each set of photophysical data (quantum yield). The samples were at equal absorbance of 0.05 at the excitation wavelength. Each absorbance value was measured three times for better accuracy in the measurements of emission quantum yield. Tetraphenylporphyrin (Φ_f = 0.11) was used as a reference and the quantum yield (Φ_f) of Por-C_n-RA_m porphyrins are tabulated in Table S2.

VIII. Photoacoustic Studies

The PA signal generated due to the irradiation of the laser pulse can be expressed as

$$PA = \varepsilon_g C_g \Gamma I \Phi_{nr} \quad (2)$$

where ε_g is the ground state molar extinction coefficient at the incident wavelength, C_g is the ground state concentration of dye molecules, Γ is the Grüneisen coefficient, I is the incident photon fluence, and Φ_{nr} is the quantum yield for non-radiative decay. The Γ is a constant that quantifies a mediums ability to conduct sound efficiently and is defined as

$$\Gamma = \frac{V_s^2 \alpha}{C_p} \qquad (3)$$

where V_s is the velocity of sound, α is the thermal expansion coefficient of the medium, C_p is the specific heat of the medium at constant pressure, C_v is the specific heat of the medium at constant volume, respectively. While Eq. 1 holds true in a linear optical absorption regime, it is recently demonstrated[21] that photoacoustic transients are produced due to the interaction between the incident laser fluence and the nonlinear absorbing medium

$$PA = \varepsilon_g C_g \Gamma I \Phi_{nr} + \varepsilon_e C_e \Gamma I^2 \ldots + \varepsilon_n C_n \Gamma I^{n+1} \qquad (4)$$

where ε_e is the first excited state molar extinction coefficient at the incident wavelength and C_e is the concentration of excited state dye molecules. [21] In this case, consistent with Kasha's rule, Φ_{nr} should equal unity for any excited state relaxation process equivalent to $S_n \rightarrow S_1$ or $T_n \rightarrow T_1$. Hence, Φ_{nr} is only relevant for the first (linear) term in Eq. 3. Thus, nonlinear absorption processes contribute quantitatively to the PA response resulting in a nonlinear PA amplification for a fluorescent dye even with a significantly large fluorescence (Φ_f), or indeed phosphorescence (Φ_{ph}), quantum yield, pending that the excited state absorption cross section is non-negligible.[22] It is also important to note that the concentration of excited state dye molecules will vary with time and thus the laser pulse width is also an important consideration when optimizing such a nonlinear PA amplification with respect to the lifetime of the excited state chromophore.

For effective correlation of the PA emission to its corresponding photophysical properties, optical and PA Z-scan (PAZ-scan) experiments were performed for all the samples. All the samples were dissolved in DMF solvent and using a 2.0 mm path length quartz cuvette, their optical density was adjusted to 0.1 at 532 nm excitation wavelength. The same sample cuvette was used for all the measurements to avoid ambiguity. Sample preparation and PAZ-scan arrangement are explained in detail in the below sections.

a. PAZ-scan measurements

Using a lens of 20 cm focal length, the light from a Q-switched, frequency doubled Nd:YAG laser (Minilite II, Continuum) with a repetition rate of 10 Hz producing 532 nm laser pulses of 3 ns pulse width was focused on the sample to perform the PAZ-scan on the samples. The 2.00 mm path length quartz cell containing the sample solution was placed in a sample holder at 45° degree with respect to the incident laser light while surrounded by water for ultrasound coupling. The sample holder was mounted on an automated XYZ translation stage (Thorlabs NRT 150) so that it could be moved gently in very small steps. As the sample translated along with the laser beam direction through the focal plane of the lens, the sample confronted a moderately increasing laser intensity which reached its maximum at focus then moving the sample forward, it experienced a gradual decrease in laser energy. Depending on the absorption properties of each dye, the optical light transmittance and the generated photoacoustic signal changed by moving the sample along the laser beam direction due to changes in the laser energy transmitted through the sample.

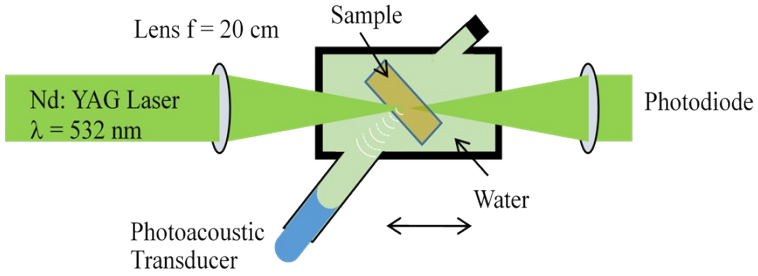

Figure S6a. Schematic of PAZ-scan setup.

To prepare the samples for both PAZ-scan and PA tomography all the samples were dissolved in solvents using a 2.0 mm path length quartz cuvette in order to prepare solutions of 0.1 optical density at 532 nm excitation wavelength which is equivalent to a linear absorption coefficient (α) of 115 m^{-1} at this wavelength. While preparing the dyes for PAZ-scan, the UV-Vis absorption spectra of samples over the wavelength range of 200-800 nm were defined using the Agilent Cary 60 UV-Vis Spectrophotometer and optical absorption of each sample was checked before and after PAZ-scan measurements to assure stability of the sample. The photoacoustic response of each sample was detected by a 10 MHz focused water immersion transducer and the laser light transmitted through the sample was collected by a photodiode. The beam waist of the laser light was measured to be about 70 μm at focal point of the lens where the sample experiences the highest intensity of the laser. The energy of the laser pulses before it reaches the focusing lens was 60 μ J. A neutral density filter of 1.00 OD was placed in front of the detector to ensure the linearity of the optical detector.

Table S3. Molar absorption coefficients (ε) of Por-C_n-RA_m series of complexes at 532 nm & 680 nm.

Extinction coefficient	532 nm	680 nm
Por-C_{12}-RA_1	0.48 x 10^4	0.12 x 10^4
Por-C_{12}-RA_2	1.05 x 10^4	1.02 x 10^4
Por-C_{12}-RA_3	0.75 x 10^4	2.36 x 10^4
Por-C_8-RA_4	0.5 x 10^4	7.43 x 10^4
ZnTPP	0.42 x 10^4	0

Generally, the amplitude of the PA signal is linearly proportional to the input fluence. However, as the excitation laser intensity increases, mechanisms such as saturation of the optical absorption (SA) or multiphoton/multi-step absorption (RSA), and thermal dependence of the Grüneisen coefficient can occur resulting in a nonlinear enhancement of the photoacoustic signal with increasing the excitation pulse fluence. RSA absorption is the mechanism observed in all **Por-C_n-RA_m** dyes as well as in the reference ZnTPP dye. A comparable trend was observed in our previous study for the sample of ZnTPP in THF, where a nonlinear dependence of PA on the input fluence as well as on the optical absorption were observed.[22] This study resulted in redefining the general equation of PA when RSA absorption is the dominant mechanism. The curve shapes in Figure 2b (in main article) is considering the nonlinear optical absorption (RSA behavior) in **Por-C_n-RA_m** porphyrins. In our experiments, ZnTPP in DMF showed weaker nonlinear optical properties at employed excitation pulse fluence which can explain relatively similar curve shapes of ZnTPP in plots of PA vs. fluence and absorption vs. fluence.

The nonlinear PA response with increasing the laser fluence has been studied by another group as well.[23-25] Danielli et al., have described the photoacoustic equation for the case of nonlinear optical absorption at high excitation pulse fluence. In case of a low excitation pulse fluence where nonlinear optical behavior is negligible, the general PA equation is defined as;

$$q(F) \propto \Gamma . \eta_{th} . \mu_a . F$$

in which 'q' is the PA signal, 'Γ' is the Grüneisen parameter, 'η_{th}' is the percentage of absorbed energy that is converted to heat, 'μ_a' is the optical absorption coefficient (cm^{-1}), and 'F' is the local optical fluence ($J.cm^{-2}$). While at high excitation fluence, the PA signal is described as;

$$q(F) \propto \Gamma_0 . \eta_{th} . \mu_a . F + k_1 . F^2 + k_2 . \eta_{th} . (\mu_a . F)^2$$

where 'k_1' is the two photon/multi-step absorption coefficient, and 'k_2' is a linear approximation coefficient of the Grüneisen parameter. Another factor that should be taken into account is the heat distribution within the sample. For a sample of high concentration, the heat distribution around each absorbing molecule is affected by the presence of other molecules. Hence, for 'N' number of molecules in the excited region, the thermal nonlinearity term is proportional to N^2 rather than to N.[23] Therefore, increasing the sample concentration and hence its increasing the linear optical absorption, by itself may lead to nonlinear enhancement of PA amplitude. It is worth to mention that in a concentrated dye sample, quenching of radiative emission may occur which in turn leads to an increase in PA (nonradiative) emission. The combination of all these effects leads to a nonlinear proportionality of PA amplitude to the optical absorption.

In **Por-C_n-RA_m** samples, below 200 $mJ.cm^{-2}$ laser fluence, the PA signal is linearly proportional to their optical absorption. The curve shapes for **Por-C_{12}-RA_1**, for instance, show similar trends in PA signal and optical absorption at the laser fluences up to 200 $mJ.cm^{-2}$ (Figure S6b). At higher laser fluence (higher than 200 $mJ.cm^{-2}$) the nonlinear optical properties come into effect. A similar behavior is observed for other **Por-C_n-RA_m** porphyrins.

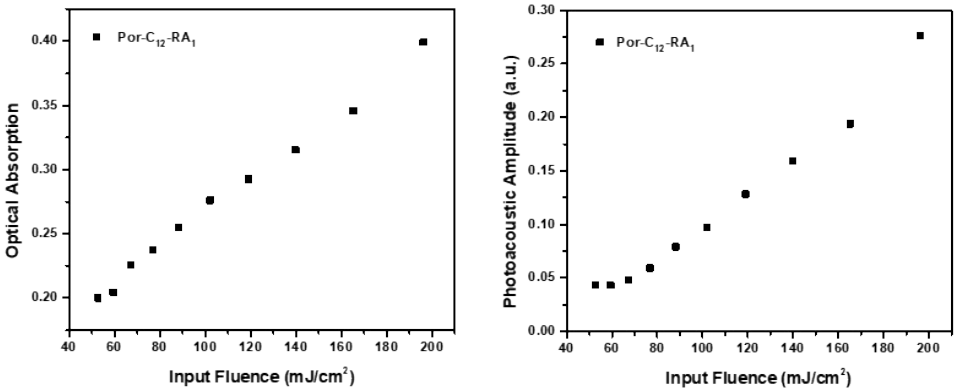

Figure S6b. Photoacoustic response and optical absorption of Por-C_{12}-RA_1 plotted with laser fluence.

Using the experimental data obtained from concentration studies on **Por-C_n-RA_m** porphyrins, we have plotted the PA amplitude vs. optical absorption for all dyes at both low (20 $mJ.cm^{-2}$) and high (400 $mJ.cm^{-2}$) laser fluence (Figure S6c & S6d). At low excitation fluence a linear dependence is observed whereas at high laser fluence, PA changes with optical absorption nonlinearly.

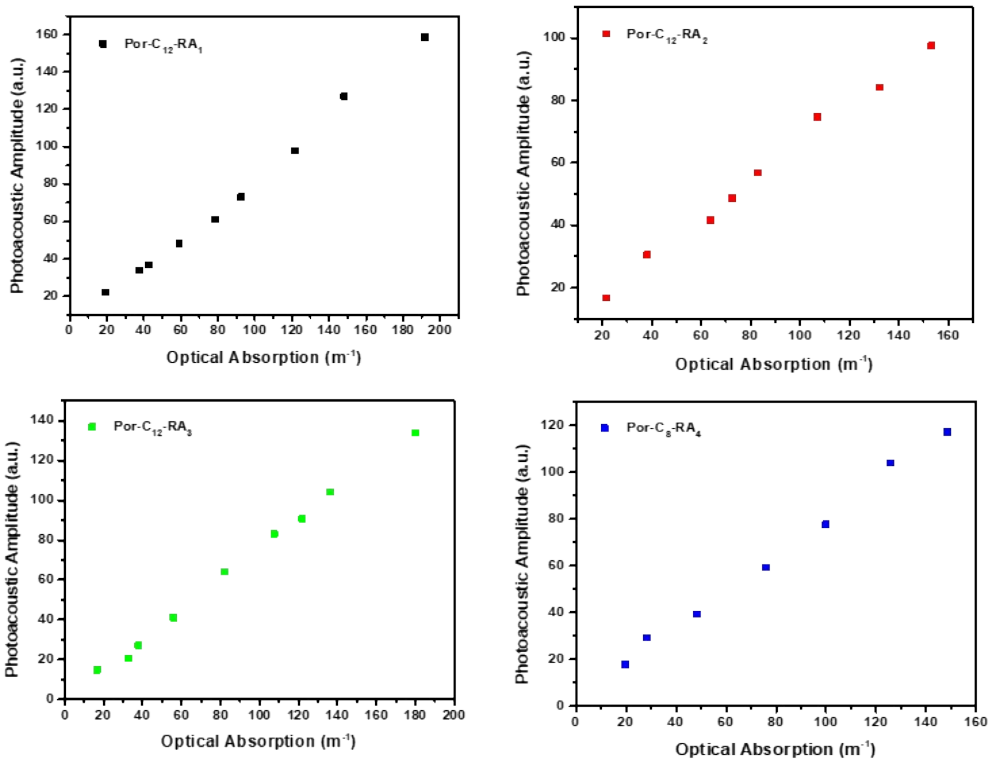

Figure S6c. Photoacoustic response as a function of optical absorption of Por-C_n-RA_m compounds plotted at low (20 mJ.cm^{-2}) laser fluence.

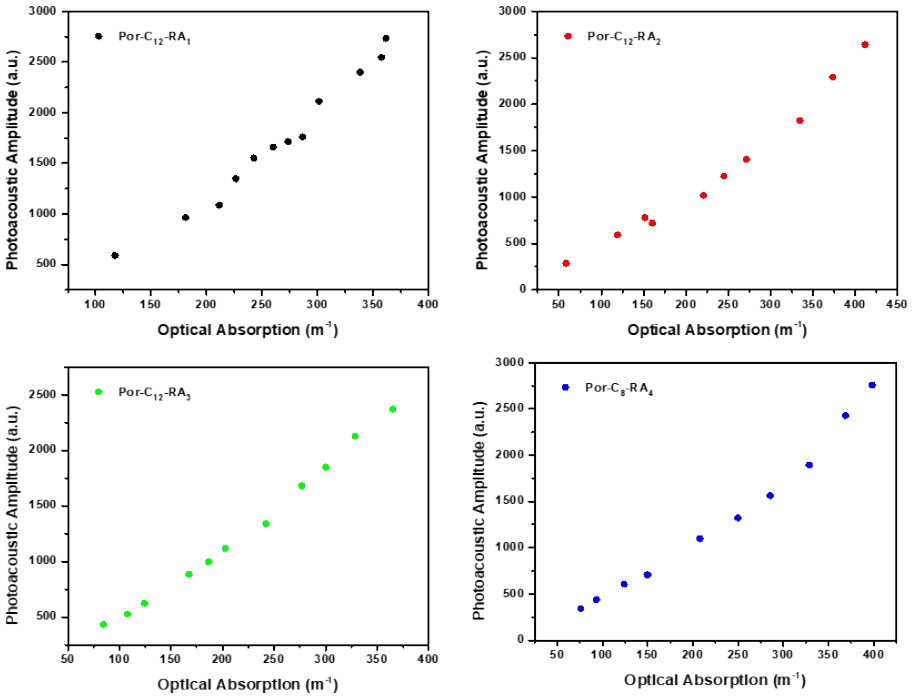

Figure S6d. Photoacoustic response as a function of optical absorption of Por-C_n-RA_m compounds plotted at high (400 mJ.cm^{-2}) laser fluence.

b. Photoacoustic Tomography (PAT)

Photoacoustic imaging was performed by injecting **Por-C_n-RA_m** solutions into 1 mm diameter borosilicate glass tubes and then placed parallel inside the sample housing unit filled with water. A combination of two linear translation stages (Thorlabs NRT 150) with increment movement size of 0.2 mm in longitudinal direction and 0.5 in the direction along the capillary tube length was used to move the sample holder along a planar 2D trajectory. A 10 MHz focused transducer with 25.5 mm focal length (Olympus V311-SU) was positioned in 2.54 cm vertical translation from the tubes. A right angle prism was situated in the setup to direct the laser beam of the Nd: YAG laser on the tubes. The photoacoustic signal was amplified with 30 dB gain on a pulser-receiver (Olympus 5072PR) and digitized using an oscilloscope (WaveRunner 625Zi, Lecroy). At each scanning step, the signal was averaged over 20 laser pulses. A LabVIEW interface was used to acquire the signal data while communicating with the stage controllers to control over scanning movements. The PA image was then reconstructed using MATLAB to compute the absolute value of the Hilbert envelope of the acquired signal at each position.

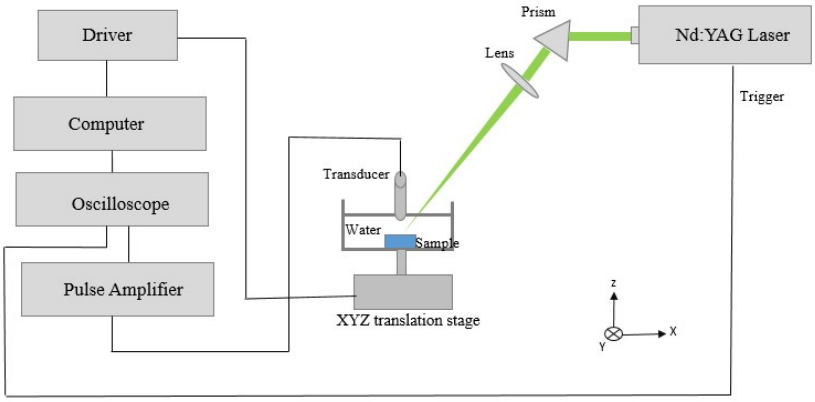

Figure S7. Experimental setup of the photoacoustic tomography (PAT) apparatus.

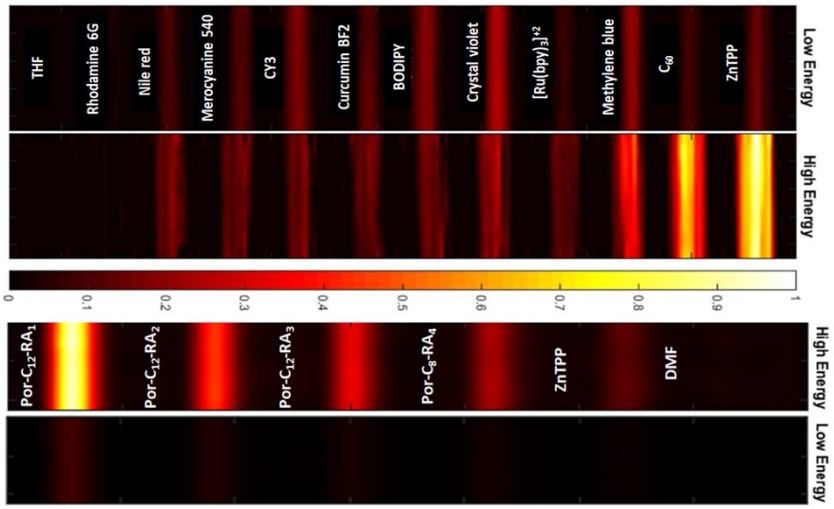

Figure S8. PAT comparison between Por-C_n-RA_m compounds and previously reported small molecules. PAT image recorded at the low laser fluence of 20 mJ/cm^2 and high laser fluence of 400 mJ/cm^2 at λ_{exc}= 532 nm; dimension = 32 mm×5 mm. All samples had 0.15 O.D. at 532 nm in the 1 mm path length borosilicate capillary tubes. The x-axis color scale represents the normalized acoustic intensity.

IX. TGA measurements

Figure S9 shows the TGA curves for all the samples. It is revealed that the TG curves of all the complexes show a continuous weight loss starting from 150 °C to 990 °C, until stable ZnO oxides are formed at around 950 °C or above. The initial weight loss of about 22.83%, 23.84%, 27.67% and 33.94% observed between 200 °C and 450 °C for **Por-C_{12}-RA_1**, **Por-C_{12}-RA_2**, **Por-C_{12}-RA_3** and **Por-C_8-RA_4** respectively, are attributed to the removal of ethnyl-phenyl rings. At 450 °C–550 °C, up to 50% of the total weights had been lost which correspond to the loss of alkoxy-phenyl groups. The organic moiety decomposes further with increasing temperature. At around 410 °C–4450 °C, up to 70% of the total mass had been lost; correspondingly there is a large peak in DTA curves attributed to the collapse of macrocyclic ligand. Further in the range of 500 °C–950 °C, the weight losses reach up to 97% which are attributed to the removal of pyrrole groups and complete decomposition of macrocyclic rings finally leaving behind zinc oxide. Simultaneously, there are some peaks in 200 °C–950 °C region in the DTA curves indicating the major loss in this region. The small peaks correspond to the loss of substituents on porphyrin ring and the large peaks correspond to the collapse of the porphyrin skeleton.

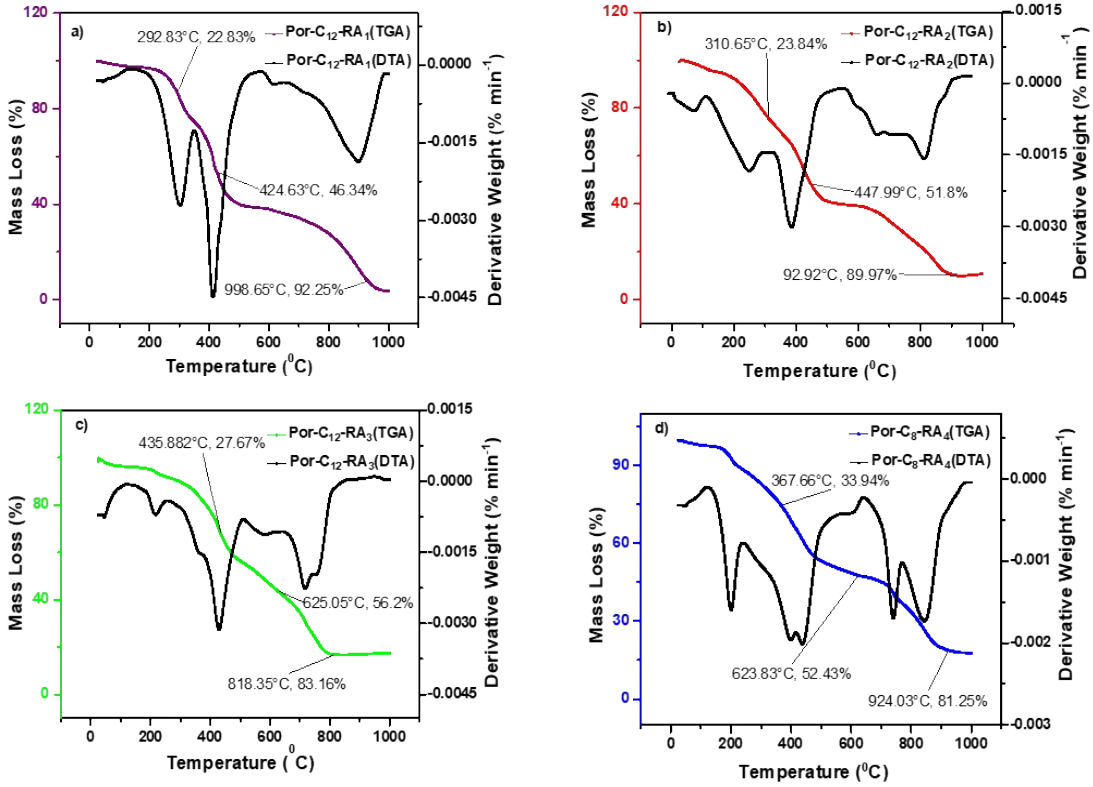

Figure S9. TGA curve of (a) Por-C_{12}-RA_1; (b) Por-C_{12}-RA_2; (c) Por-C_{12}-RA_3 and (d) Por-C_8-RA_4

X. EDX spectra

Spectrum details

Project: Por-C_{12}-RA_1 Spectrum name: Spectrum 1

Electron Image

Image Width: 351.4 µm

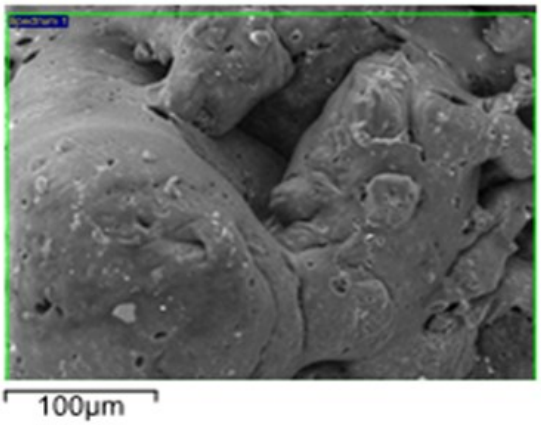

Acquisition conditions

Acquisition time (s) : 30.0 Process time : 5

Accelerating voltage (kV) : 15.0

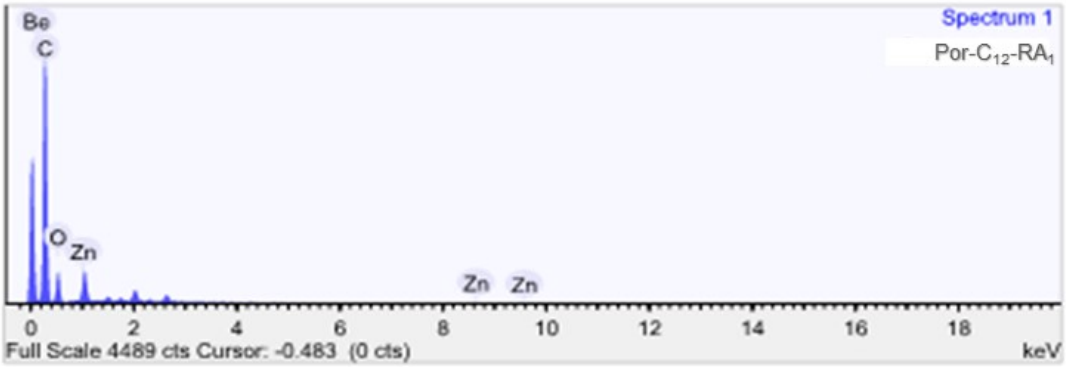

Quantification Settings

Quantification method : All elements (normalised) Coating element : None

Summary results

Element	Weight %	Weight % σ	Atomic %
Carbon	72.212	0.540	80.337
Oxygen	22.168	0.539	18.515
Zinc	5.620	0.221	1.149

Spectrum details

Project: Por-C_{12}-RA_2 Spectrum name: Spectrum 1

Electron Image

Image Width: 351.4 µm

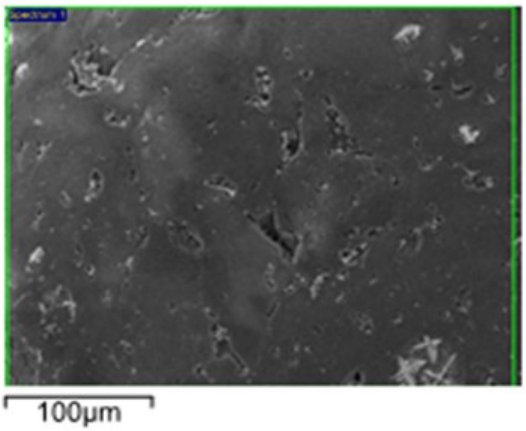

Acquisition conditions

Acquisition time (s) : 30.1 Process time : 5

Accelerating voltage (kV) : 15.0

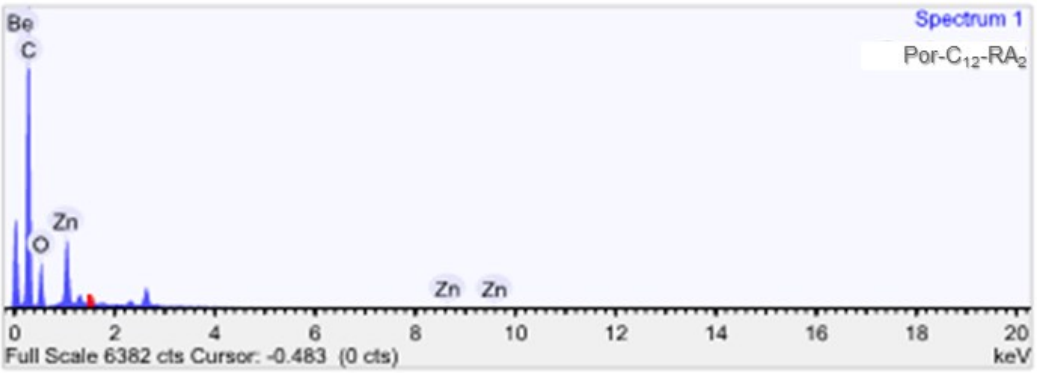

Quantification Settings

Quantification method : All elements (normalised) Coating element : None

Summary results

Element	Weight %	Weight % σ	Atomic %
Carbon	68.352	0.390	78.297
Oxygen	23.160	0.387	19.917
Zinc	8.487	0.193	1.786

Spectrum details

Project: Por-C_{12}-RA_3 Spectrum name: Spectrum 1

Electron Image

Image Width: 175.7 µm

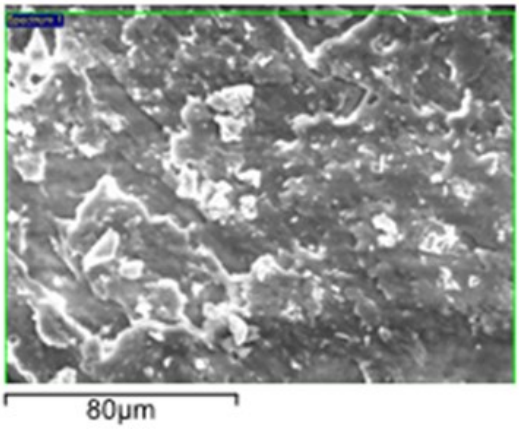

Acquisition conditions

Acquisition time (s) : 30.0 Process time : 5

Accelerating voltage (kV) : 15.0

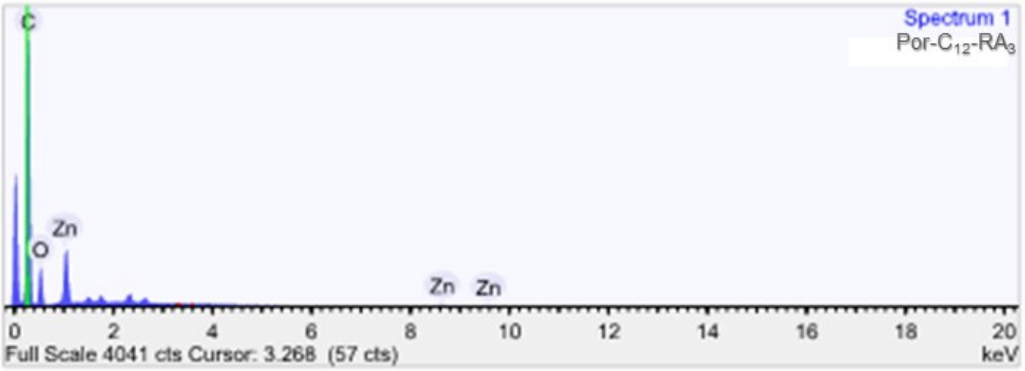

Quantification Settings

Quantification method : All elements (normalised) Coating element : None

Summary results

Element	Weight %	Weight % σ	Atomic %
Carbon	69.936	0.499	79.487
Oxygen	22.088	0.495	18.847
Zinc	7.976	0.241	1.666

Spectrum details

Project: Por-C_8-RA_4 Spectrum name: Spectrum 1

Electron Image

Image Width: 351.4 µm

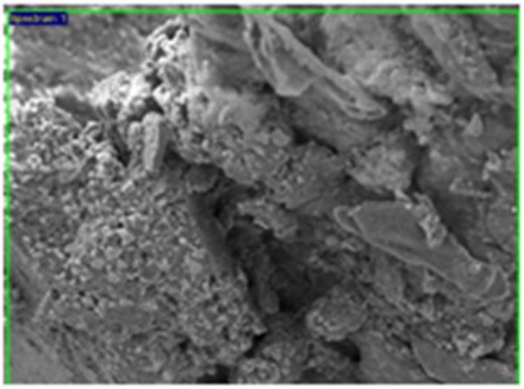

Acquisition conditions

Acquisition time (s) : 30.1 Process time : 5

Accelerating voltage (kV) : 15.0

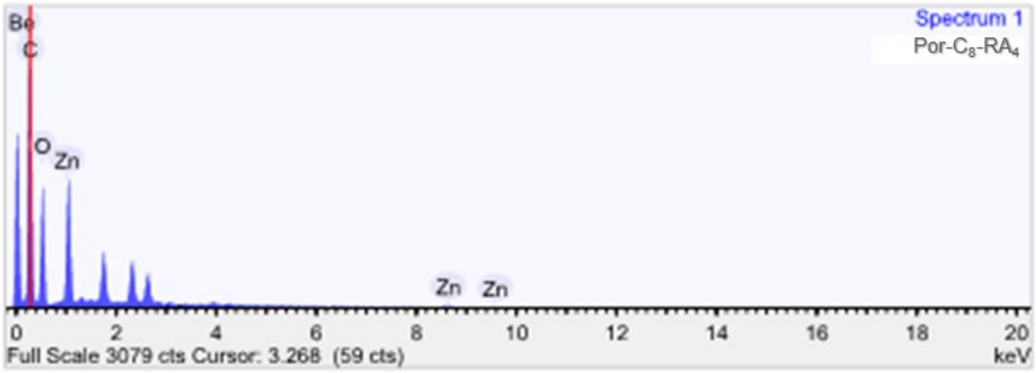

Quantification Settings

Quantification method : All elements (normalised) Coating element : None

Summary results

Element	Weight %	Weight % σ	Atomic %
Carbon	55.139	0.464	66.851
Oxygen	33.685	0.463	30.660
Zinc	11.176	0.262	2.490

XI. NMR spectra

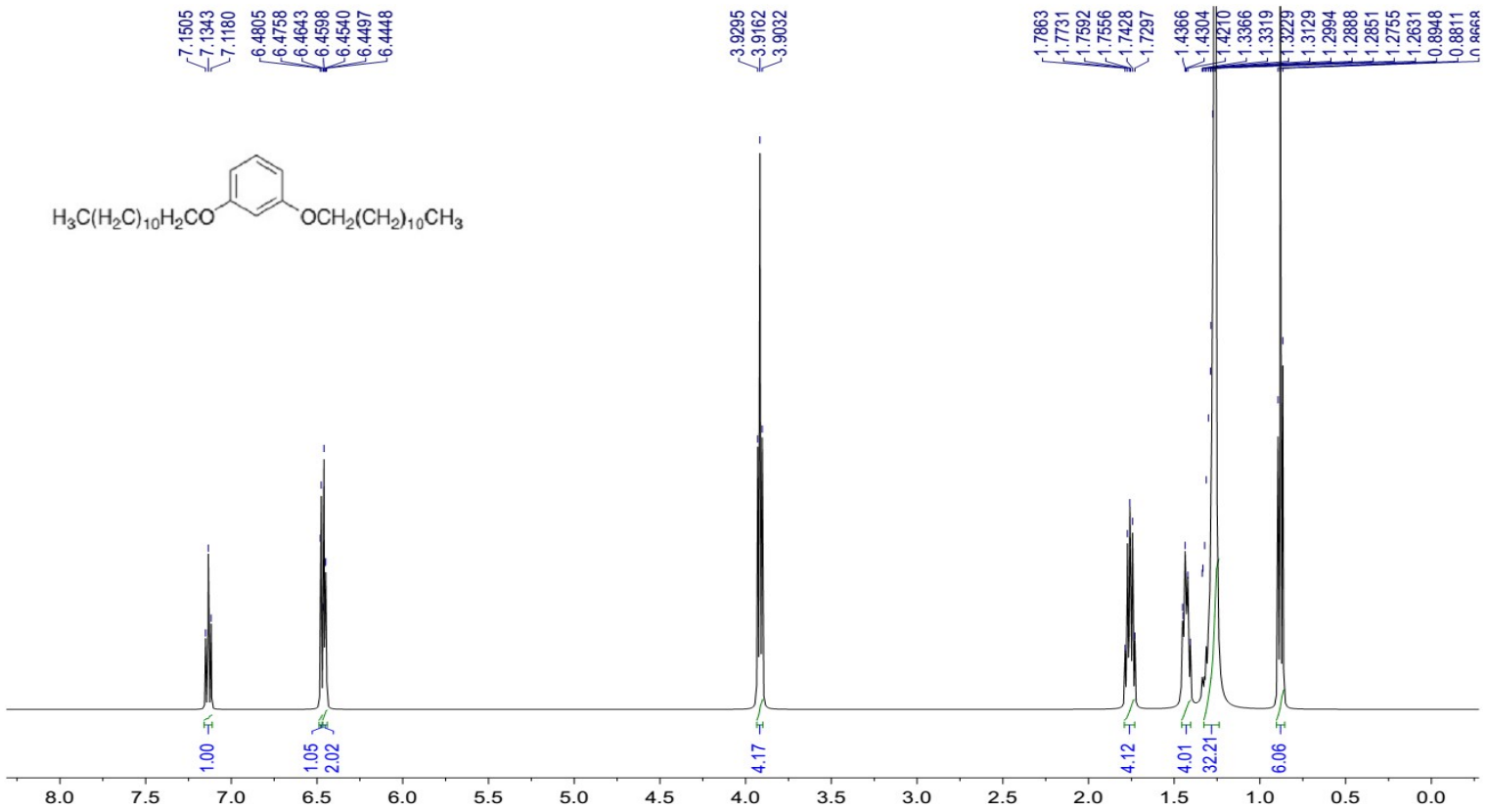

Figure S10a. ^{1}HNMR of 1,3-di(dodecyloxy)benzene (5a) in $CDCl_3$

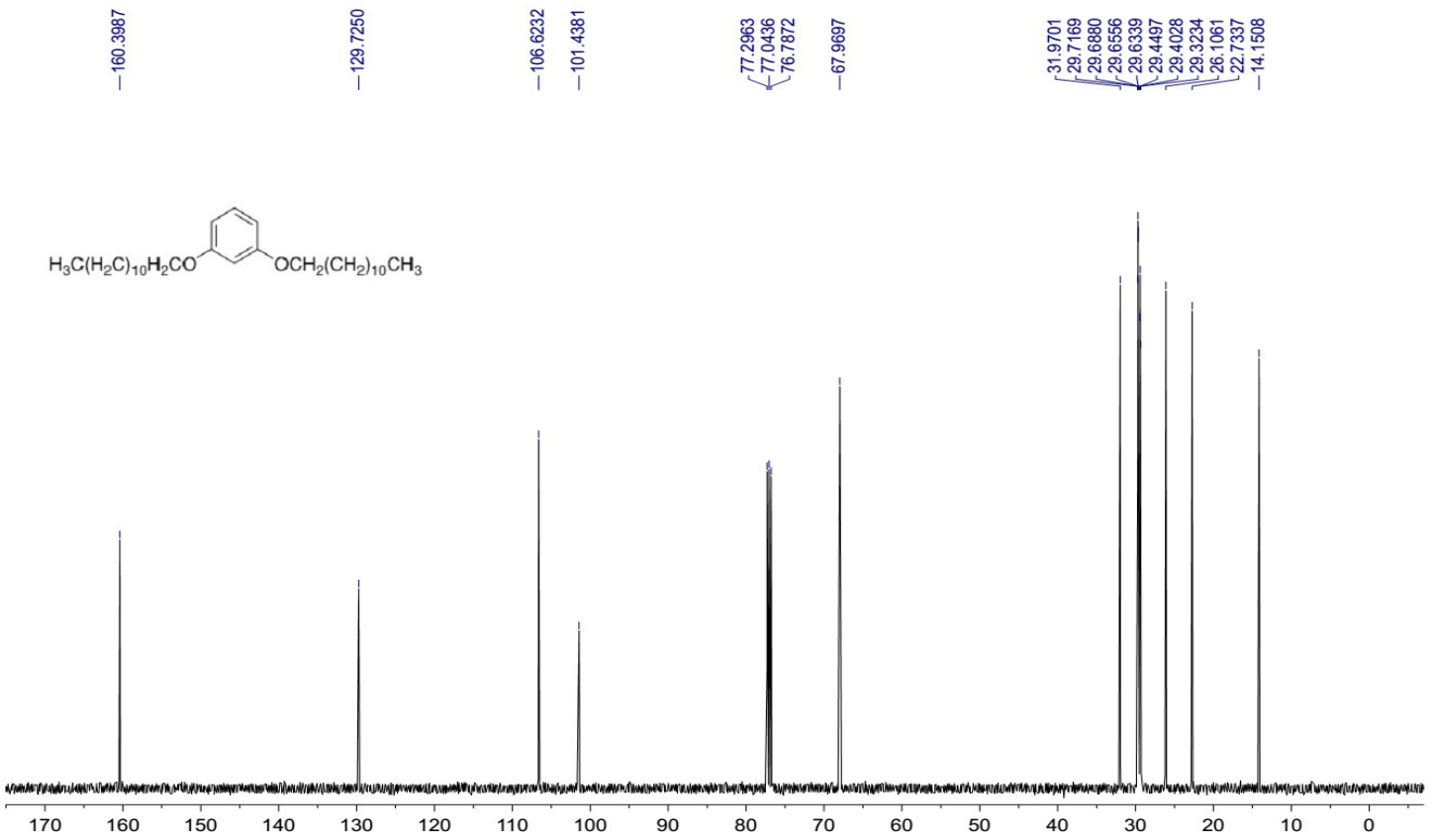

Figure S10b. ^{13}CNMR of 1,3-di(dodecyloxy)benzene (5a) in $CDCl_3$

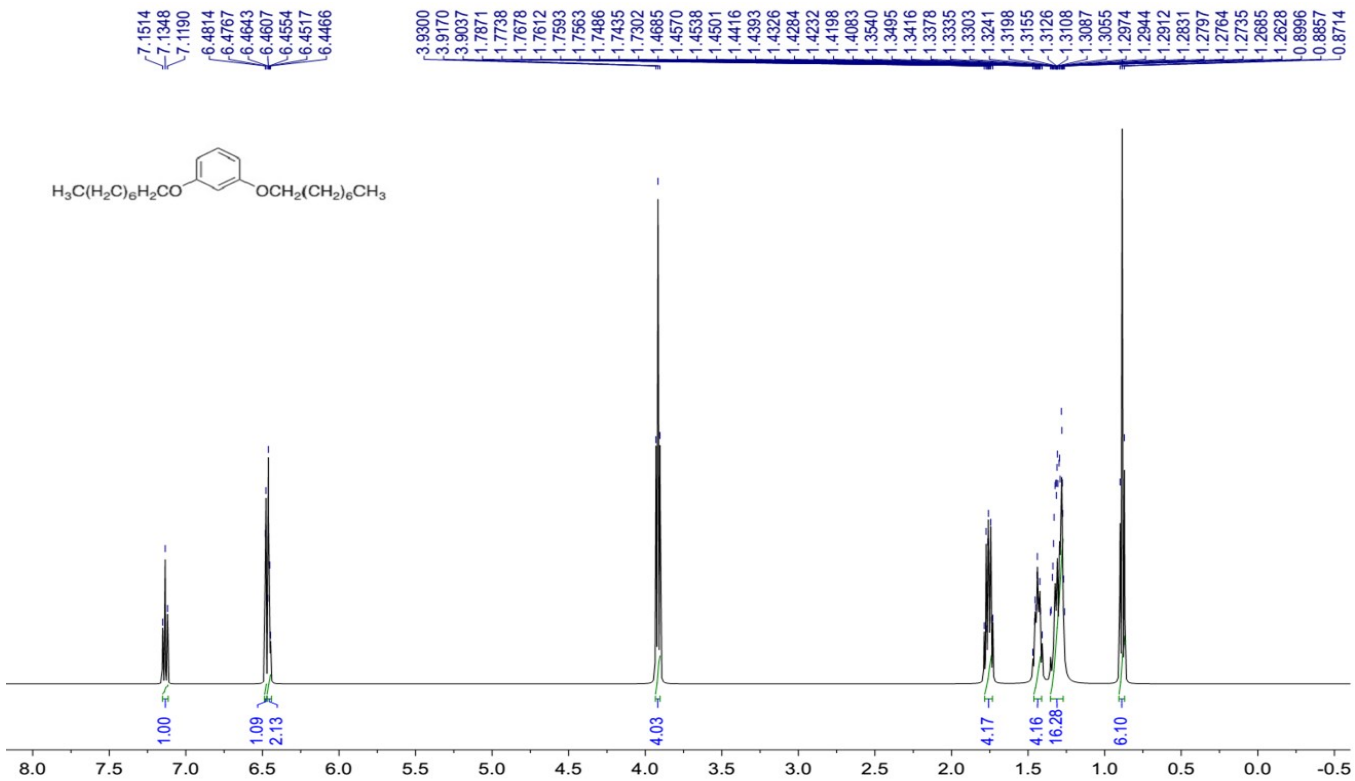

Figure S10c. ^{1}HNMR of 1,3-di(octyloxy)benzene (5b) in $CDCl_3$

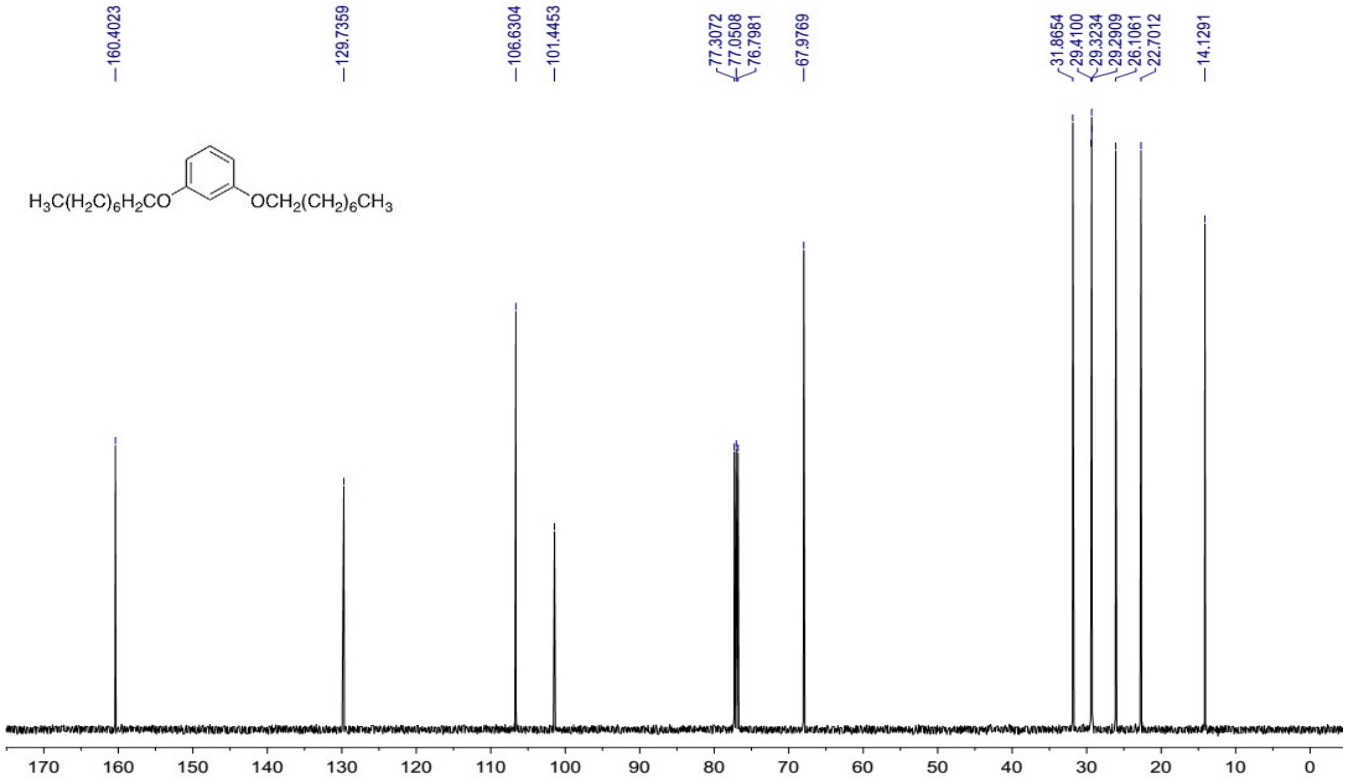

Figure S10d. ^{13}CNMR of 1,3-di(octyloxy)benzene (5b) in $CDCl_3$

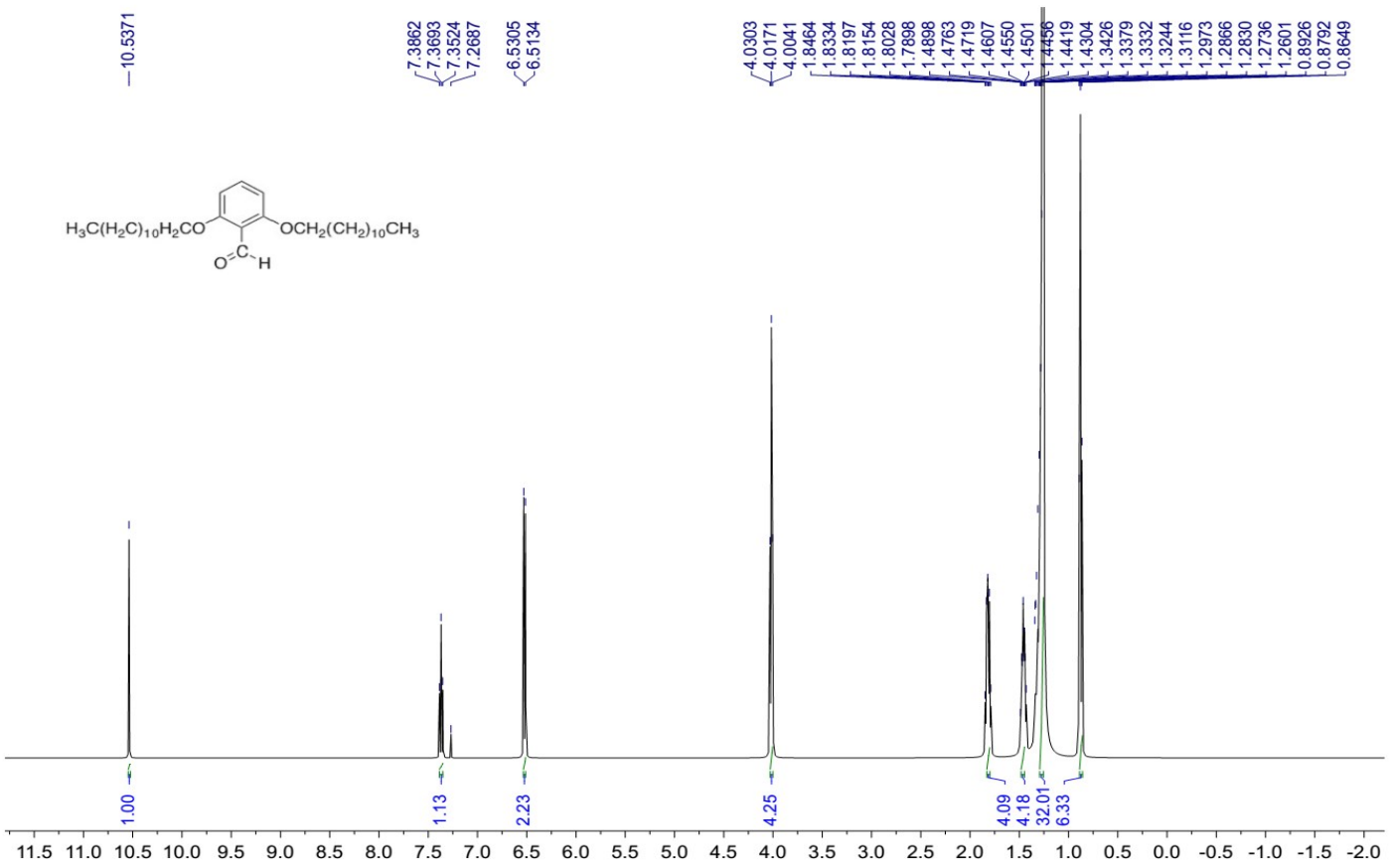

Figure S11a. ^{1}HNMR of 2,6-bis(dodecyloxy)benzaldehyde (6a) in $CDCl_3$

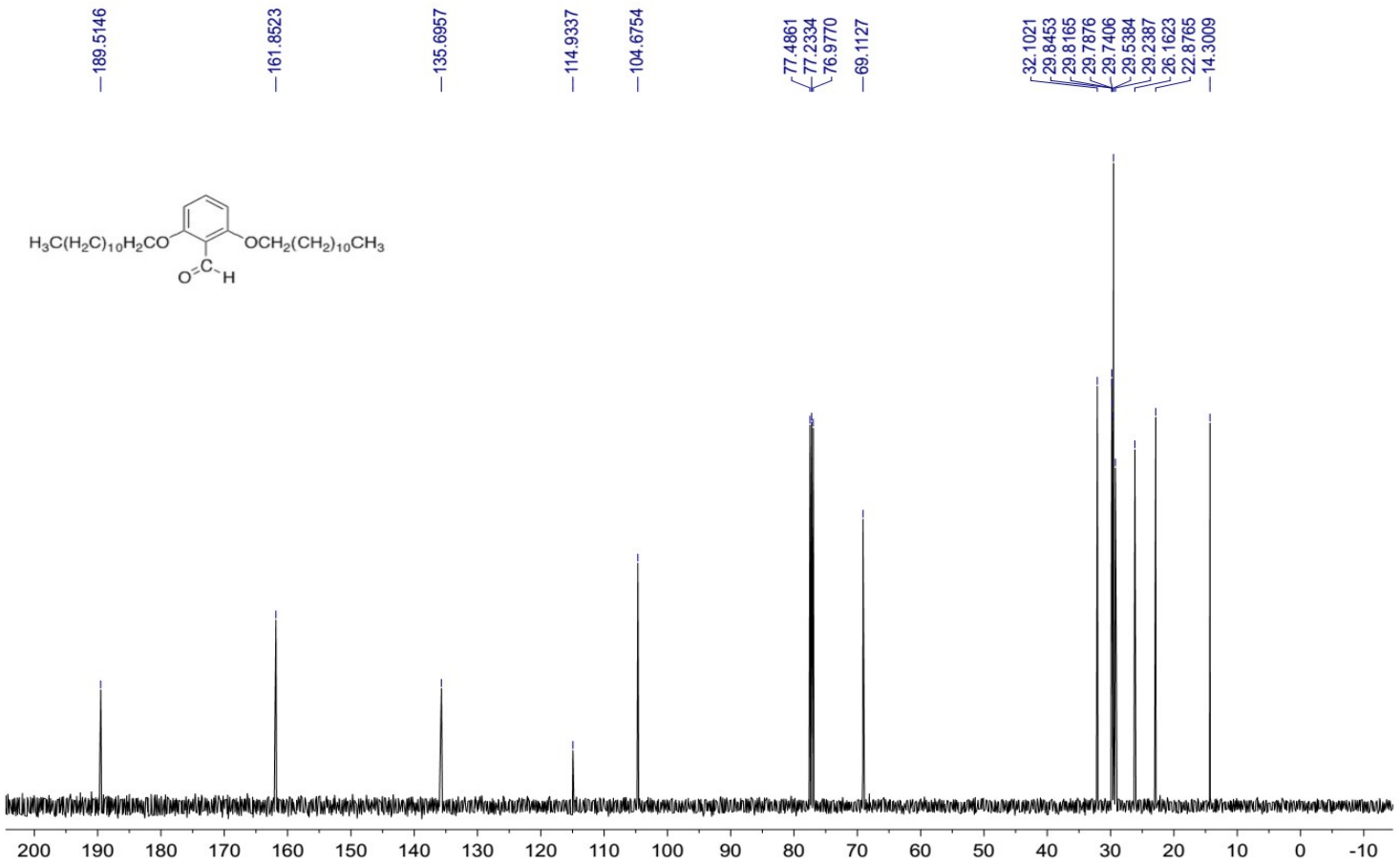

Figure S11b. ^{13}CNMR of 2,6-bis(dodecyloxy)benzaldehyde (6a) in $CDCl_3$

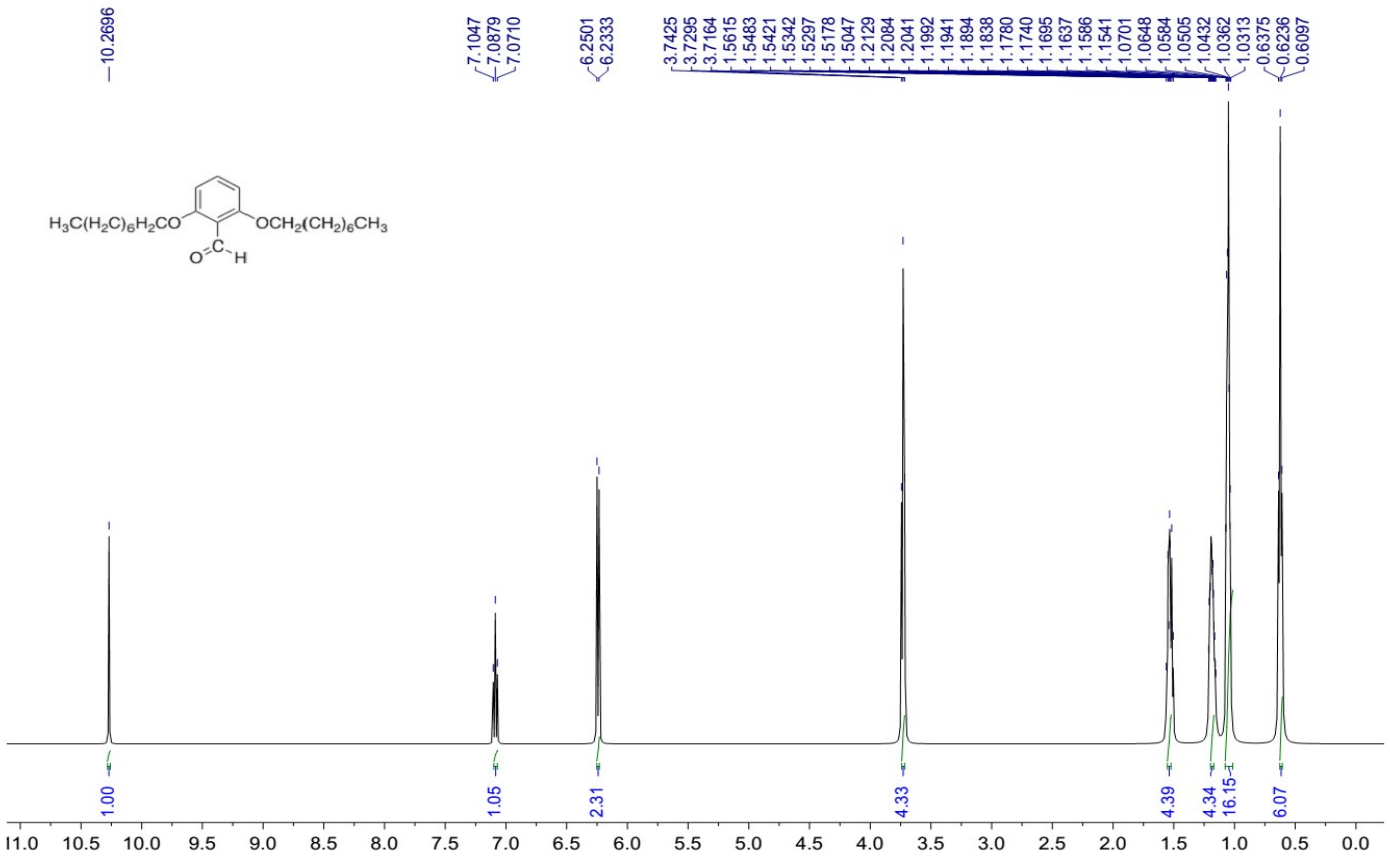

Figure S11c. ^{1}HNMR of 2,6-bis(octyloxy)benzaldehyde (6b) in $CDCl_3$

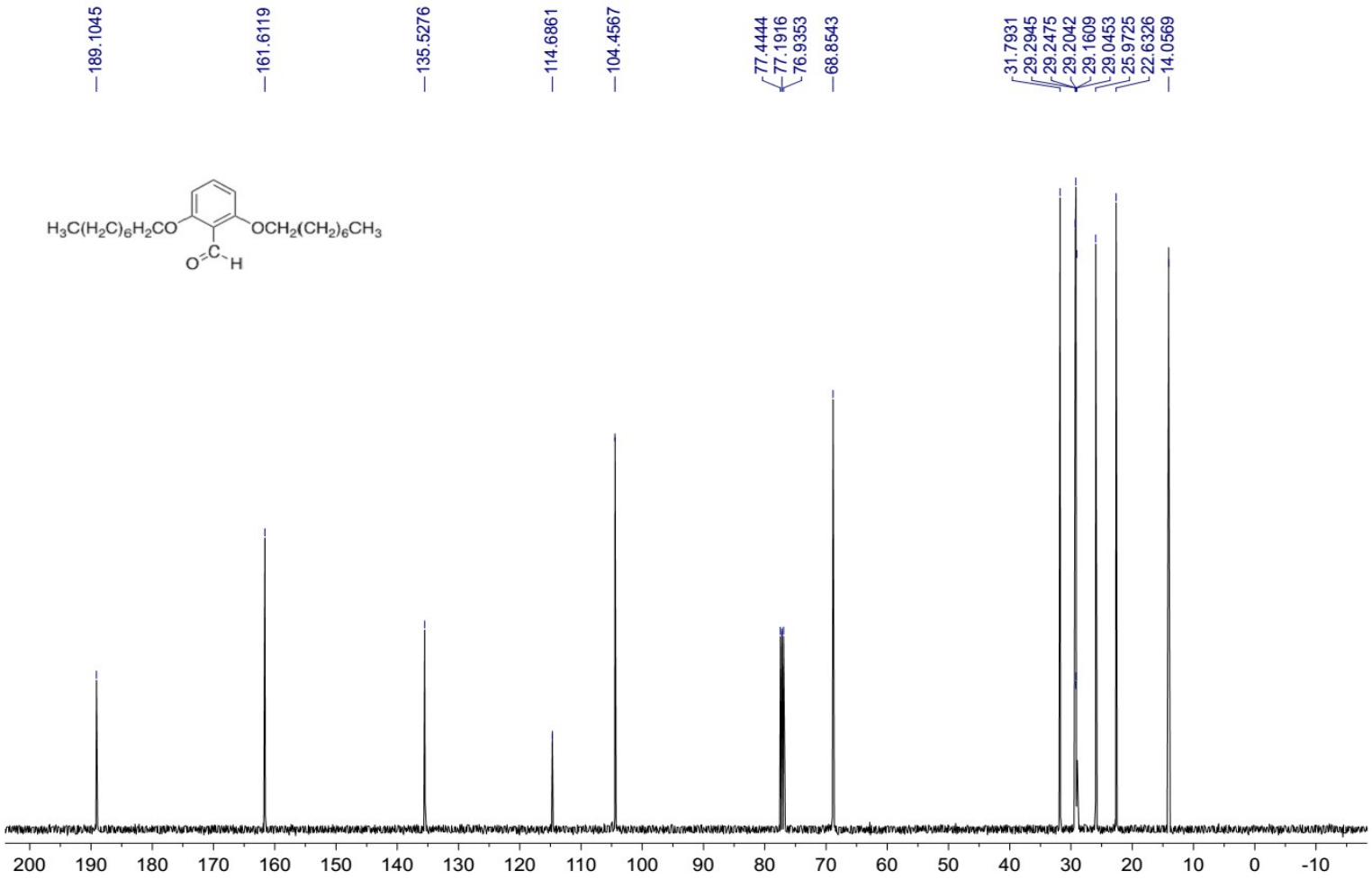

Figure S11d. ^{13}CNMR of 2,6-bis(octyloxy)benzaldehyde (6b) in $CDCl_3$

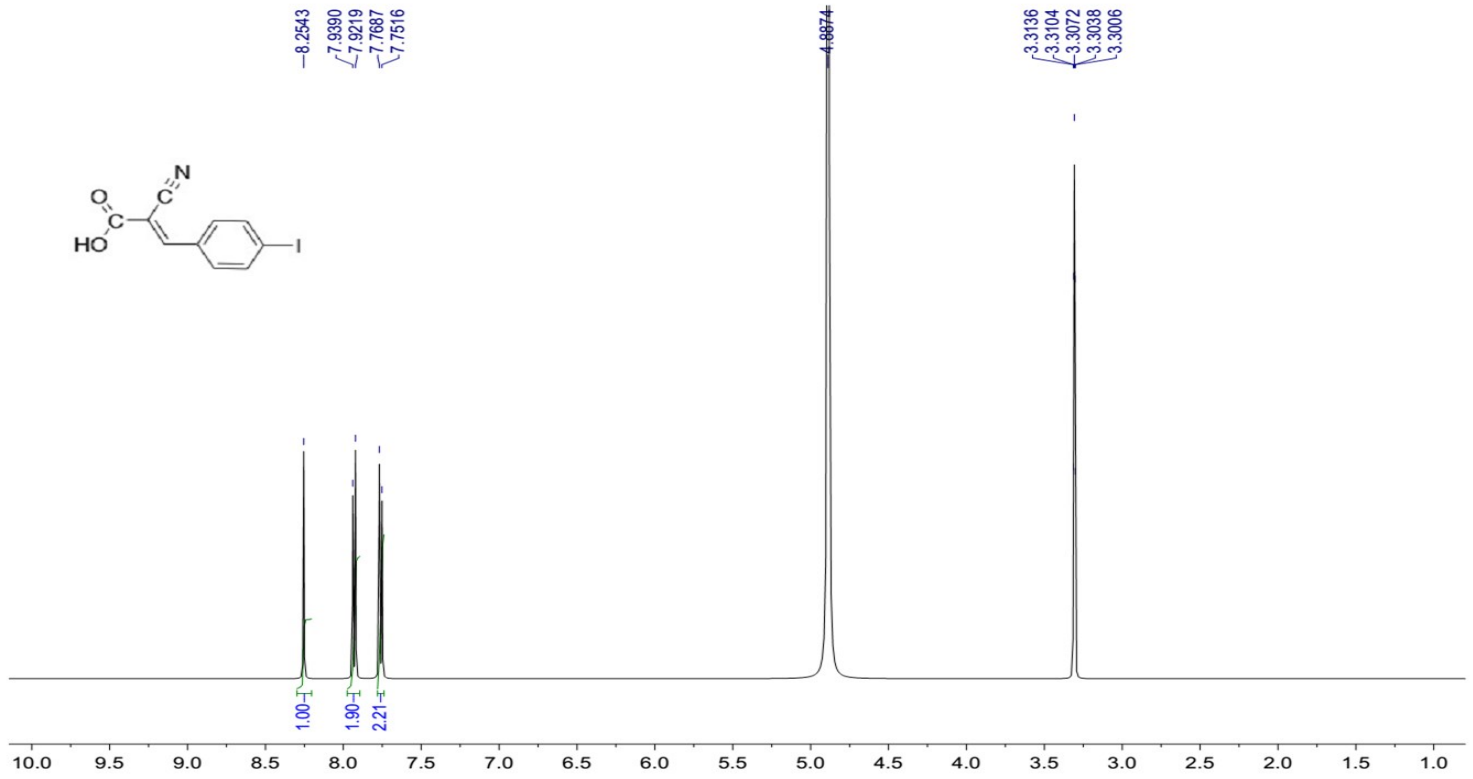

Figure S12a. ^{1}HNMR of 2-cyano-3-(4-iodophenyl)acrylic acid (3) in CD_3OH

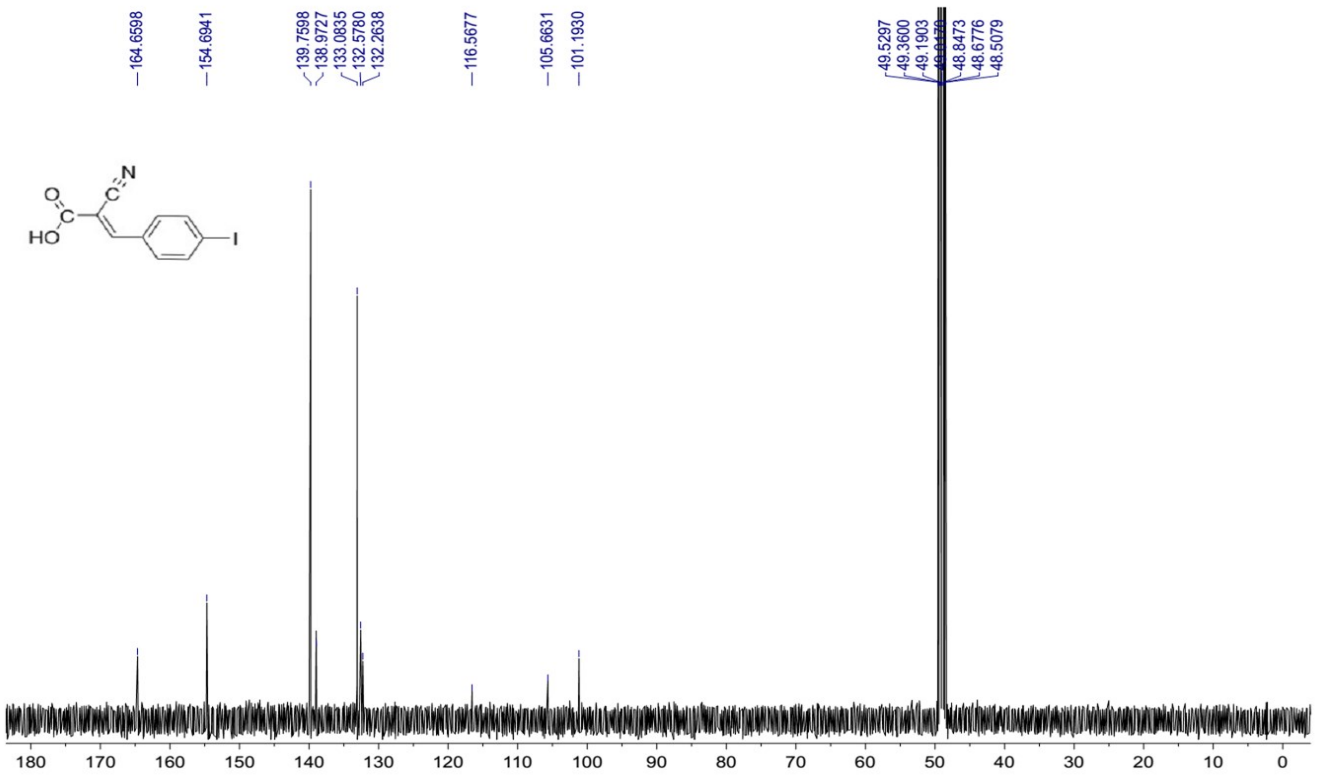

Figure S12b. ^{13}CNMR of 2-cyano-3-(4-iodophenyl)acrylic acid (3) in CD_3OH

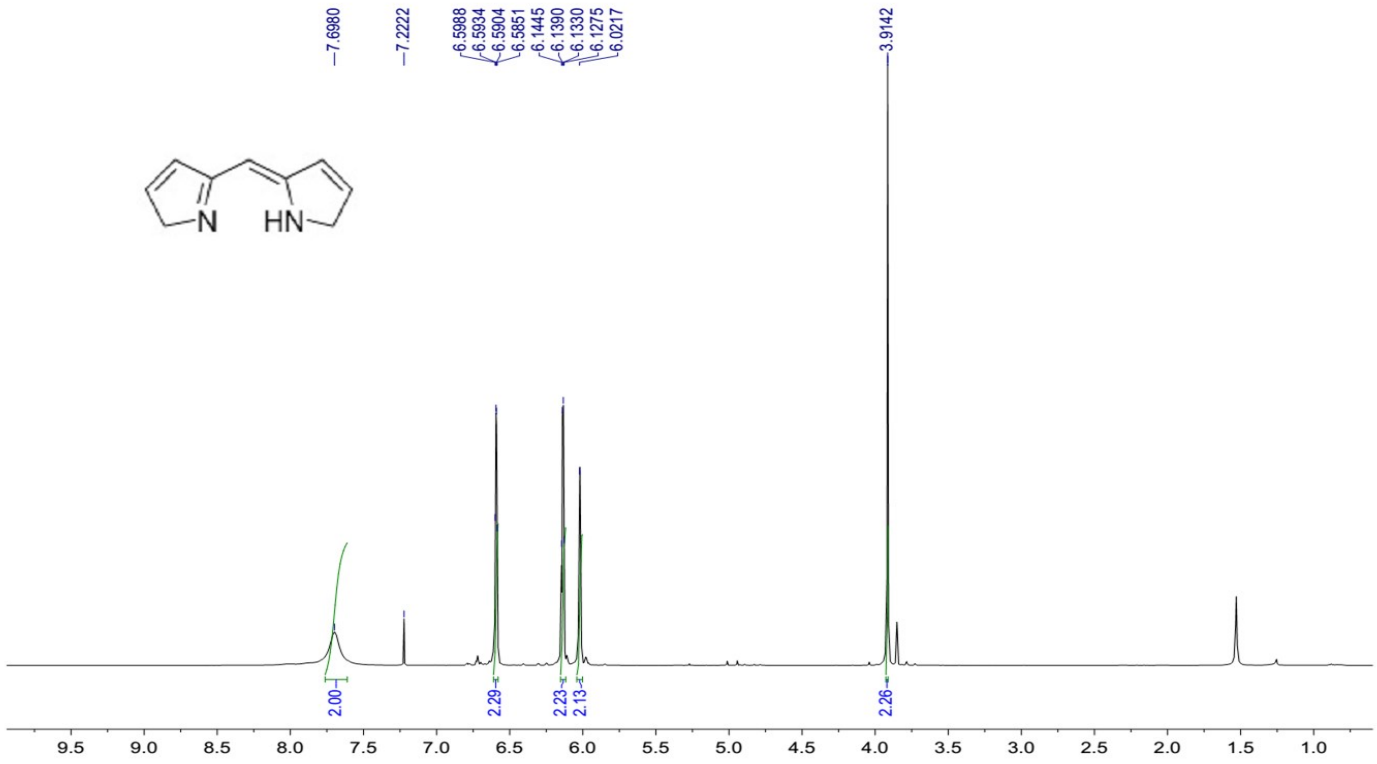

Figure S13a. ^{1}HNMR of di(1H-pyrrol-2-yl)methane (9) in $CDCl_3$

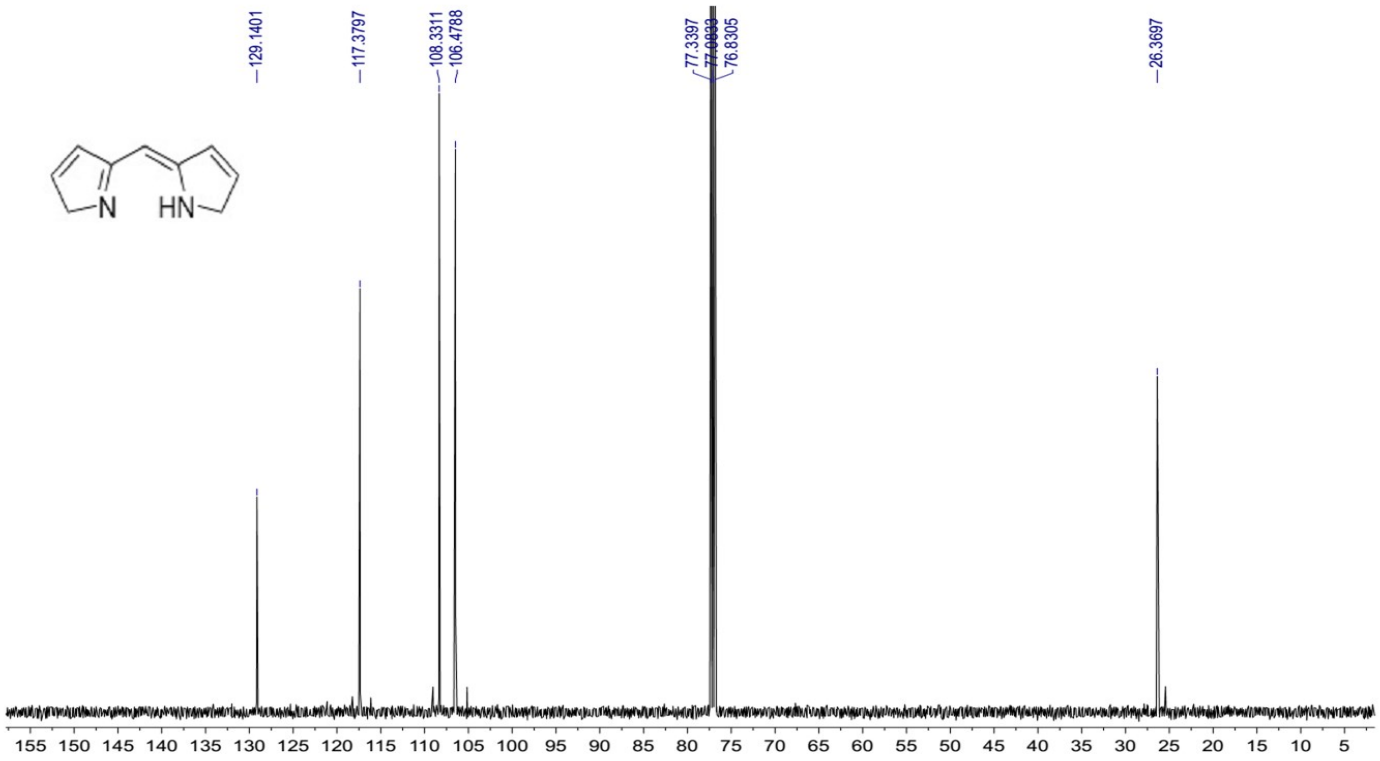

Figure S13b. ^{13}CNMR of di(1H-pyrrol-2-yl)methane (9) in $CDCl_3$

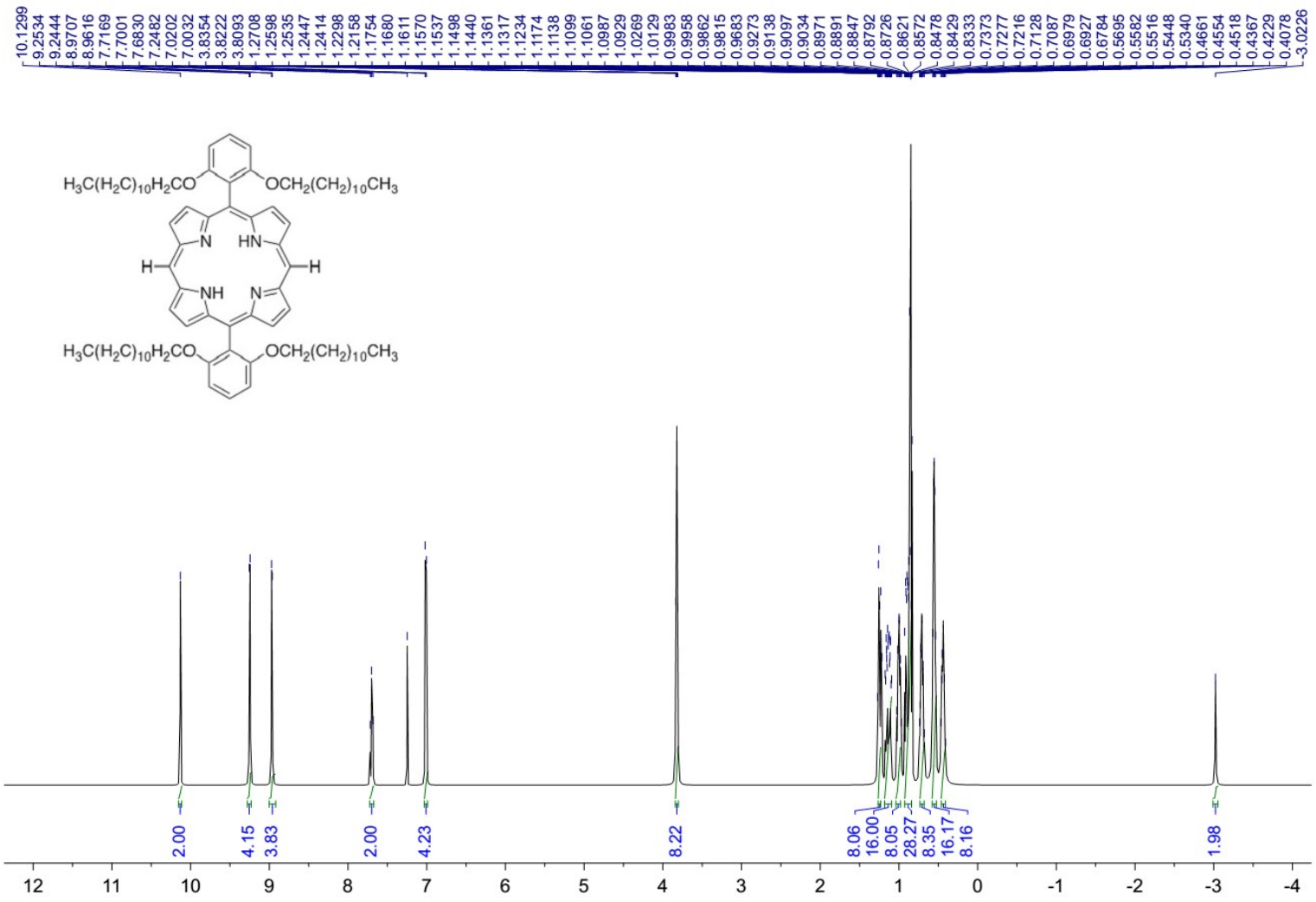

Figure S14a. ^{1}HNMR of 5,15-bis(2,6-di(dodecyloxy)phenyl)porphyrin (10a) in $CDCl_3$

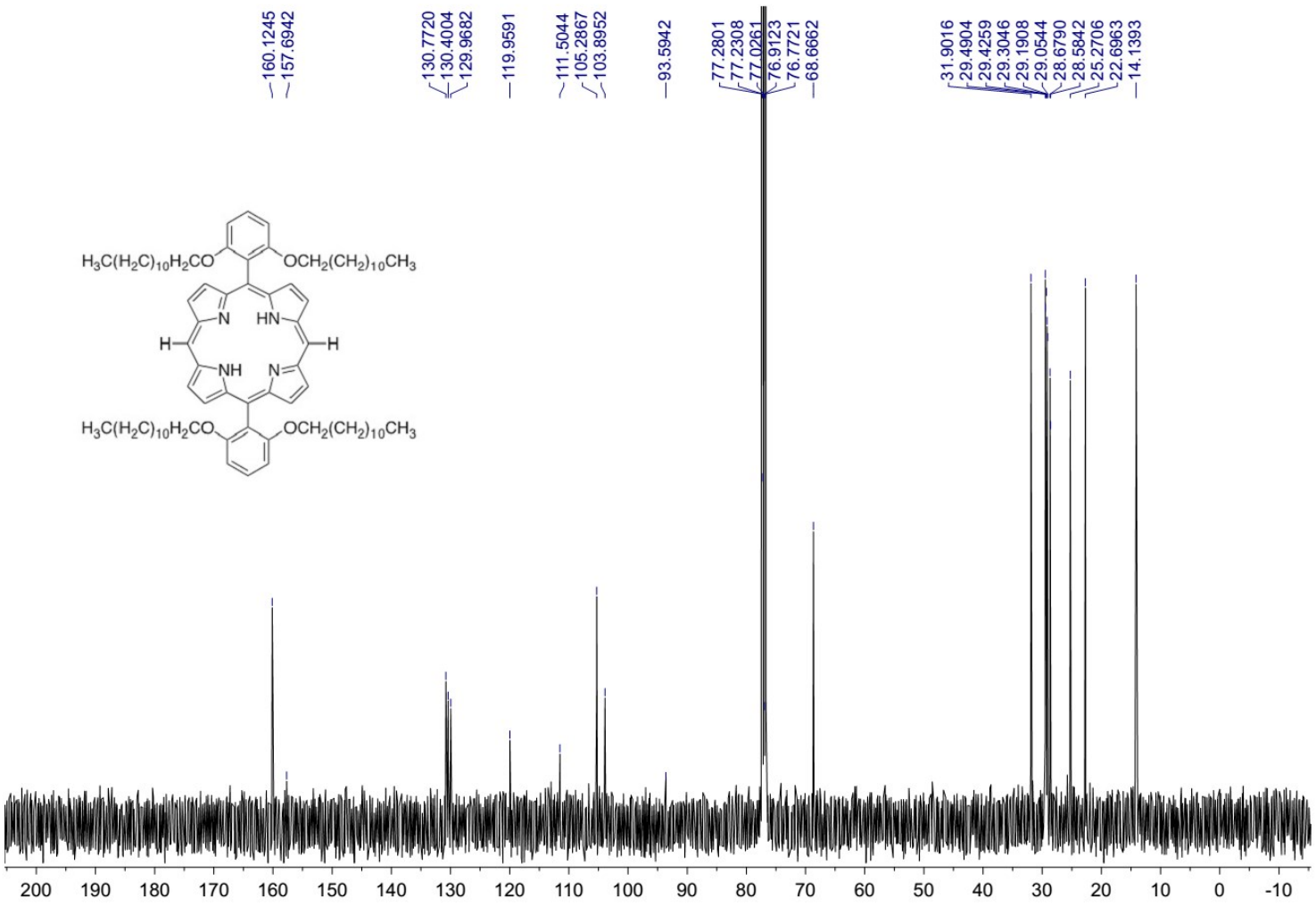

Figure S14b. ^{13}CNMR of 5,15-bis(2,6-di(dodecyloxy)phenyl)porphyrin (10a) in $CDCl_3$

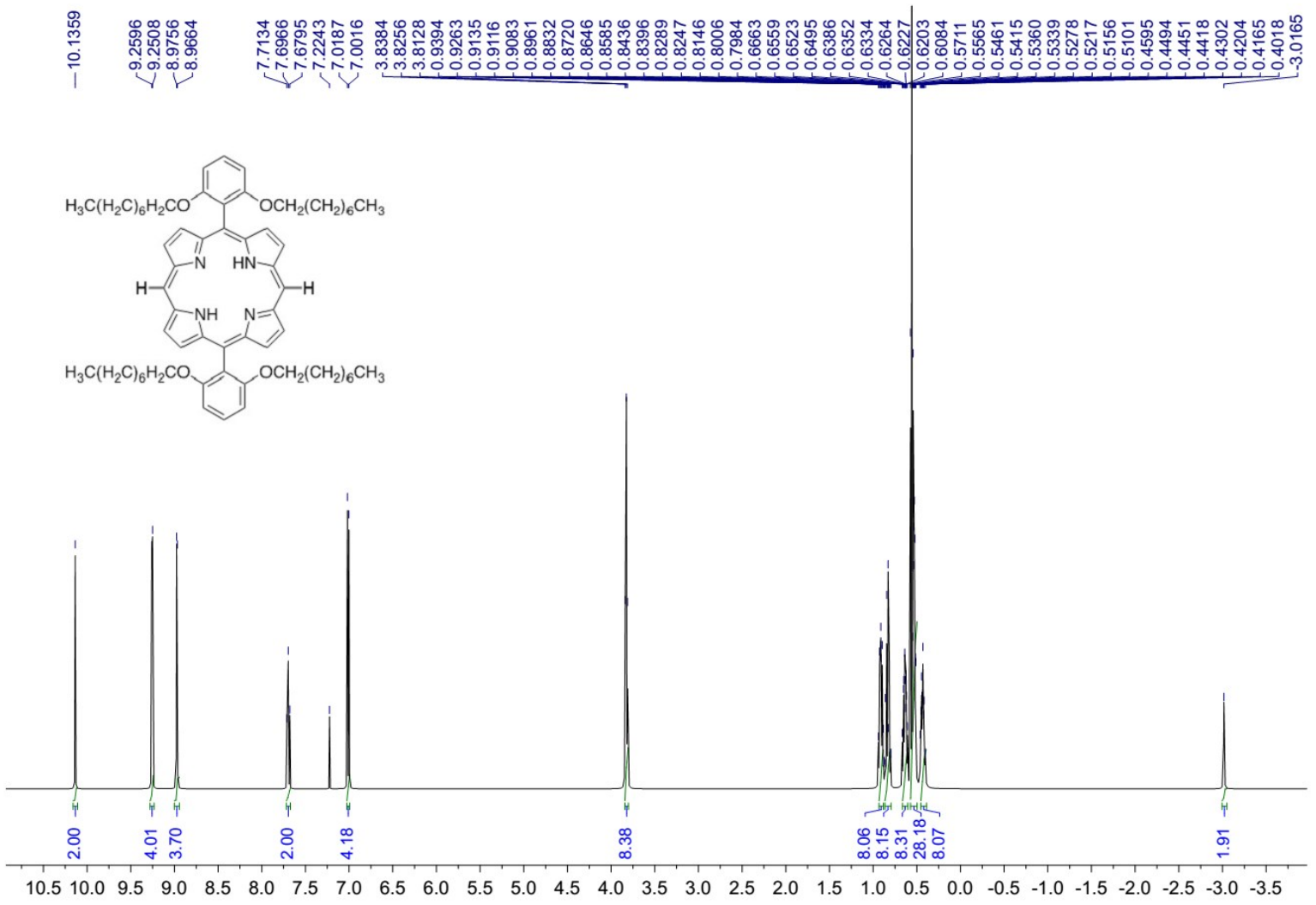

Figure S14c. ^{1}HNMR of 5,15-bis(2,6-di(octyloxy)phenyl)porphyrin (10b) in $CDCl_3$

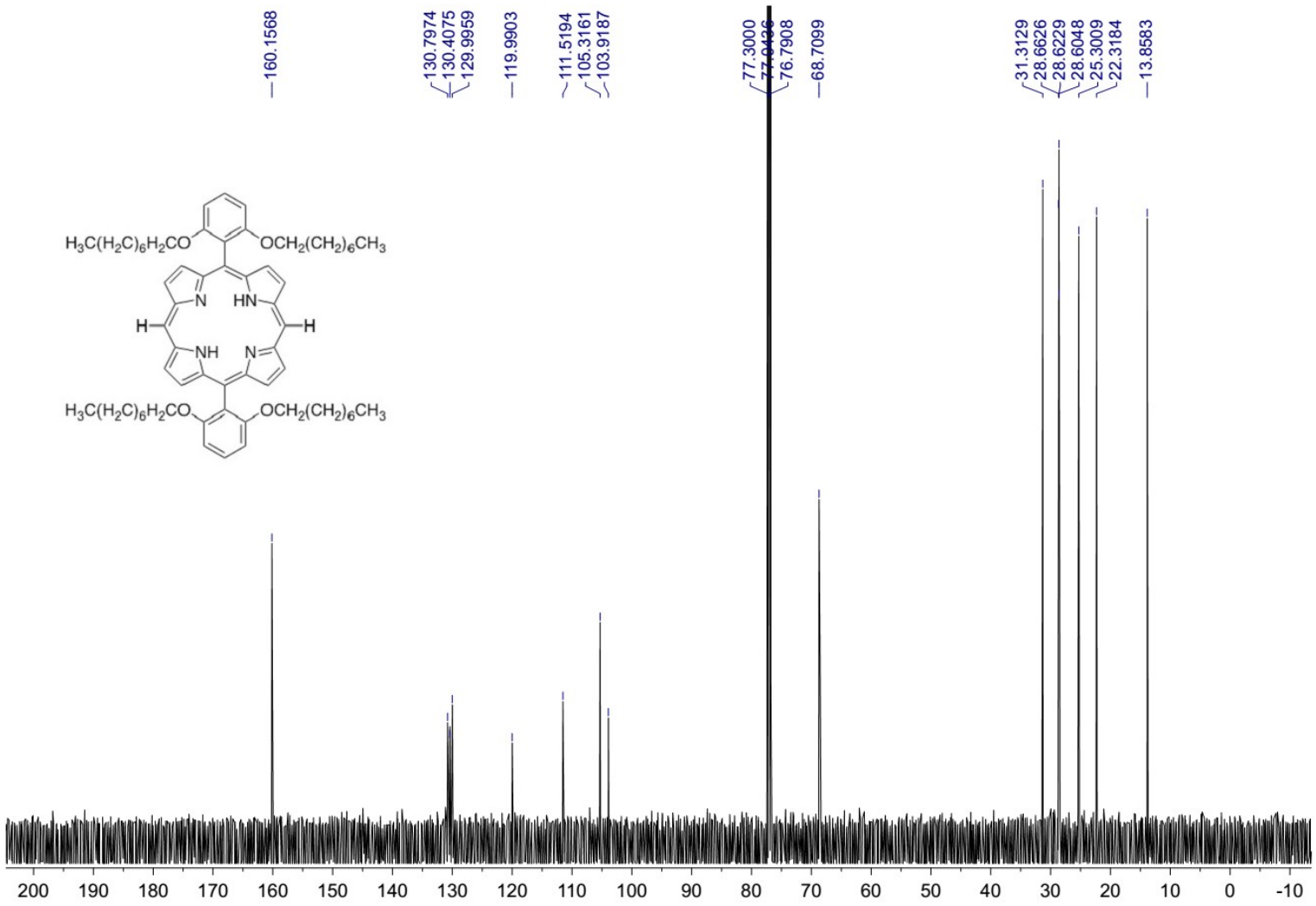

Figure S14d. ^{13}CNMR of 5,15-bis(2,6-di(octyloxy)phenyl)porphyrin (10b) in $CDCl_3$

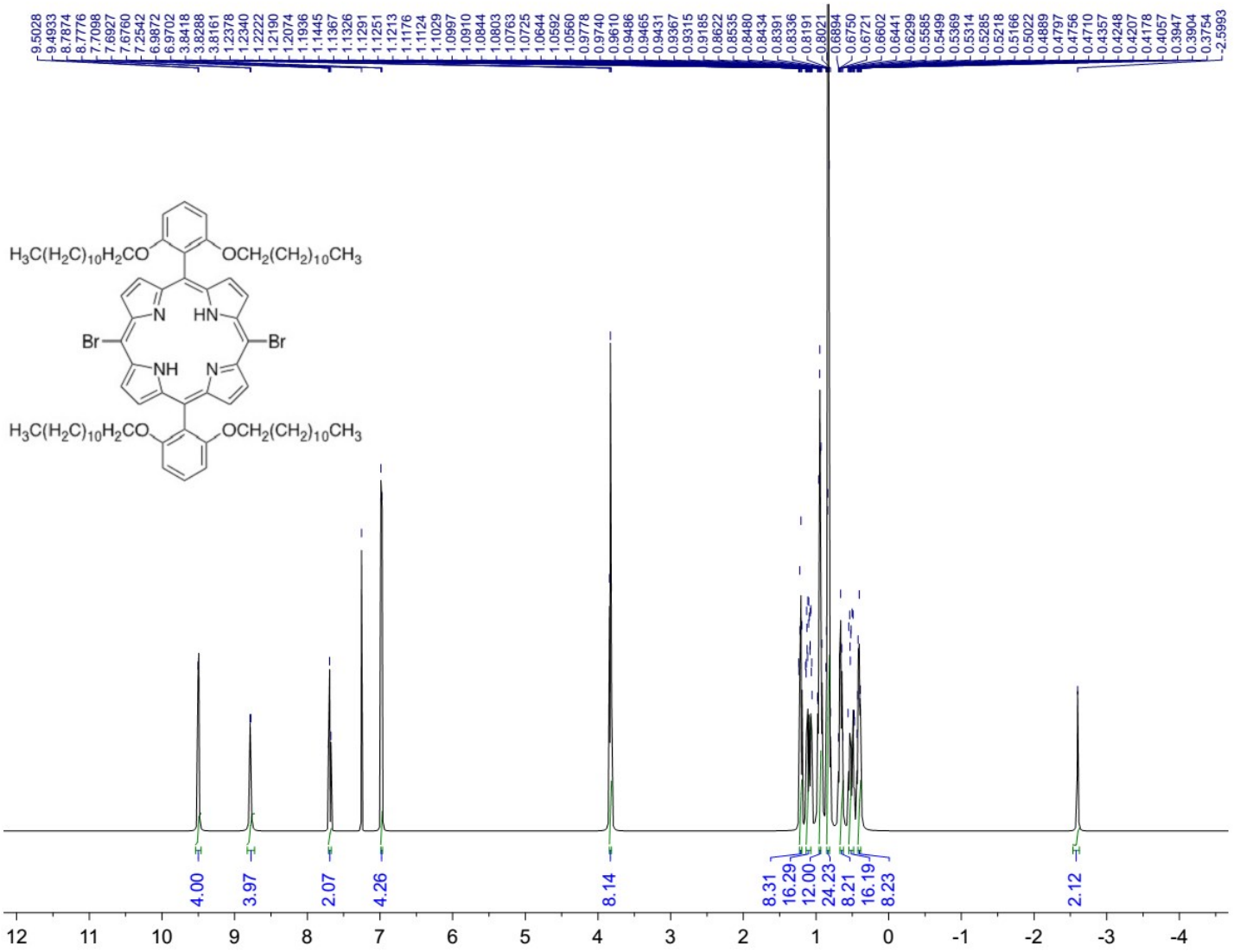

Figure S15a. ^{1}HNMR of 5,15-bisbromo-10,20-bis(2,6-di(dodecyloxy)phenyl)porphyrin (11a) in $CDCl_3$

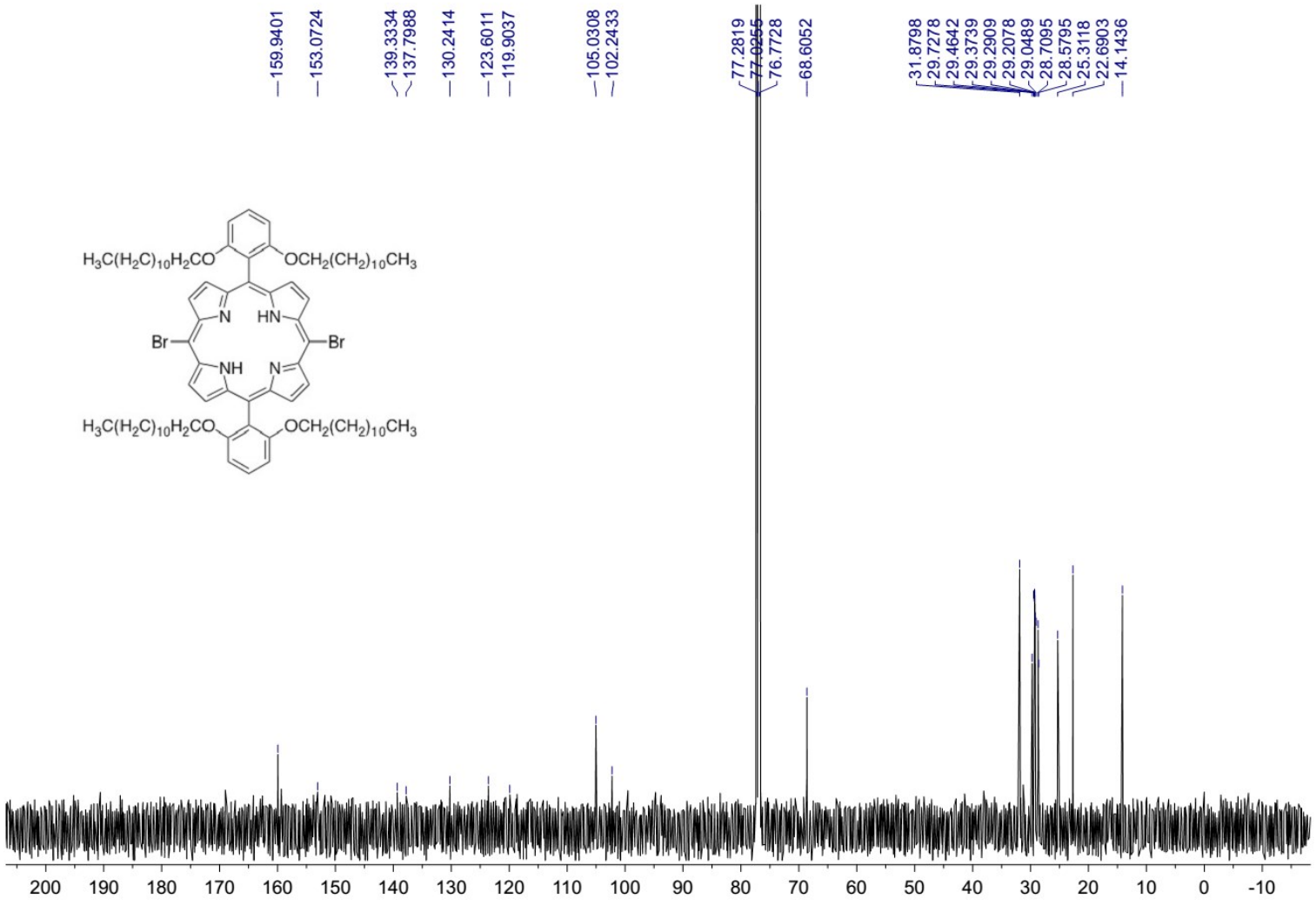

Figure S15b. ^{13}CNMR of 5,15-bisbromo-10,20-bis(2,6-di(dodecyloxy)phenyl)porphyrin (11a) in $CDCl_3$

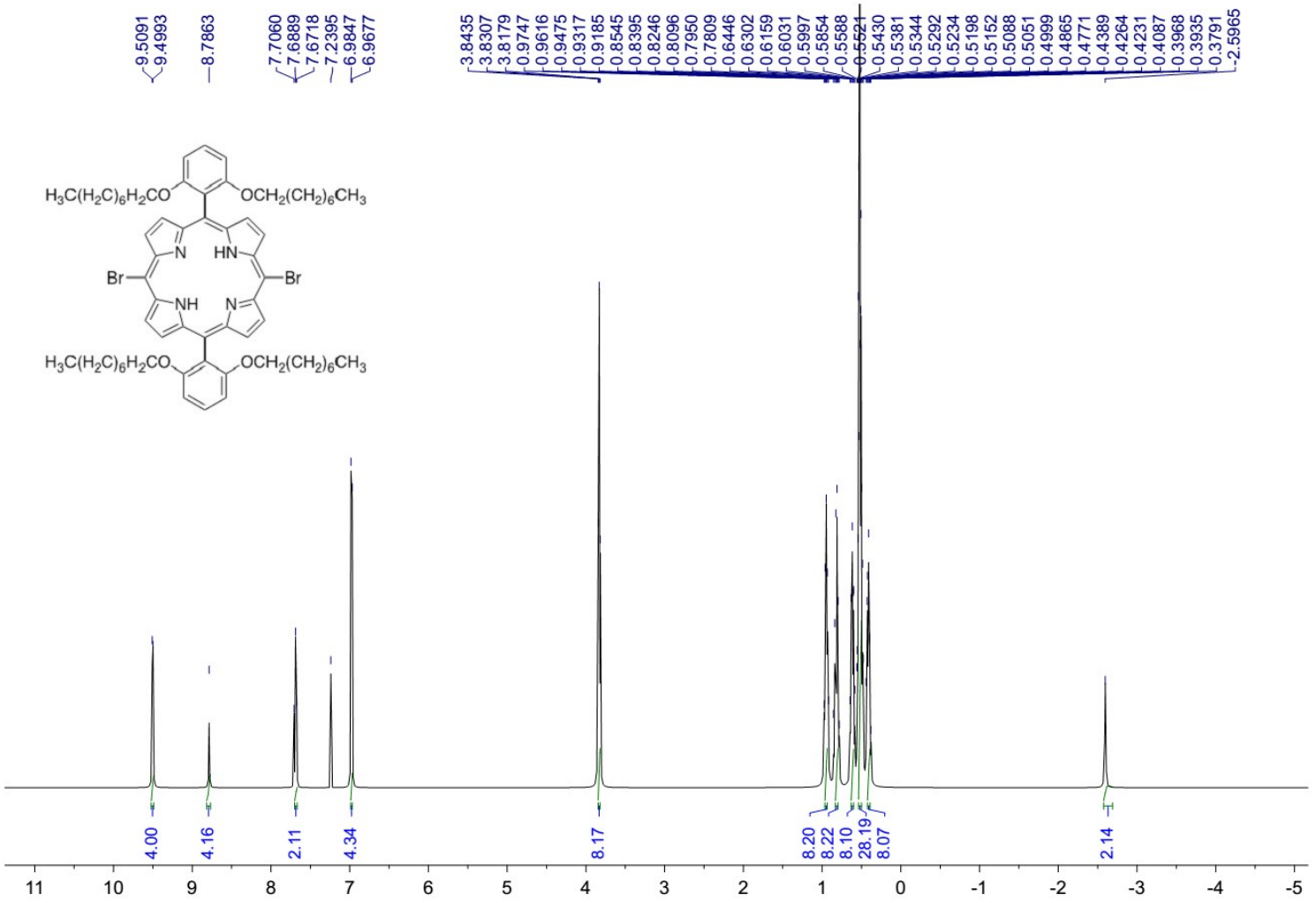

Figure S15c. ^{1}HNMR of 5,15-bisbromo-10,20-bis(2,6-di(octyloxy)phenyl)porphyrin (11b) in $CDCl_3$

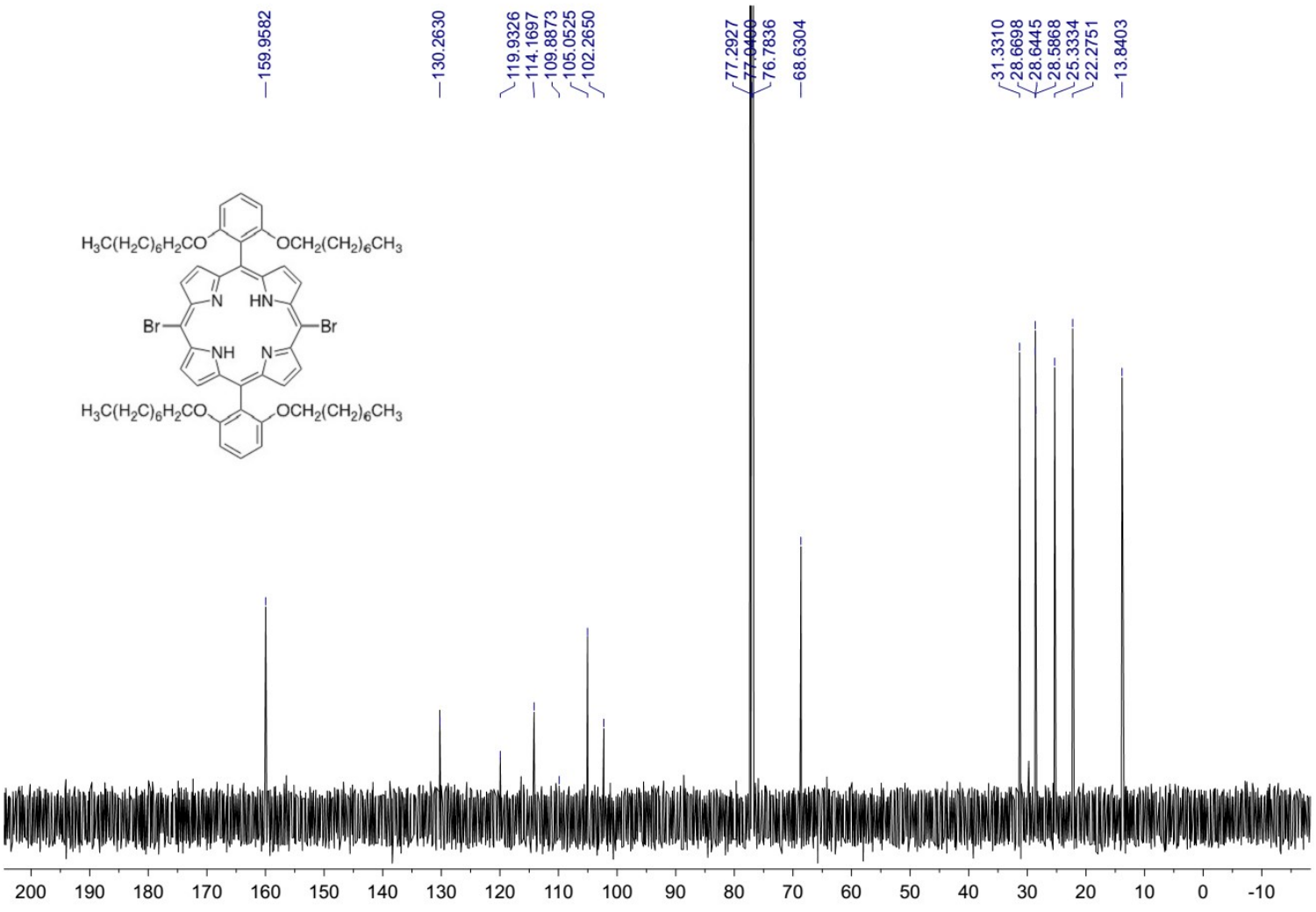

Figure S15d. ^{13}CNMR of 5,15-bisbromo-10,20-bis(2,6-di(octyloxy)phenyl)porphyrin (11b) in $CDCl_3$

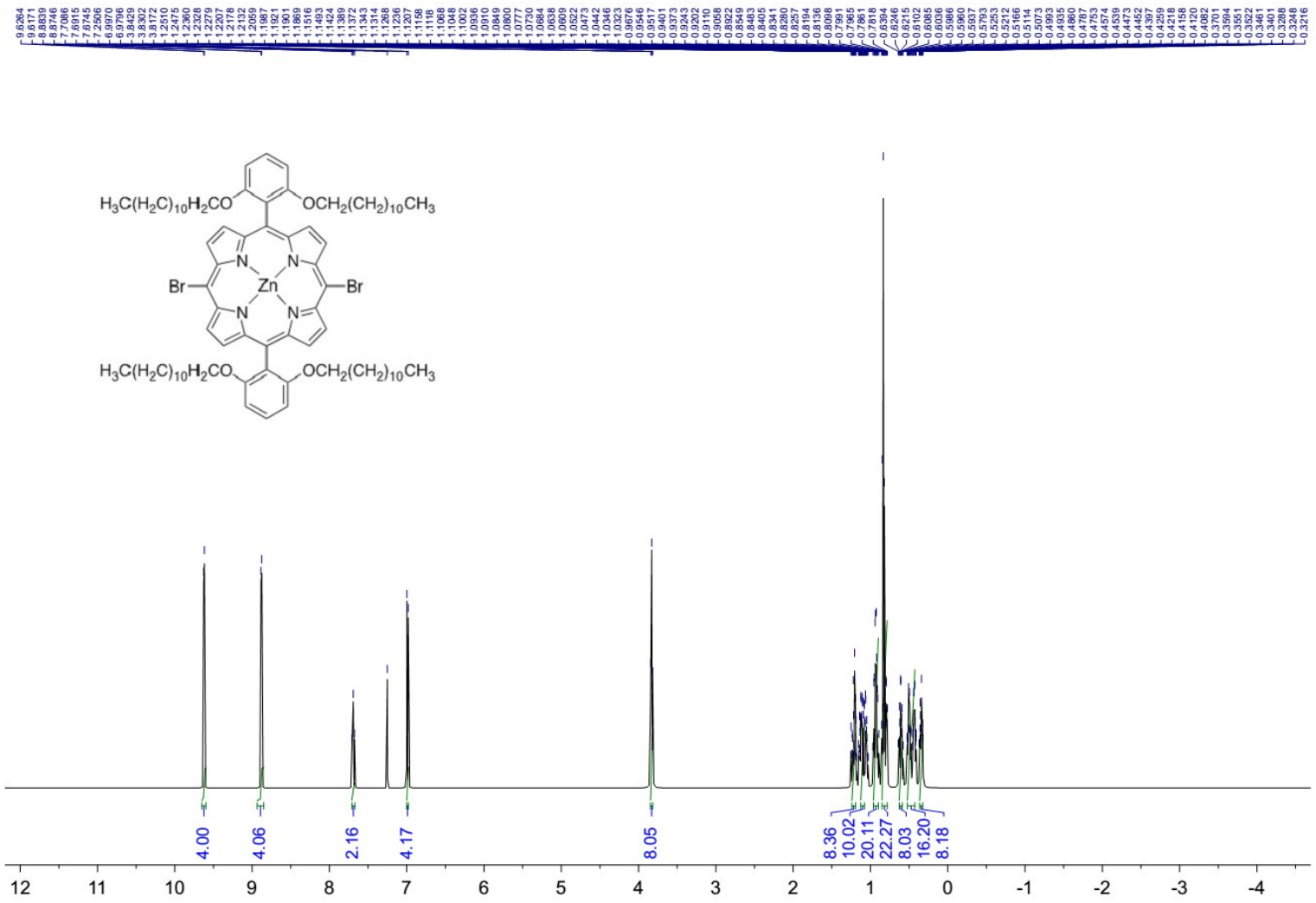

Figure S16a. ^{1}HNMR of [5,15-bisbromo-10,20-bis(2,6-di(dodecyloxy)phenyl)porphinato]zinc(II) (12a) in $CDCl_3$

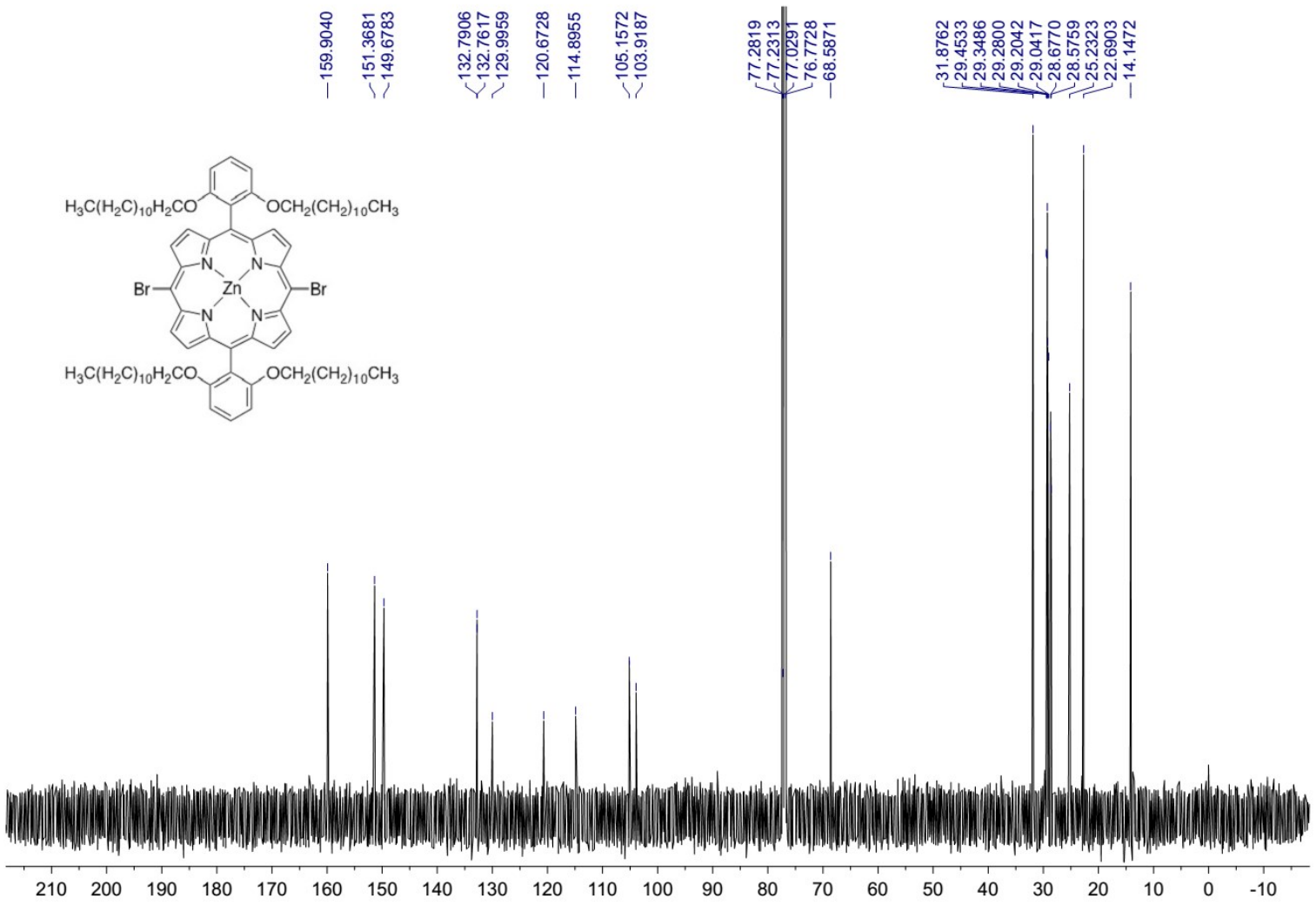

Figure S16b. ^{13}CNMR of [5,15-bisbromo-10,20-bis(2,6-di(dodecyloxy)phenyl)porphinato]zinc(II) (12a) in $CDCl_3$

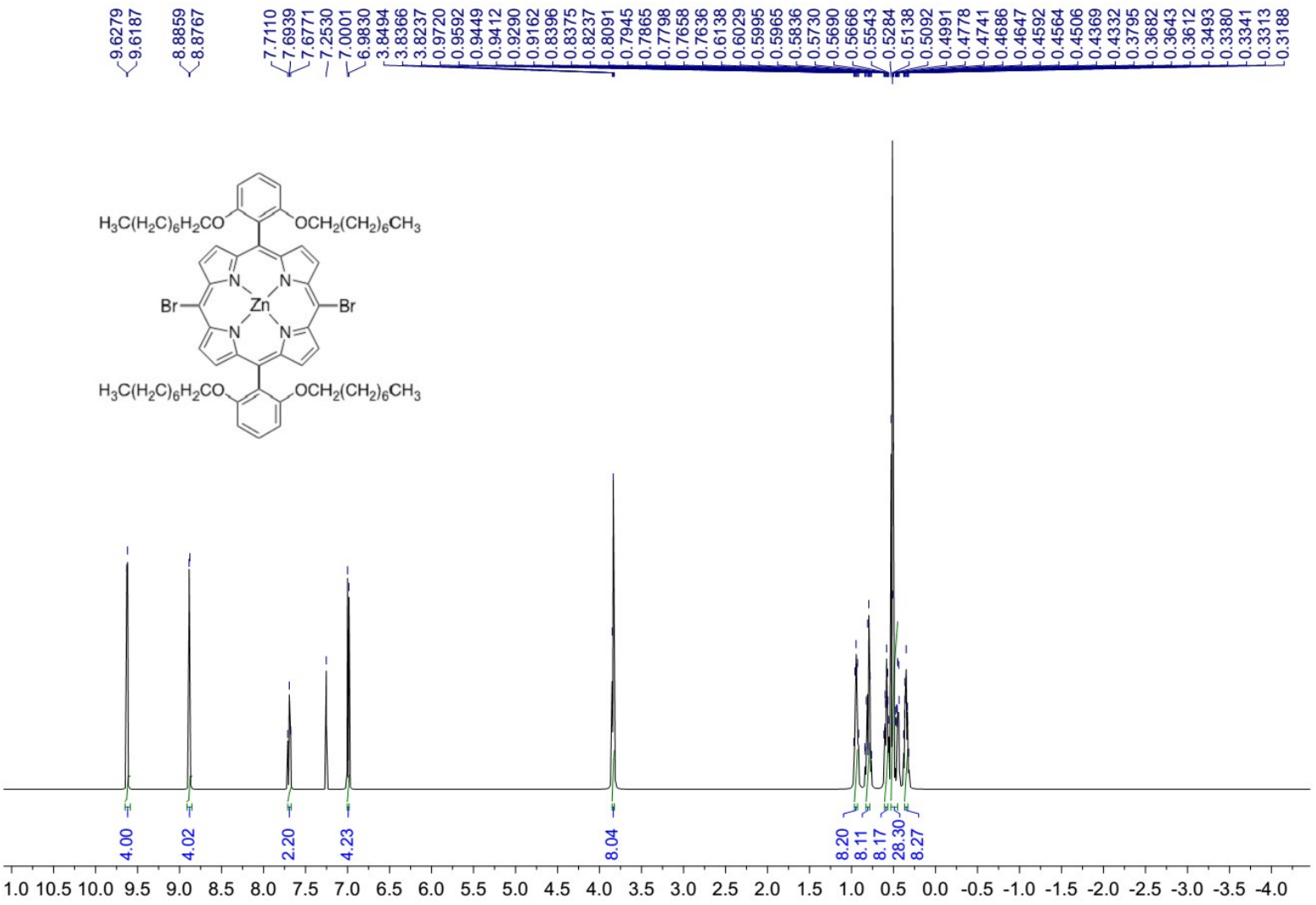

Figure S16c. ^{1}HNMR of [5,15-bisbromo-10,20-bis(2,6-di(octyloxy)phenyl)porphinato]zinc(II) (12b) in $CDCl_3$

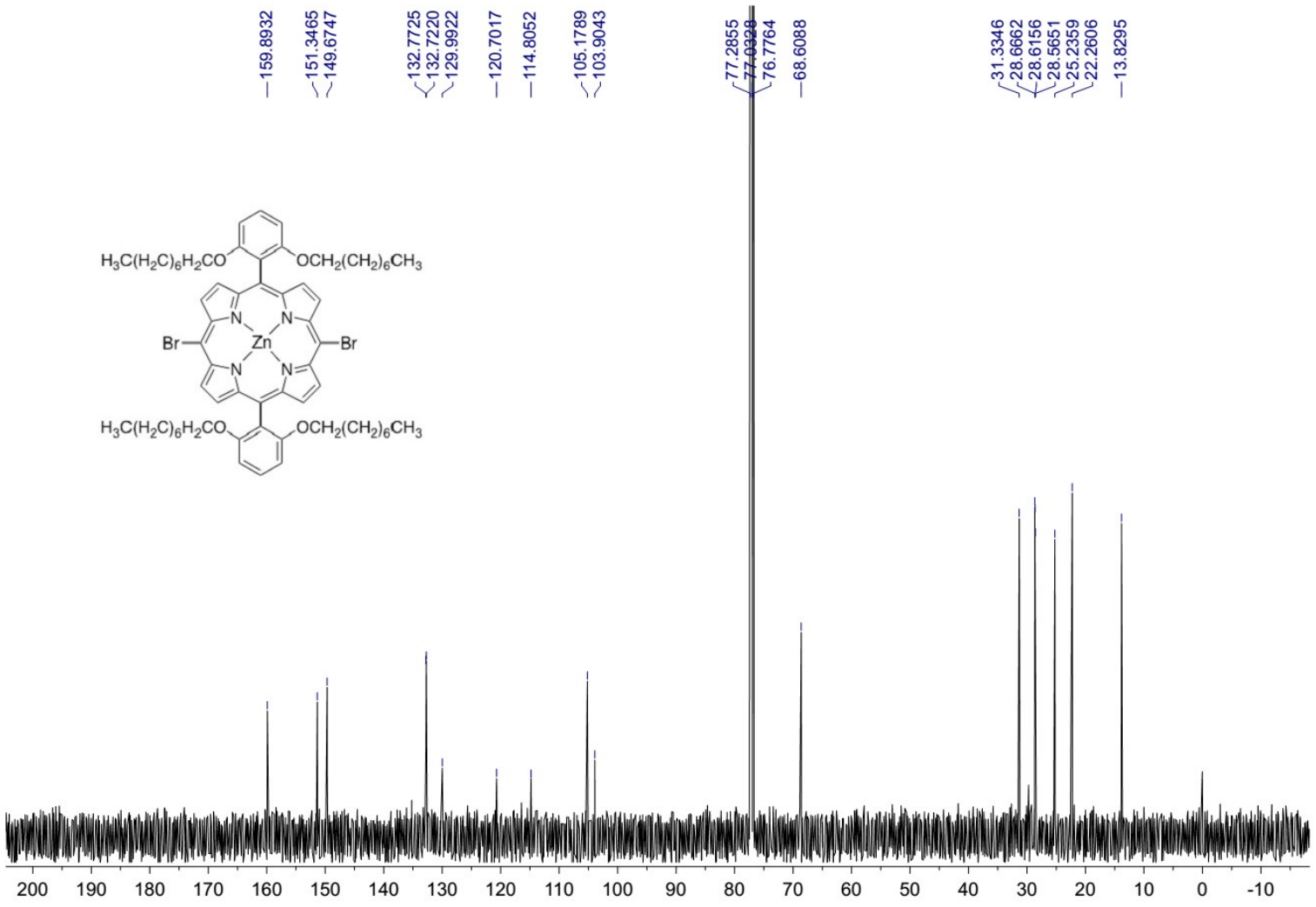

Figure S16d. ^{13}CNMR of [5,15-bisbromo-10,20-bis(2,6-di(octyloxy)phenyl)porphinato]zinc(II) (12b) in $CDCl_3$

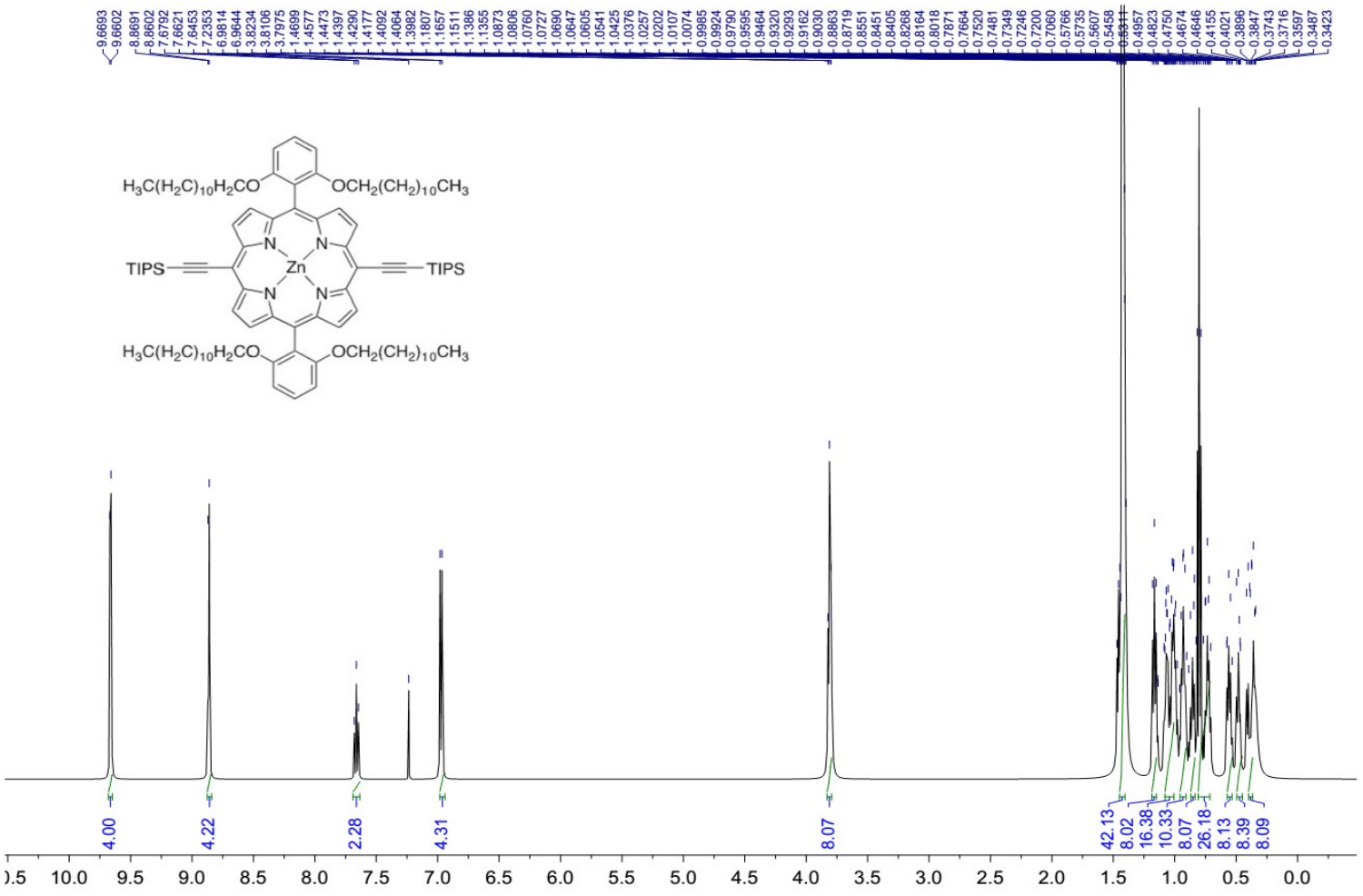

Figure S17a. ^{1}HNMR of [5,15-bis(2,6-di(dodecyloxy)phenyl)-10,20-bis(triisopropylsilyl)ethynyl)porphinato]zinc(II) (13a) in $CDCl_3$

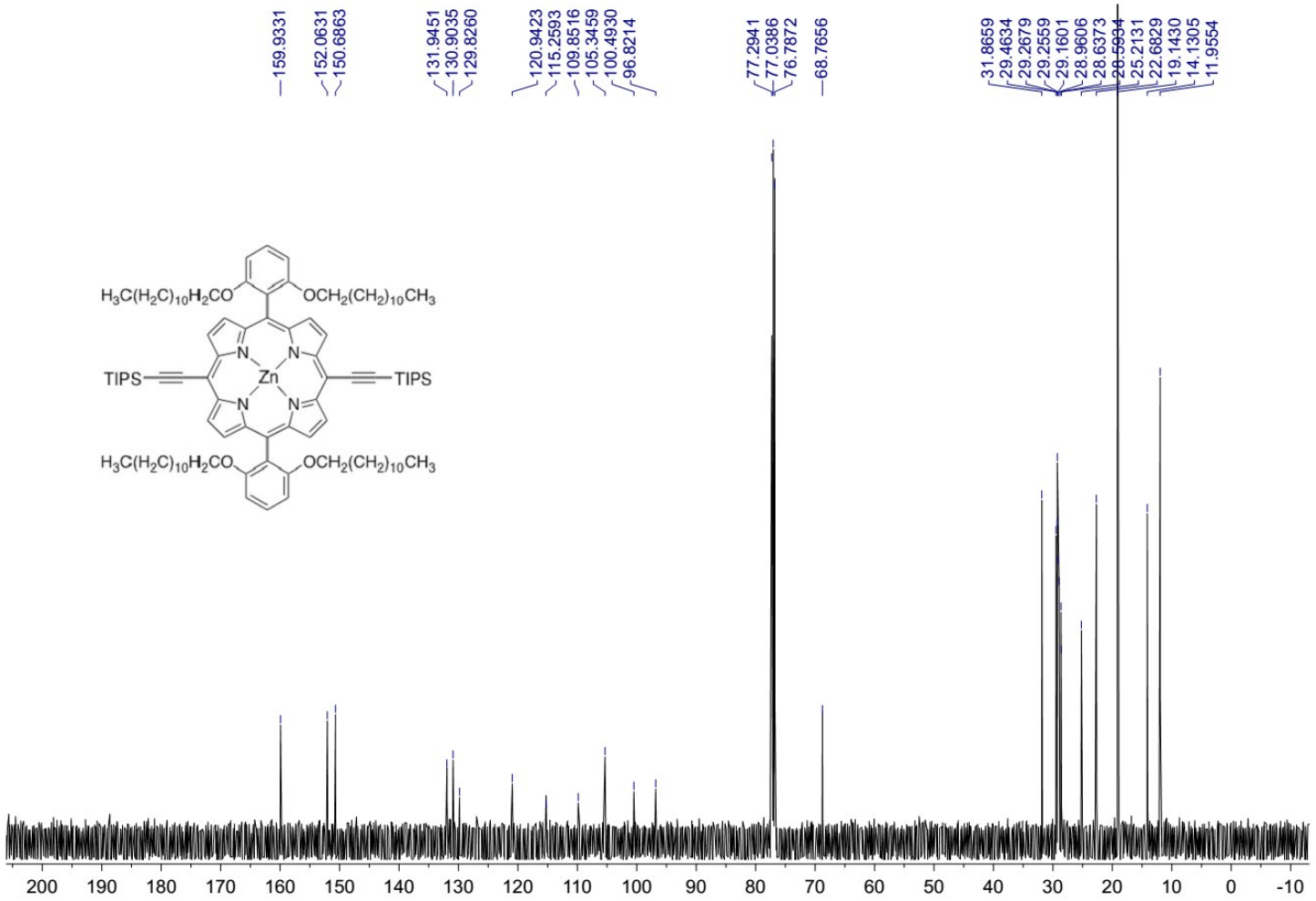

Figure S17b. ^{13}CNMR of [5,15-bis(2,6-di(dodecyloxy)phenyl)-10,20-bis(triisopropylsilyl)ethynyl)porphinato]zinc(II) (13a) in $CDCl_3$

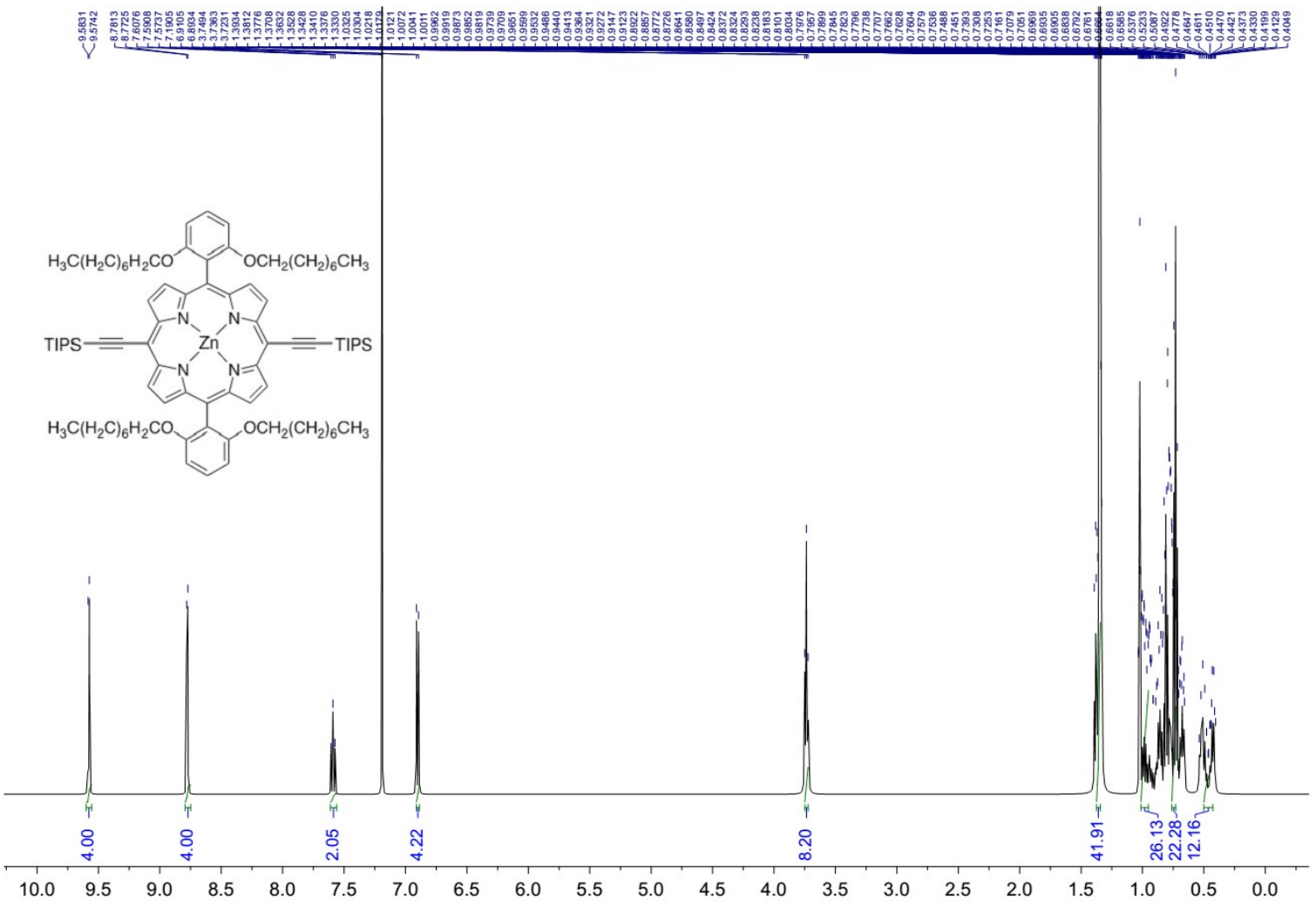

Figure S17c. ^{1}HNMR of [5,15-bis(2,6-di(octyloxy)phenyl)-10,20-bis(triisopropylsilyl)ethynyl)porphinato]zinc(II) (13b) in $CDCl_3$

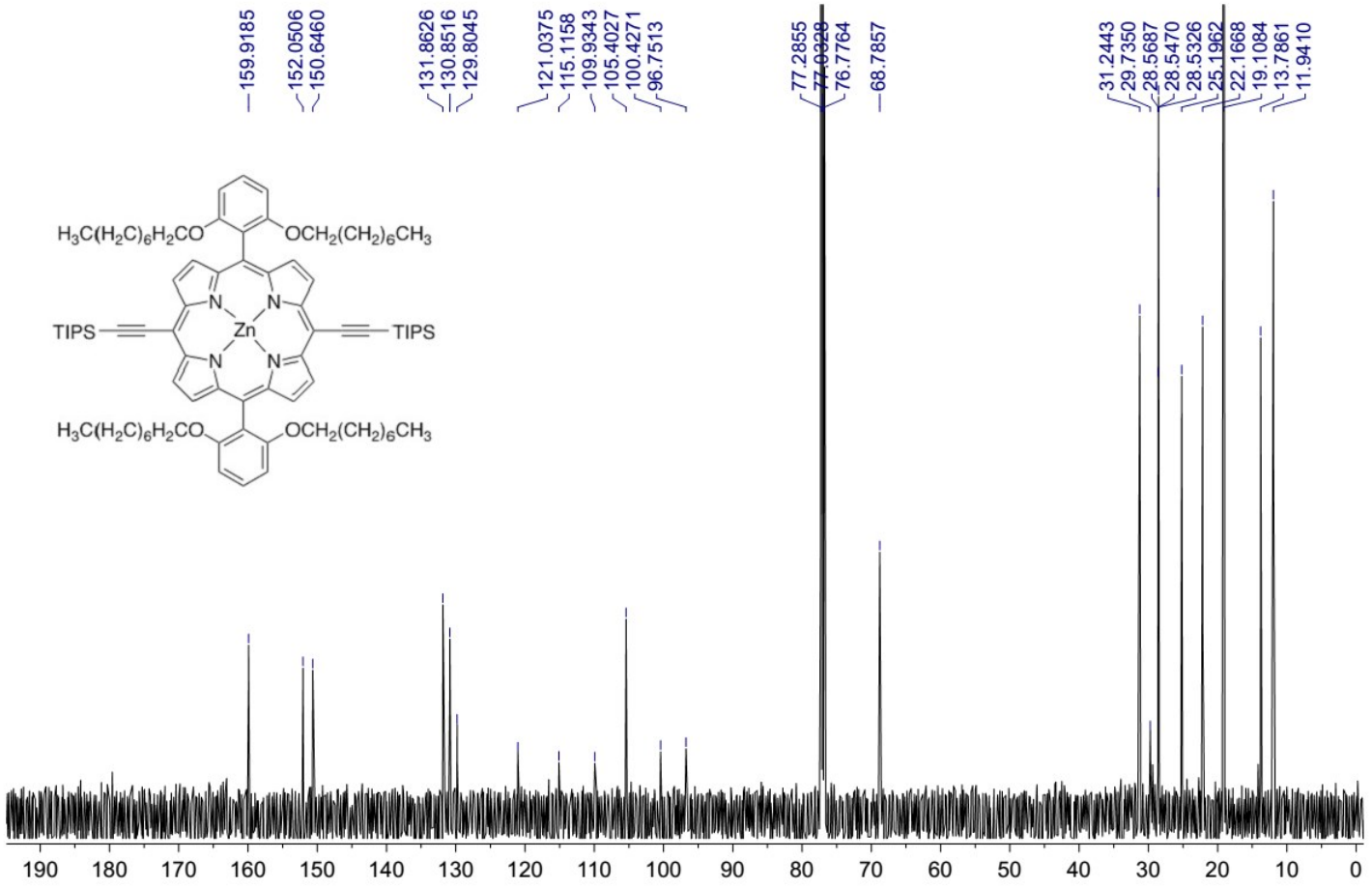

Figure S17d. ^{13}CNMR of [5,15-bis(2,6-di(octyloxy)phenyl)-10,20-bis(triisopropylsilyl)ethynyl)porphinato]zinc(II) (13b) in $CDCl_3$

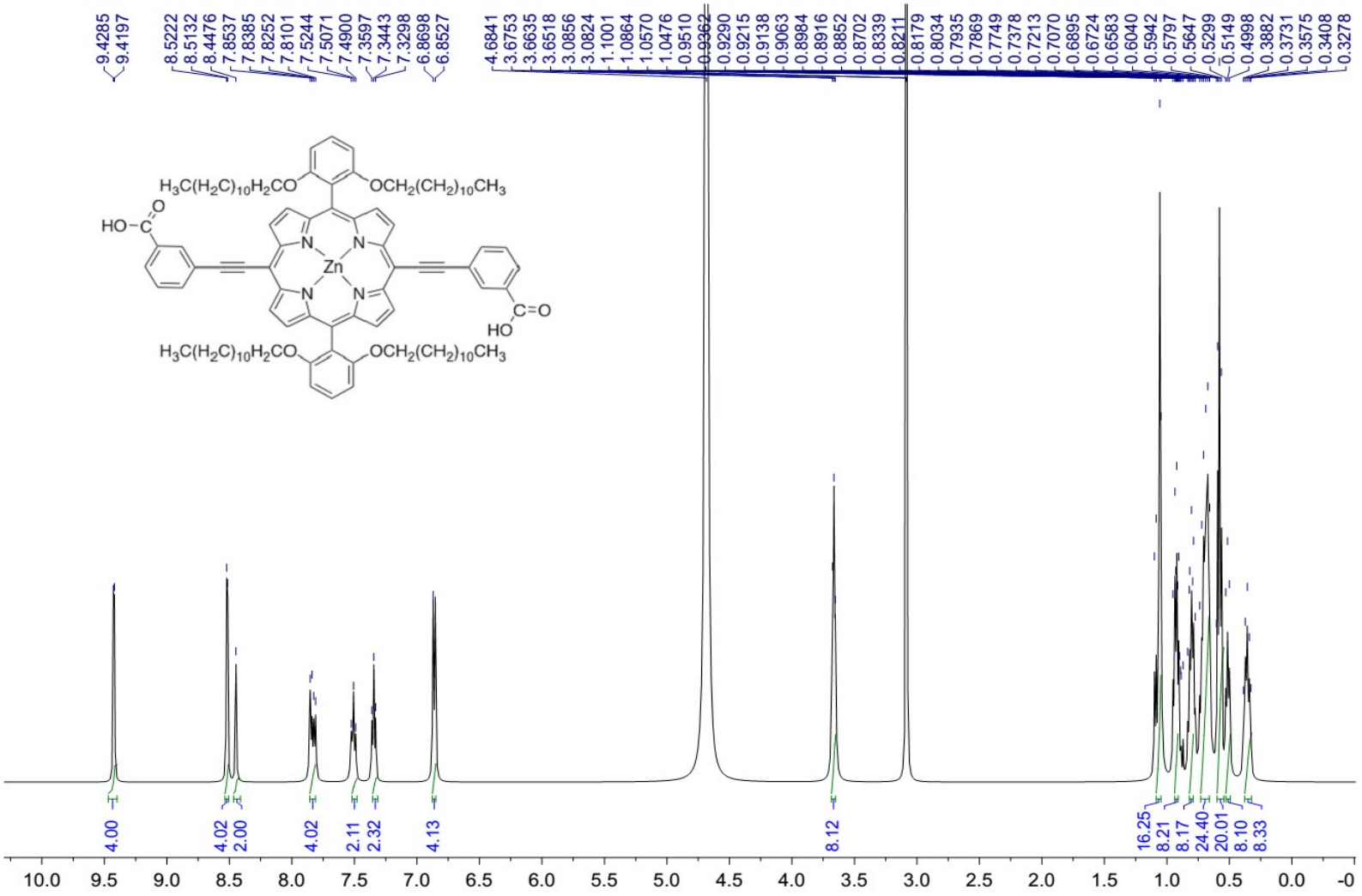

Figure S18a. ^{1}HNMR of [5,15-bis(2,6-di(dodecyloxy)phenyl)-10,20-bis(3-carboxylphenyl)ethynyl)porphinato]zinc(II) (Por-C_{12}-RA_1) in CD_3OH

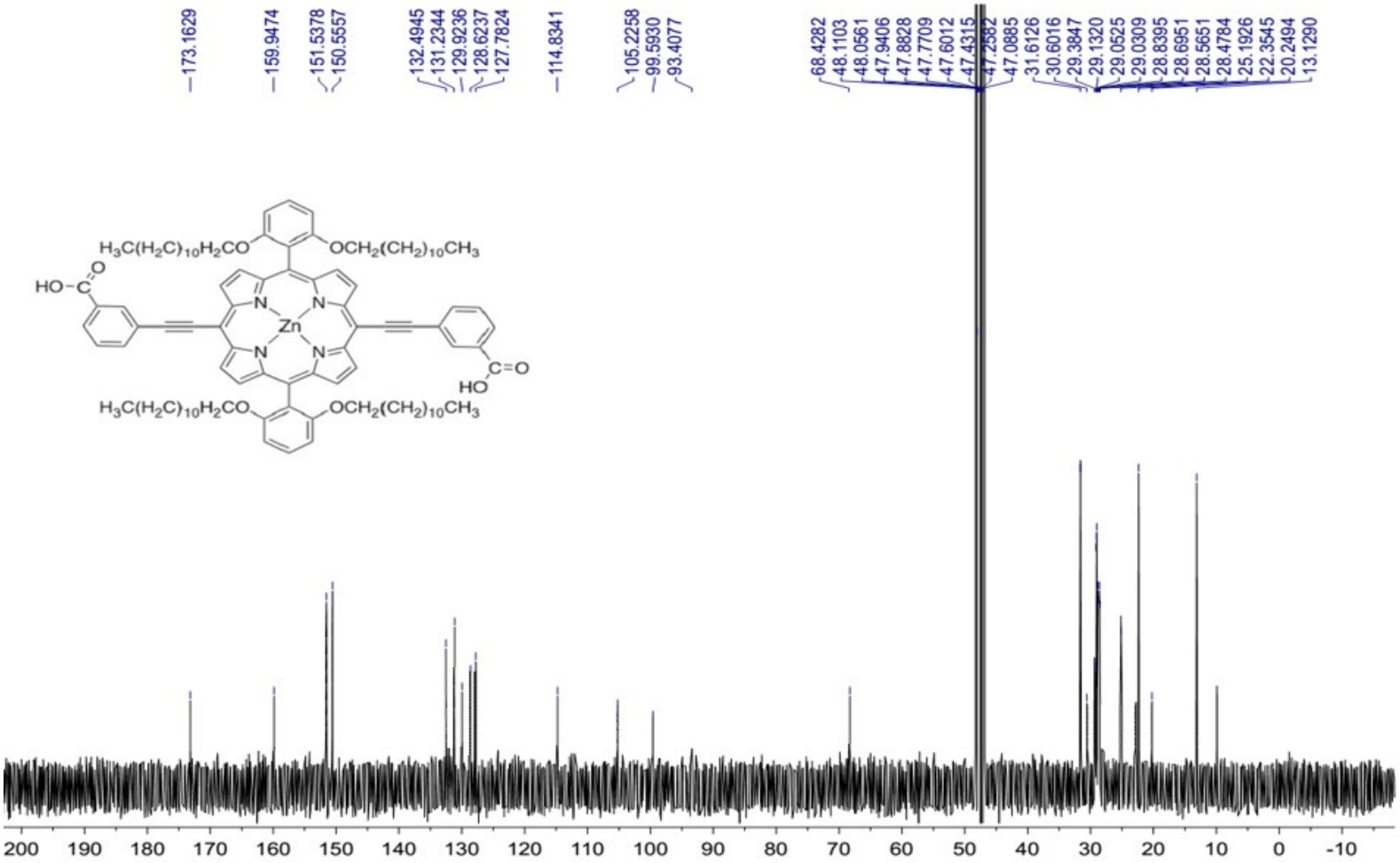

Figure S18b. ^{13}CNMR of [5,15-bis(2,6-di(dodecyloxy)phenyl)-10,20-bis(3-carboxylphenyl)ethynyl)porphinato]zinc(II) (Por-C_{12}-RA_1) in CD_3OH

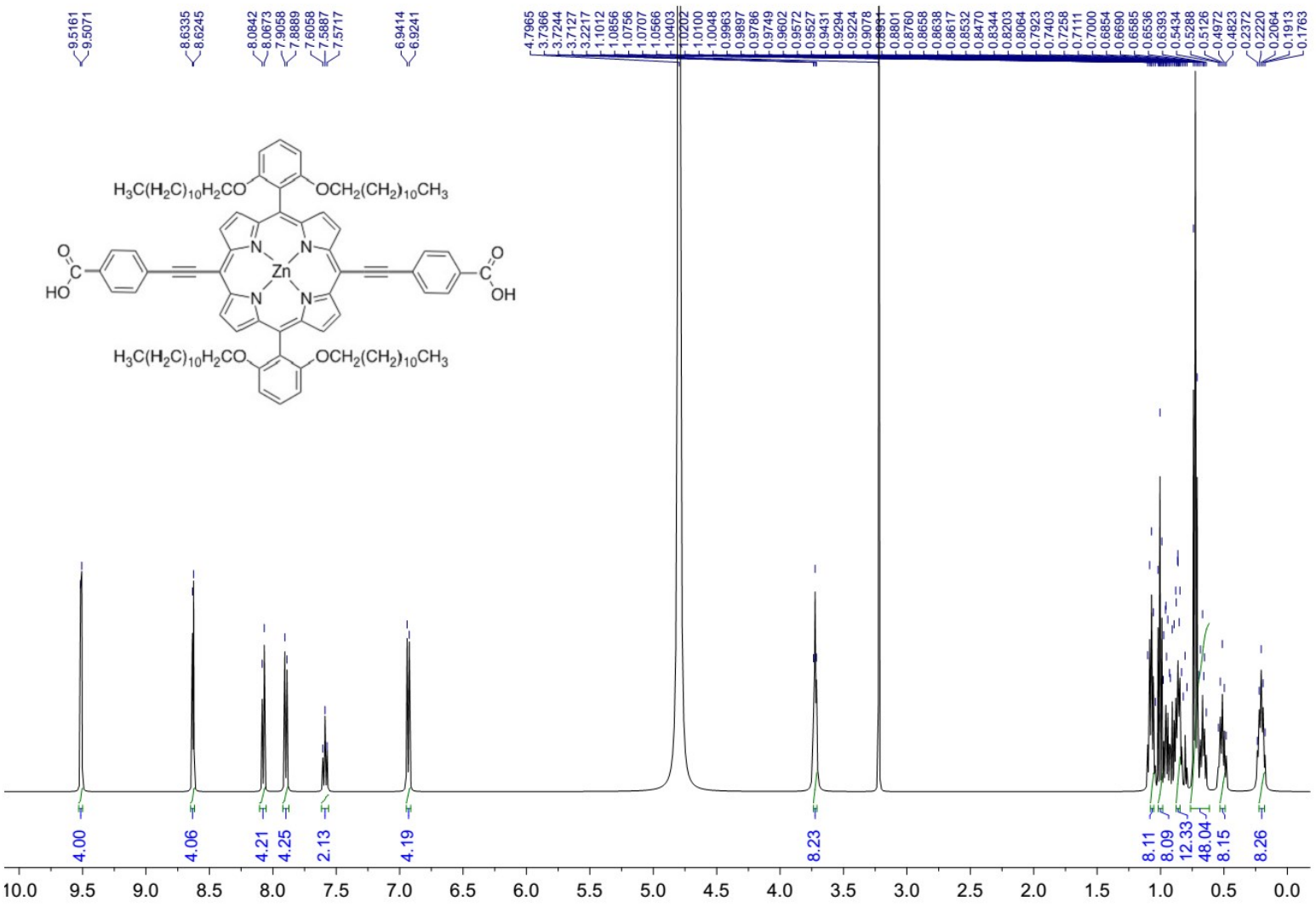

Figure S19a. ^{1}HNMR of [5,15-bis(2,6-di(dodecyloxy)phenyl)-10,20-bis(4-carboxylphenyl)ethynyl)porphyrinato]zinc(II) (Por-C_{12}-RA_2) in CD_3OH

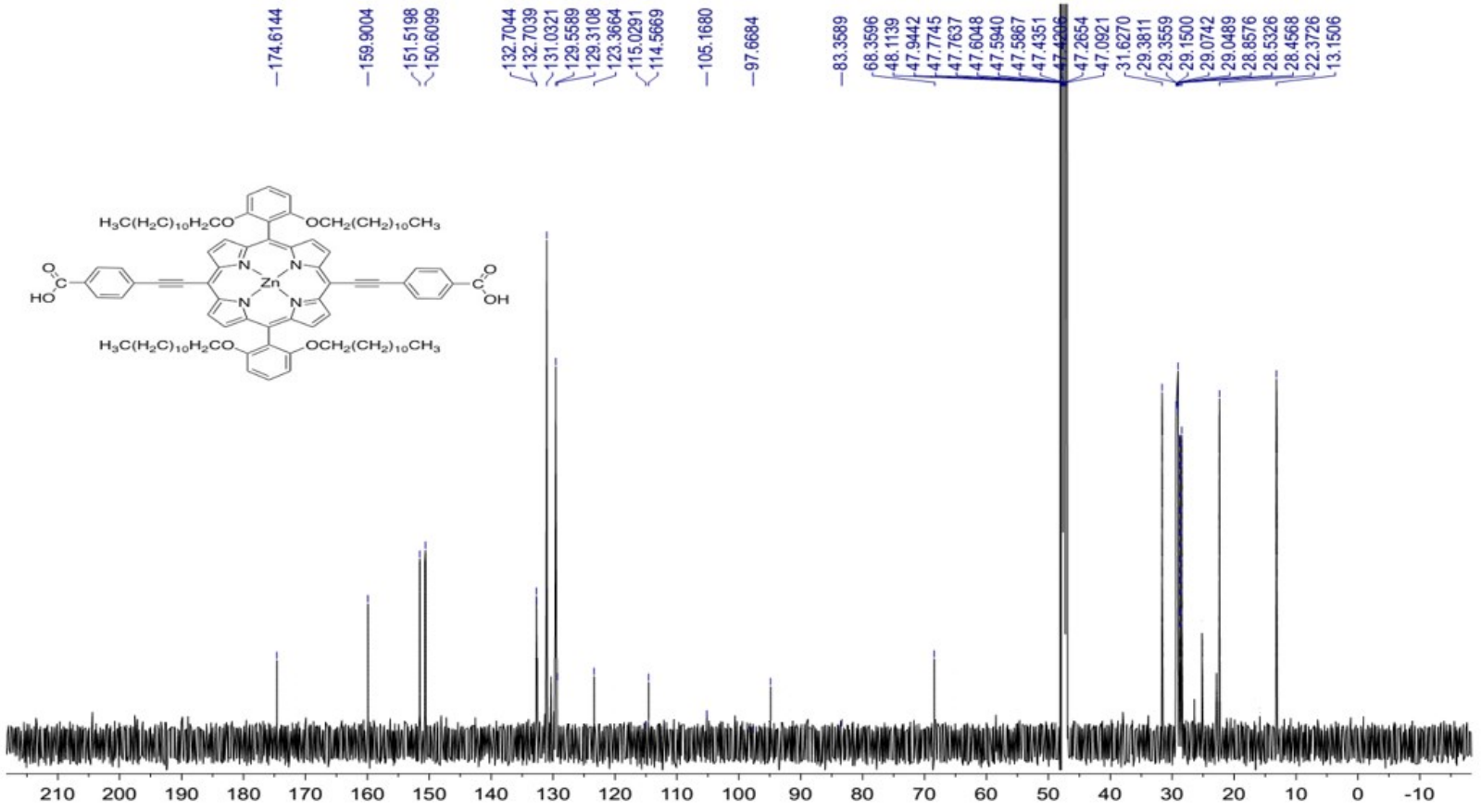

Figure S19b. ^{13}CNMR of [5,15-bis(2,6-di(dodecyloxy)phenyl)-10,20-bis(4-carboxylphenyl)ethynyl)porphyrinato]zinc(II) (Por-C_{12}-RA_2) in CD_3OH

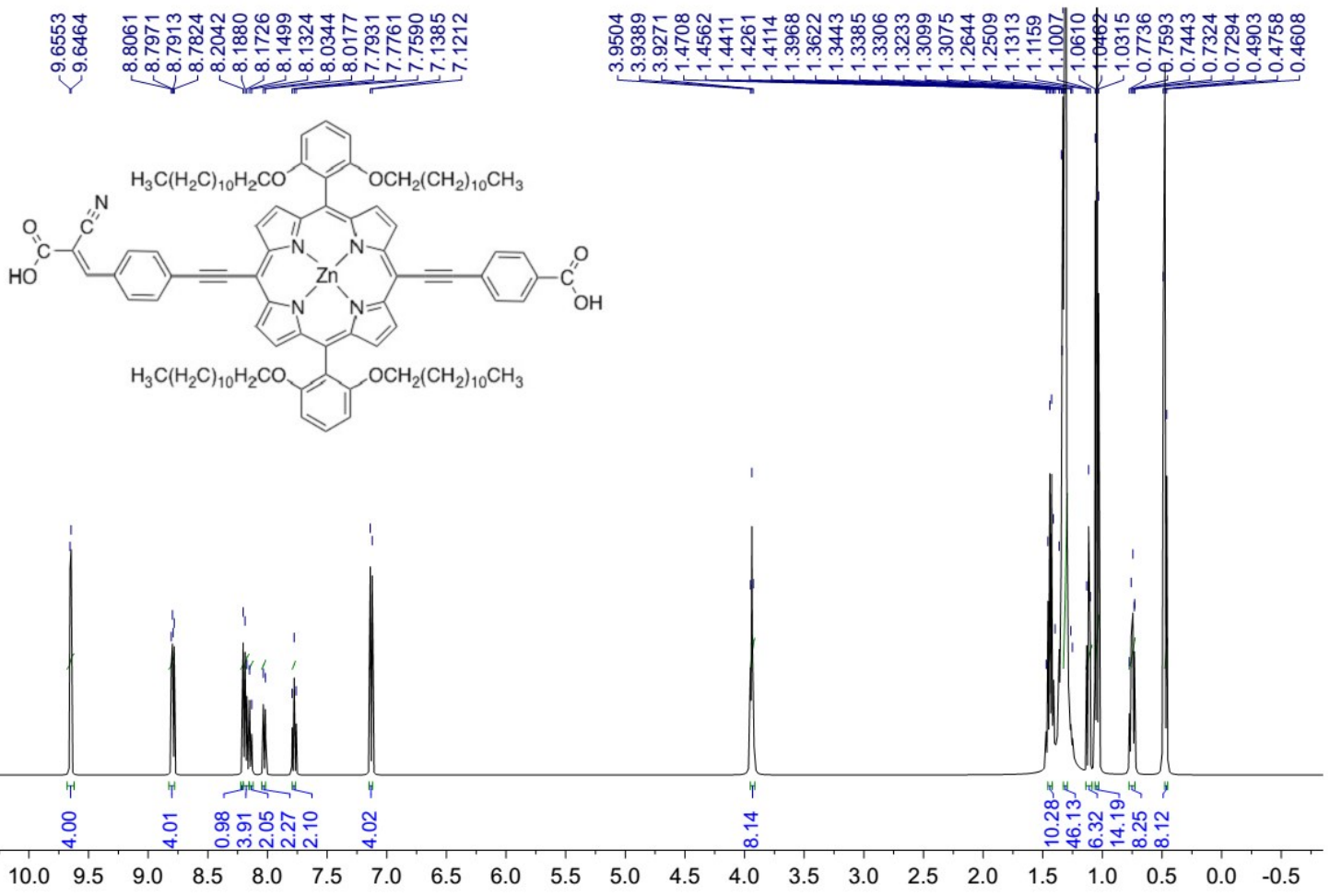

Figure S20a. ^{1}HNMR of [5,15-bis(2,6-di(dodecyloxy)phenyl)-10-[(4-carboxylphenyl)ethynyl]-20-[(4-(2-cyanopropenoicacid)phenyl)ethynyl] porphyrinato]zinc(II) (Por-C_{12}-RA_3) in CD_3OH

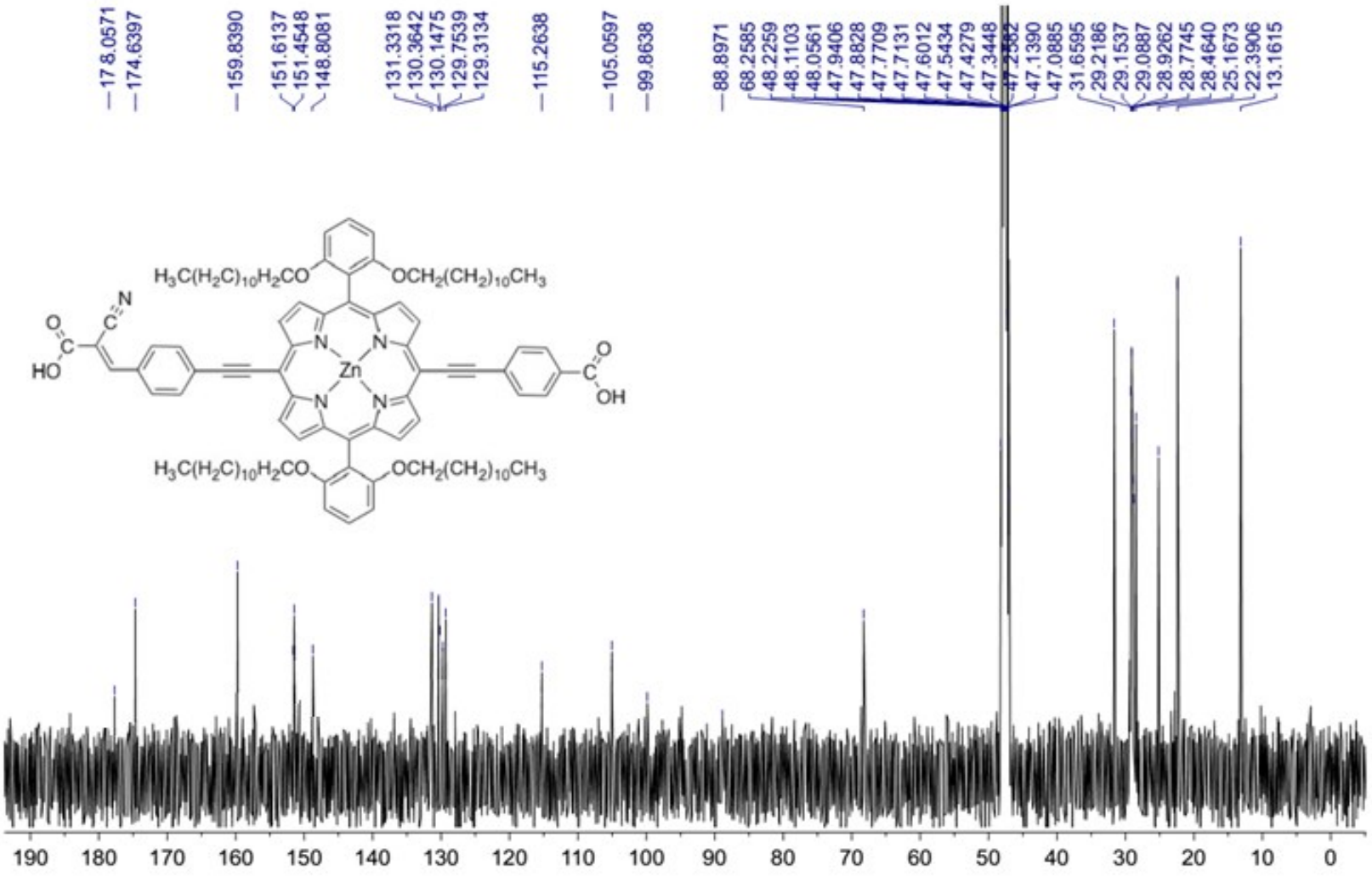

Figure S20b. ^{13}CNMR of [5,15-bis(2,6-di(dodecyloxy)phenyl)-10-[(4-carboxylphenyl)ethynyl]-20-[(4-(2-cyanopropenoicacid)phenyl)ethynyl] porphyrinato]zinc(II) (Por-C_{12}-RA_3) in CD_3O

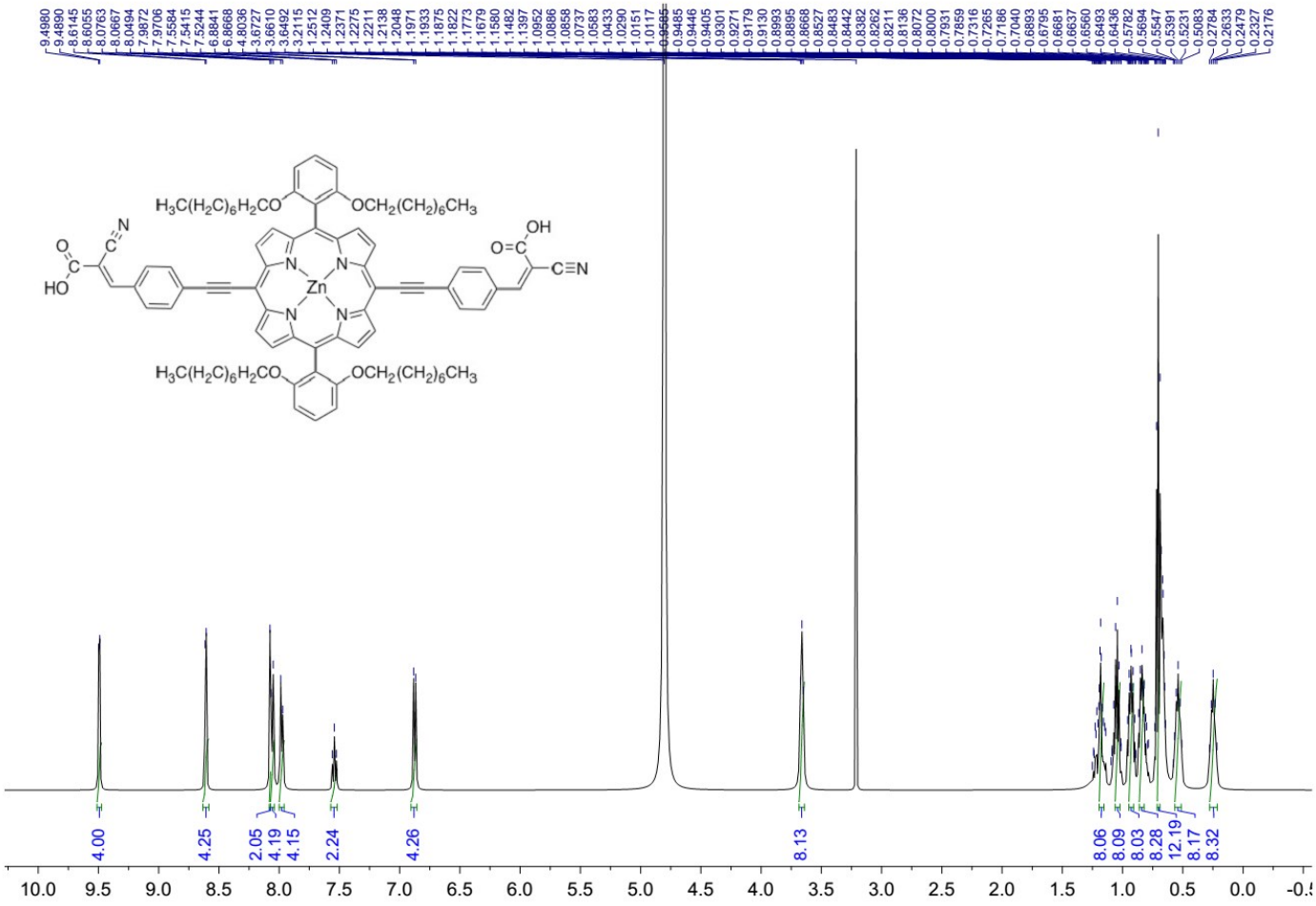

Figure S21a. ^{1}HNMR of [5,15-bis(2,6-di(octyloxy)phenyl)-10,20-[(4-(2-cyanopropenoicacid)phenyl)ethynyl]porphyrinato]zinc(II) (Por-C_8-RA_4) in CD_3OH

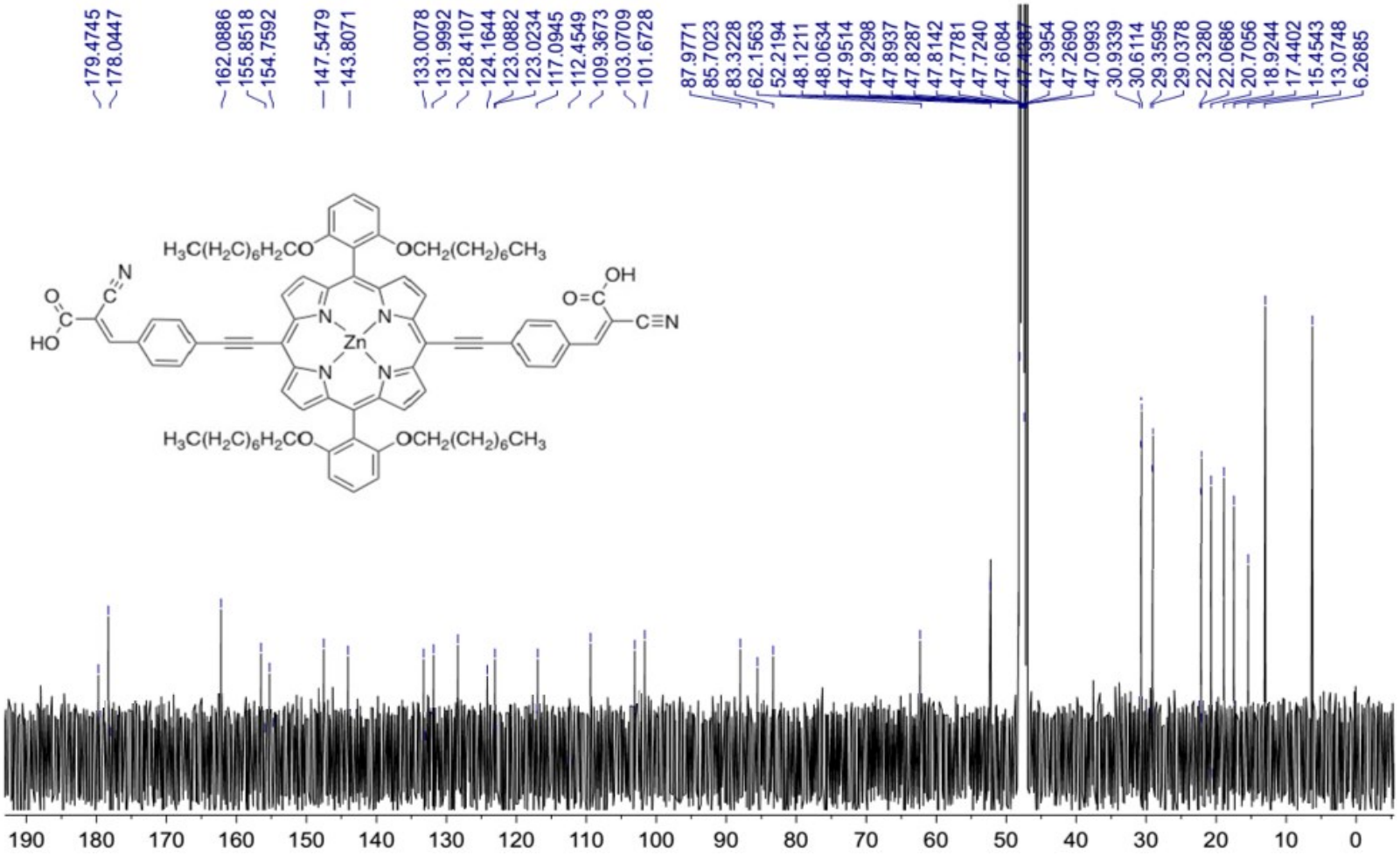

Figure S21b. ^{13}CNMR of [5,15-bis(2,6-di(octyloxy)phenyl)-10,20-[(4-(2-cyanopropenoicacid)phenyl)ethynyl]porphyrinato]zinc(II) (Por-C_8-RA_4) in CD_3OH

XVI. References

1. Gaussian09, R. A., 1, MJ Frisch, GW Trucks, HB Schlegel, GE Scuseria, MA Robb, JR Cheeseman, G. Scalmani, V. Barone, B. Mennucci, GA Petersson et al., Gaussian. *Inc., Wallingford CT* **2009**.
2. Lee, C.; Yang, W.; Parr, R., Density-functional exchange-energy approximation with correct asymptotic behaviour. *Phys. Rev. B* **1988,** 37, 785-789.
3. Hay, P. J.; Wadt, W. R., Ab initio effective core potentials for molecular calculations. Potentials for K to Au including the outermost core orbitals. *The Journal of Chemical Physics* **1985,** 82, (1), 299-310.
4. Hay, P. J.; Wadt, W. R., Ab initio effective core potentials for molecular calculations. Potentials for the transition metal atoms Sc to Hg. *The Journal of chemical physics* **1985,** 82, (1), 270-283.
5. Hehre, W. J.; Ditchfield, R.; Pople, J. A., Self—consistent molecular orbital methods. XII. Further extensions of gaussian—type basis sets for use in molecular orbital studies of organic molecules. *The Journal of Chemical Physics* **1972,** 56, (5), 2257-2261.
6. Hariharan, P. C.; Pople, J. A., The influence of polarization functions on molecular orbital hydrogenation energies. *Theoretical Chemistry Accounts: Theory, Computation, and Modeling (Theoretica Chimica Acta)* **1973,** 28, (3), 213-222.
7. Zhao, Y.; Truhlar, D. G., The M06 suite of density functionals for main group thermochemistry, thermochemical kinetics, noncovalent interactions, excited states, and transition elements: two new functionals and systematic testing of four M06-class functionals and 12 other functionals. *Theoretical Chemistry Accounts: Theory, Computation, and Modeling (Theoretica Chimica Acta)* **2008,** 120, (1), 215-241.
8. Yanai, T.; Tew, D. P.; Handy, N. C., A new hybrid exchange–correlation functional using the Coulomb-attenuating method (CAM-B3LYP). *Chemical Physics Letters* **2004,** 393, (1), 51-57.
9. Marten, B.; Kim, K.; Cortis, C.; Friesner, R. A.; Murphy, R. B.; Ringnalda, M. N.; Sitkoff, D.; Honig, B., New model for calculation of solvation free energies: correction of self-consistent reaction field continuum dielectric theory for short-range hydrogen-bonding effects. *The Journal of Physical Chemistry* **1996,** 100, (28), 11775-11788.
10. Tapia, O.; Goscinski, O., Self-consistent reaction field theory of solvent effects. *Molecular Physics* **1975,** 29, (6), 1653-1661.
11. Tomasi, J.; Mennucci, B.; Cammi, R., Quantum mechanical continuum solvation models. *Chemical reviews* **2005,** 105, (8), 2999-3094.
12. Nielsen, A. B.; Holder, A. J., *GaussView. User's reference*. Gaussian, Incorporated: 1998.
13. Marques, M. A.; Maitra, N. T.; Nogueira, F. M.; Gross, E. K.; Rubio, A., *Fundamentals of time-dependent density functional theory*. Springer Science & Business Media: 2012; Vol. 837.
14. Ullrich, C. A., *Time-dependent density-functional theory: concepts and applications*. OUP Oxford: 2011.
15. Mohr, B.; Enkelmann, V.; Wegner, G., Synthesis of alkyl-and alkoxy-substituted benziles and oxidative coupling to tetraalkoxyphenanthrene-9, 10-diones. *Journal of organic chemistry* **1994,** 59, (3), 635-638.
16. Katritzky, A. R.; He, H.-Y.; Long, Q.; Wilcoxb, A. L., Preparation of 2, 6-dialkoxybenzaldehydes. *Arkivoc* **2001,** 3, 3-12.
17. Littler, B. J.; Miller, M. A.; Hung, C.-H.; Wagner, R. W.; O'Shea, D. F.; Boyle, P. D.; Lindsey, J. S., Refined synthesis of 5-substituted dipyrromethanes. *The Journal of Organic Chemistry* **1999,** 64, (4), 1391-1396.
18. Lakowicz, J. R., Introduction to fluorescence. In *Principles of fluorescence spectroscopy*, 2nd ed.; Springer: 1999; pp 367-373.
19. Lakowicz, J. R., Introduction to fluorescence. In *Principles of fluorescence spectroscopy*, Springer: 1999; pp 1-23.
20. Williams, A. T. R.; Winfield, S. A.; Miller, J. N., Relative fluorescence quantum yields using a computer-controlled luminescence spectrometer. *Analyst* **1983,** 108, (1290), 1067-1071.
21. Frenette, M.; Hatamimoslehabadi, M.; Bellinger-Buckley, S.; Laoui, S.; La, J.; Bag, S.; Mallidi, S.; Hasan, T.; Bouma, B.; Yelleswarapu, C., Shining light on the dark side of imaging: excited state absorption enhancement of a bis-styryl BODIPY photoacoustic contrast agent. *Journal of the American Chemical Society* **2014,** 136, (45), 15853-15856.
22. Hatamimoslehabadi, M.; Bellinger, S.; La, J.; Ahmad, E.; Frenette, M.; Yelleswarapu, C.; Rochford, J., Correlation of Photophysical Properties with the Photoacoustic Emission for a Selection of Established Chromophores. *The Journal of Physical Chemistry C* **2017,** 121, (43), 24168-24178.
23. Danielli, A.; Maslov, K.; Favazza, C. P.; Xia, J.; Wang, L. V., Nonlinear photoacoustic spectroscopy of hemoglobin. *Applied physics letters* **2015,** 106, (20), 203701.
24. Danielli, A.; Maslov, K.; Xia, J.; Wang, L. V. In *Wide range quantitative photoacoustic spectroscopy to measure non-linear optical absorption of hemoglobin*, Photons Plus Ultrasound: Imaging and Sensing 2012, 2012; International Society for Optics and Photonics: 2012; p 82233H.
25. Danielli, A.; Yao, J.; Krumholz, A.; Wang, L. V. In *Effects of calibration factors and intensity dependent non-linearity on functional photoacoustic microscopy*, Photons Plus Ultrasound: Imaging and Sensing 2011, 2011; International Society for Optics and Photonics: 2011; p 78993C.